LOCKHEED MISSILES AND SPACE COMPANY
A Division of Lockheed Aircraft Corporation

Technical Memorandum

TM 53-40-143

LMSC/803185

STATIC LOADS ON THE SATURN I-APOLLO LAUNCH VEHICLE

August 1963

Prepared By: J. P. Reding
J. P. Reding
Aerodynamic Design
Aerodynamics

Prepared By: Lars-Eric Ericason
Lars-Eric Ericason
Staff Engineer
Aero-Mechanics

Approved By:
B. W. Marsh
Manager
Aero-Mechanics

D2686

SUMMARY

An analysis of the Saturn I-Apollo static force distribution has been performed to provide the basis for a quasi-steady analysis of the aeroelastic stability of the vehicle. The flow field over the Saturn I-Apollo launch vehicle contains numerous regions of separated flow which drastically alter the static force distribution. The separated wake from the tower mounted escape rocket has the largest single effect upon the vehicle normal force distribution. The tower wake causes an increase in the command module loading throughout the Mach number range $.8 \leq M \leq 2.5$, and transonically a negative loading is induced on the forward service module aft of the command module shoulder by the reattaching escape rocket wake. The wake also thickens the service module boundary layer promoting the flare induced separation forward of the service module flare. Regions of flare induced separation are present over the various other body flares. In general, flare induced separation produces a negative loading on the cylinder forward of the flare in the region of the detached flare shocks and increases the loading over the flare. If the separation reattaches aft of the flare shoulder a negative load results in this region which is similar to the negative service module load caused by the reattaching escape rocket wake.

SUMMARY (Cont'd)

An approximation to the static load distribution is presented in Appendix B for the two configurations of major interest (the basic configuration and the current flight configuration). This approximation amounts to replacing the various regions of positive and negative loading over the body by 18 discrete body force vectors plus a fin loading vector. This lumped force approximation has been accomplished to facilitate the utilization of the data in a quasi-steady aerodynamic analysis of the response of the elastic vehicle.

TABLE OF CONTENTS

DEFINITION OF SYMBOLS

C_A	Forebody axial force coefficient, $\frac{\text{forebody axial force}}{1/2\ \rho\ U^2\ S}$
C_N	Normal force coefficient, $\frac{\text{Normal force}}{1/2\ \rho\ U^2\ S}$
C_{N_α}	Normal force coefficient slope, $\partial C_N / \partial \alpha$ per degree
$C_{N_{\alpha X}}$	Local normal force coefficient slope
$C_{N_{\alpha L}}$	Lumped normal force coefficient slope
C_p	Pressure coefficient, $\frac{p - p_\infty}{1/2\ \rho\ U^2}$
e	Reference length, 1st stage diameter - 1 caliber = 257 inches
d	Local diameter, calibers
M	Mach number
S	Reference area, $\frac{\pi\ C^2}{4}$, square feet
U	Free stream velocity, ft/sec
u	Component of free stream velocity normal to body axis, ft/sec
Xc.p.	Center of pressure, calibers
α	Angle of attack, degrees
ρ	Free stream density, slugs/ft^3

Subscript

$\alpha = 0^\circ$	Denotes zero angle of attack characteristics
ϕ	Denotes radial position, degrees
α_2	Refers to second slope in triple slope approximation of angle of attack characteristics
α_3	Refers to third slope of triple slope approximation of angle of attack characteristics

LIST OF FIGURES (Cont'd)

LIST OF FIGURES

INTRODUCTION

In May 1962 Lockheed Missiles and Space Company was retained by the Aeroballistics Laboratory of the NASA Marshall Space Flight Center in a consultant capacity to determine the aeroelastic stability of the Saturn I launch vehicle with an Apollo payload. The quasi-steady aerodynamic analysis technique developed at LMSC (Reference 1) uses the static aerodynamic load distribution over the vehicle as an input.

This report presents the results of an analysis of the static load distribution over the Saturn I-Apollo vehicle where the effects of the numerous regions of separated flow have been included. These data were used in the quasi-steady dynamic analysis of Reference 2.

Since the Apollo payload with its escape system has the most important effect on the vehicle dynamics a test program was conducted in the Unitary Plan Wind Tunnels of the Ames Research Center to accurately determine the load distribution over the forward portion of the launch vehicle. A dual balance segmented model was used so that command module, service module, and service module flare loads could be determined for a basic configuration which at that time represented the flight configuration (Fig. 1). Other forebody configurations were also investigated in order to facilitate the analysis and to provide some data needed for extrapolation

INTRODUCTION (Cont'd)

to other escape rocket and tower configurations. The proposed test program for configurations other than the basic configuration was, however, greatly curtailed because it was considered to be research testing which Ames could not admit due to a heavy test schedule. Figure 2 presents sketches of the configurations tested and References 3 and 4 present the data obtained from the test program. These data were used in conjunction with the results of various other static force and pressure tests (References 5, 6 and 7) to determine the static load distribution over the entire vehicle.

Subsequent to the completion of this analysis a configuration change was made as may be seen in Figure 3, which presents a sketch of the current "flight configuration." The analysis has, therefore, been extended using the data of Reference 8 to determine the loading over the "flight configuration."

Appendix A presents an empirical pressure integration technique used to integrate the data of Reference 5, while Appendix B includes a triple slope approximation to the non-linear angle of attack characteristics of the various discrete normal force coefficients which approximates the static force distribution of the "flight configuration." These data are intended to facilitate the inclusion of the separated flow force distribution into a multi-degree of freedom dynamic simulation.

SEPARATED FLOW EFFECTS

The Saturn I-Apollo configuration offers the aerodynamicist a unique opportunity to investigate the effects of separated flow on the aerodynamic characteristics of large launch vehicles. Figure 4 illustrates the flow field over the Saturn I-Apollo vehicle at a Mach number of 1.35. Almost every type of flow separation is present: Retarded spike separation exists forward of the escape rocket disk; the escape rocket wake impinging upon the command module is similar to separated flow from the blunt tip of a short spike; flare-induced separation is evident forward of the service module flare, the second stage adapter ring, and the small tail flare; the separation aft of the second stage adapter ring is of the hammerhead or base wake variety. An examination of the aerodynamic characteristics of the Saturn I-Apollo vehicle with escape rocket removed reveals the presence of nose-induced transonic separation. In the following discussion the aerodynamic characteristics of various types of separation will be compared with the Saturn I-Apollo component characteristics.

Spiked-Body Separation

For a spiked blunt body the spike tip, acting as the wake source, produces a region of separated flow which impinges on the blunt aft body or windshield. The spike greatly reduces the axial force of the windshield (see Figure 5). The axial force reduction is a result of the decreased average velocity or dynamic pressure field within the separated flow region.

Accompanying the reduction in the average velocity are large velocity gradients that, when coupled with the differential movement of the reattachment with angle of attack, produce a large increase in the normal force derivative near $\alpha = 0^{\circ}$. Also a product of the differential movement of the reattachment is the large stabilizing axial force moment. Thus, as illustrated in Figure 5, the addition of a spike to a blunt conical windshield produces a reduced axial force, an increased normal force derivative, and a more stable pitching moment derivative. As angle of attack is increased the spiked body characteristics approach attached flow spike off characteristics.[1]

The command module characteristics (Figure 6) show great similarity with the spiked-body characteristics of the conical windshield. Addition of the escape system to the command module produces an axial force reduction and a normal force derivative increase near zero angle of attack. The differences between the tower on and tower-off characteristics, axial force coefficient and normal force slope can be seen to diminish with increased angle of attack. It is evident that the escape rocket disk is equivalent to the spike tip, i.e., the disk is the source of the wake that impinges upon the command module producing the non-linear characteristics. One may postulate that removal of the escape rocket disk will

---

[1] The reader is referred to Reference 9 for a further discussion of spiked-body characteristics.

reduce the wake, and therefore, be equivalent to reducing the spike length. The effect upon the command module characteristics would then be to increase the $\alpha = 0^{o}$ axial force and decrease the normal force derivative when compared to the disk-on configuration. It will be shown later that this is precisely what happens.

Cone-Cylinder-Flare Separation

Much experimental data have been gathered on cone-cylinder-flare bodies due to the suitability of this type of configuration to re-entry body design. There are three distinct types of cone-cylinder-flare separation.[1]

1) Type I - Nose-induced separation,
2) Type II - Supersonic flare-induced separation,
3) Type III - Transonic flare-induced separation.

The three types of cone-cylinder-flare separation are illustrated in Figure 7. Type I separation appears at high subsonic Mach numbers and is caused by the large adverse pressure gradient aft of the nose cone. This type of separation appears also on cone-cylinder bodies if the cone angle is large. Type II separation is produced by the detached flare shock at supersonic Mach numbers and resembles retarded spike separation.[2] Type III separation is a possible interim case between Type I and Type II separation. Type III separation is flare-induced where, due to the short cylinder length, the separation travels forward to the cone-cylinder juncture. This type of separation resembles spike separation for less than optimum spike lengths.[3]

---

[1] A more complete discussion of cone-cylinder-flare separation is contained in Reference 10.

[2] Flow separation starting aft of the spike tip.

[3] Flow separation starting at the spike tip.

The separation-induced flare characteristics (Figure 8) are similar to the spike-induced windshield characteristics (Figure 5). The flow separation causes a reduction of the axial force coefficient and an increase in the normal force derivative of the flare. The supersonic Type II separation has less effect than the subsonic Type I separation due to the lesser extent of the separated flow region.

Figures 9 and 10 illustrate the effect of the escape rocket system on the service module flare characteristics. The flare characteristics with escape system in place resemble normal attached flow characteristics at M = 0.8. Removal of the escape system causes Type I separation to occur at the cone-cylinder juncture. This is evidenced by the characteristic non-linear normal force curve and the corresponding axial force reduction. The absence of Type I separation with the escape tower on is explained by the spike-effect of the escape rocket. The escape rocket wake completely encloses the command module and the flow attaches aft of the command module-service module juncture.

The picture supersonically is reversed. Figures 9 and 10 at M = 1.35 indicate that the airflow over the flare is attached tower-off and separated tower-on. Apparently the impinging tower wake, which contains a velocity deficit, weakens the service module boundary layer sufficiently to promote Type II flare-induced separation. It is interesting to note that the shadowgraphs (which are not suitable for reproduction in this report) indicate that the addition of the escape rocket and tower produced a

substantially thicker turbulent boundary-layer forward of the service module flare. Kuehn has shown in Reference 11 that an increase in the Reynolds number (Re_δ) based on the boundary-layer thickness (δ) at the point where the flare first affects the cylinder static pressure, promotes flare induced separation for a fully developed turbulent boundary layer. In other words, thickening the turbulent boundary layer forward of the flare promotes flare-induced separation.

The effects of thickening the boundary layer forward of the flare with the tower on can best be seen in Figure 11 where the characteristics of the flare at $\alpha = 0^\circ$ are plotted versus Mach number. Supersonically one may see that tower on the normal force derivative is increased, the axial force coefficient is reduced, and there is a general increase in stability margin. These effects are indicative of increased flare induced separation tower on. On the other hand subsonically the separated flow effects on the flare are largest tower-off where Type I nose induced separation occurs. The flare-induced separation effects on the basic configuration are present throughout the Mach number range $.5 \leq M \leq 2.5$ peaking at $M = 1.2$. The flare center of pressure for the basic configuration moves forward with increasing Mach number and is, at $M = 2.5$, forward of the attached flow center of pressure (tower-off). This is a result of the decreasing separated flow region (see flow sketches in Figure 11), i.e., the separation-induced forces are located farther forward on the flare for higher Mach numbers. The forward center of pressure shift at $M = 1.35$ for the tower-off configuration has the

same cause. A mild flare-induced separation is obtained on the tower-off configuration at low supersonic Mach numbers. The deviation between the supersonic attached flow tower-off characteristics and the analytical predictions of References 12 and 13[1] will be discussed in connection with the service module characteristics.

PRESSURE DISTRIBUTION

The pressure distribution over the forward portion of the Saturn I-Apollo vehicle produces supporting evidence for the preceding arguments. By comparing tower-on and tower-off pressure distributions both subsonically and supersonically the detailed separated flow effects may be examined. By examining the pressure distributions in detail the the phenomenon responsible for certain pecularities, such as the subsonic separation over the flare with the tower on, and the reduced flare effectiveness caused by adding a cylinder aft of the flare, etc. may be understood. Since the pressure distribution indicates that negative service module loads should be present a brief discussion of service module force characteristics is included in this section to substantiate the pressure data trends.

Subsonic Pressure Distribution

The pressure distribution over the forward portion of the Saturn I-Apollo vehicle is rather complicated subsonically since quite different separation phenomenon exist for the two configurations. However, by comparing the

---

[1] The second order shock expansion method of Reference 13 has been programmed for digital computer solution at LMSC (Ref. 14). This program was used to obtain the results shown.

M = 0.9 pressure distributions for tower on and tower off configurations to one another (as shown in Figure 12) and to the theoretical attached flow pressure distribution (see Sketch 1) one may see the various separated flow effects.[1]

At $\alpha = 0^\circ$ the aft command module pressures are lower with tower on which indicates that the tower wake completely encloses the command module. At $\alpha = 4^\circ$ the pressure level is reduced somewhat more on the leeward side. On the windward side, however, the aft command module pressures are increased substantially above the tower off levels, because the wake impinges on the command module and the high pressures associated with flow reattachment are realized.

The effect of separated flow on the pressure distribution aft of the command module-service module juncture is more subtle. One may see from the data of Figure 12 that the forward service module pressures are more negative for the tower on configuration than for the tower off configuration. In both cases the windward side pressures are more negative than the leeward side pressures which is indicative of separated flow. This may be explained by consulting Sketch 1 on the following page.

---

[1] It should be noted that the pressure data of Figures 11 and 12 for the configuration with escape system removed was obtained on a somewhat shorter service module. The data presented have been obtained by keeping the same forward and aft service module pressure levels and stretching the distrubution out over the longer cylinder length. Cylinder length does have some effect on the pressure peaks, particularly at M = 0.9. However, the effect is believed to be minor in this case and unimportant for the comparison of general trends.

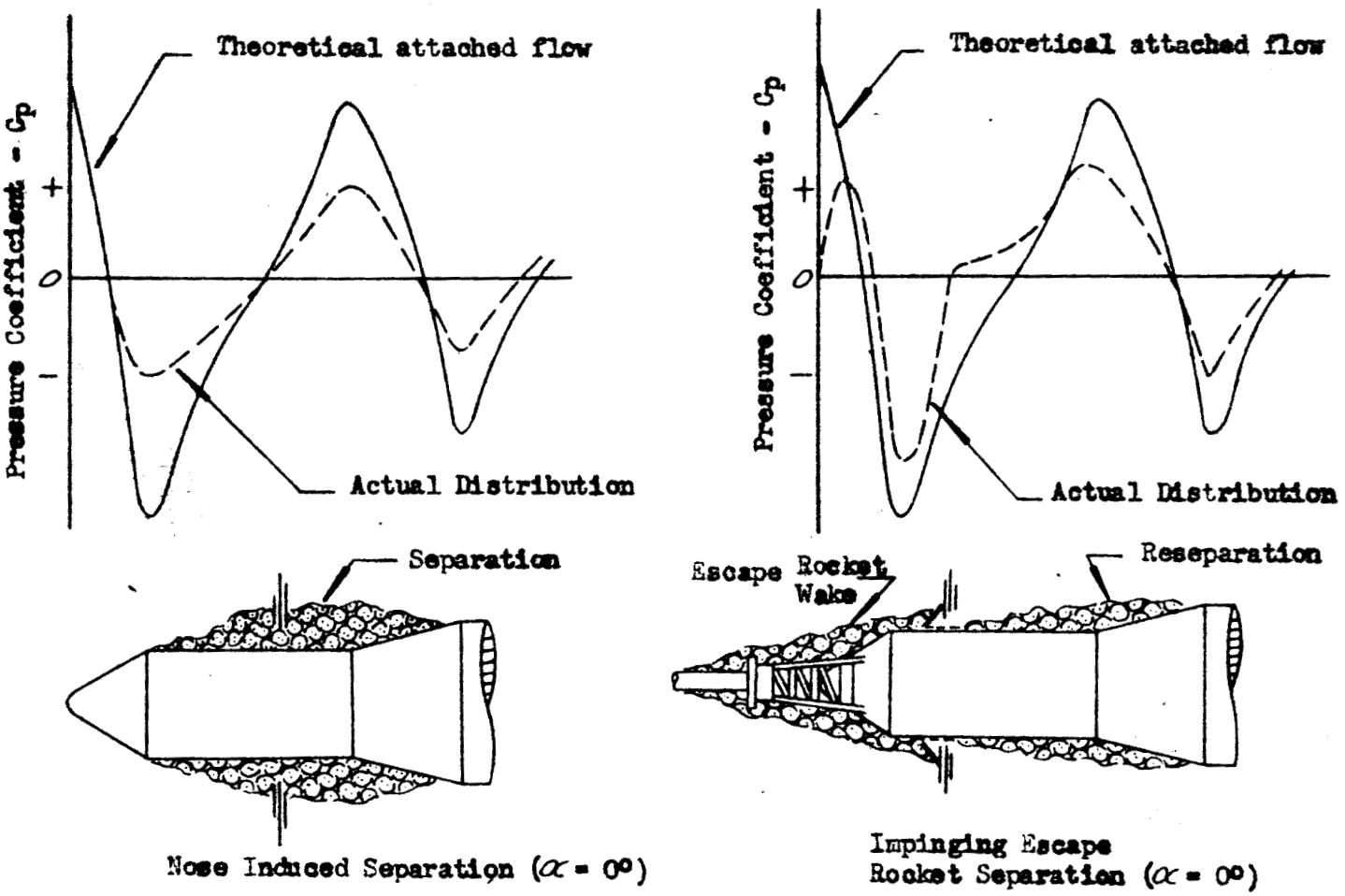

Sketch 1

By comparing the theoretical attached flow pressure distribution with the actual pressure distribution one may see how flow separation affects the tower off configuration. The negative and positive pressure peaks over the body are reduced by separation and the pressure gradients are also reduced. With increasing angle of attack the separated boundary layer on the windward side is thinned out by cross-flow effects and is strengthened permitting a larger pressure gradient. Thus, the windward pressure distribution approaches the theoretical attached flow distribution producing more negative pressures aft of the cone-cylinder juncture and higher positive

pressures on the aft service module and flare. The converse is true on the leeward side, but the effects are relatively small. The thickening and weakening[1] of an already thick and weak separated flow layer does not produce any spectacular effects.

The separated flow effects for the tower on configuration are more subtle. The wake from the escape rocket impinges at the command module shoulder and reattaches on the service module aft of the shoulder. At high subsonic Mach numbers local normal shocks produce a sudden pressure rise that the reattaching flow cannot withstand and reseparation occurs. The pressure rise through the normal shock accounts for the positive pressure coefficients over the aft service module. The reattaching tower wake only partially destroys the large negative pressure region aft of the command module shoulder and the pressures are, therefore, more negative tower on than tower off (Fig. 12).

With increasing angle of attack the windward reattachment point moves forward onto the command module and the pressures aft of the command module approach attached flow values, producing more negative pressures directly aft of the command module and more positive pressures on the aft service module and flare. In general, the converse is true on the leeward side. The exception is the leeward pressure on the service module immediately aft of the command module which becomes more negative with increasing angle of attack. This local effect is probably due to the aft movement of the leeward reattachment causing less of the reattachment pressure rise to be felt upstream at the

---

[1] Due to cross flow effects

command module-service module juncture. This effect could also contribute to the windward side pressure drop when the reattachment moves from the service module onto the command module. The large reduction of the leeward negative pressure farther aft of the command module (at .55 caliber in Figure 12) may partly be caused by this aft movement of the reattachment, but most of the pressure rise should be contributed to the thickening of the attaching boundary layer allowing the pressure rise through the local normal shocks to be felt farther upstream.

The flare pressure distributions shown in Figure 12 reveal marked differences in tower on and tower off characteristics. At $\alpha = 0^{o}$ the tower on pressure levels are higher than the corresponding tower off pressure levels. The primary factor contributing to the higher tower on pressure levels is the smaller region of separated flow. Tower off the separation is larger and the flare pressures are reduced more. The shock-induced separation tower on is thinner and the flare characteristics are similar to attached flow in that windward and leeward side increments due to angle of attack are nearly equal. The tower off pressure distribution over the flare is similar to the tower on pressure distribution over the command module. Thus, the windward side pressure increase due to angle of attack is much greater than the leeward side pressure reduction. The large separation tower off[1] produces a

---

1 The Type I nose-induced separation discussed earlier.

wake-like flow that at $\alpha = 0^{\circ}$ completely encloses the service module and flare. Consequently, the flare characteristics for the nose-induced separation tower off are similar to the command module characteristics in the escape rocket wake tower on[1].

The shock-induced separation on the service module with tower on is thinner and the flare can make its presence known by displacing the free stream through the separation layer producing more attached-flow-like flare characteristics.

The pressure distributions aft of the service module flare are generally similar tower on and tower off. The negative pressures at $\alpha = 0$ are less in magnitude tower off than tower on. This is because the more extensive separation tower off, with flow reattachment farther aft of the flare shoulder, destroys more of the negative pressures produced by expanding the flow around the shoulder. Both the tower on and the tower off pressures are less in magnitude than for attached flow. The leeward side pressures change little with angle of attack while the windward pressures approach attached flow values for both configurations, as the windward side reattachment moves forward of the shoulder onto the flare. This shoulder effect also reduces the positive pressures on the aft flare suggesting that the addition of a cylindrical aft body to the flare will reduce the flare normal force derivative. This expected effect is verified by force measurements as will be shown later.

---

[1] The similarity between nose-induced Type I separation on a cone-cylinder-flare body and the separation from the tip of a spike of less than optimum length was pointed out earlier.

Supersonic Pressure Distribution

The supersonic pressure distributions (Figure 13) require little explanation after this somewhat exhaustive discussion of the subsonic distribution. The tower off configuration exhibits almost completely attached flow characteristics. At M = 1.43 a small flare-induced separation is indicated by the increased leeward pressure forward of the flare at $\alpha = 4^{\circ}$.

For the tower on configuration the wake from the escape rocket impinges upon the command module at zero angle of attack. The pressure rise through the shock formed at the impingement produces the pronounced peak appearing in the pressure distribution on the aft command module. The outer higher velocity portion of the wake passes through the impingement zone and reattaches on the service module aft of the command module shoulder. The pressure increase due to reattachment deforms the pressure distribution on the forward service module (compare tower off). The boundary layer on the service module is thickened by the reattaching wake and the flare-induced separation is more severe tower on. This is evidenced by the larger leeward pressure drop on the flare at angle of attack (compare tower off in Figure 13).

At angle of attack the wake impinges farther forward on the windward side of the command module and the reattachment point moves forward. At $\alpha = 4^{\circ}$ in Figure 13 the windward side reattachment has moved forward onto the command module. This is revealed by the windward side pressure distribution. The positive pressure peak on the aft command module approaches attached

flow values (compare 13a and 13b). Furthermore, the negative pressure distribution on the forward service module no longer shows any reattachment deformation. The leeward side impingement[1] on the command module moves aft with increasing angle of attack. At $\alpha = 4^{\circ}$ in Figure 13 the wake no longer causes any impingement shock on the leeward command module as can be seen from the pressure distribution. In absence of the impingement shock higher velocity flow is expanding around the leeward shoulder and the negative pressure on the service module at the shoulder is increased and approaches attached flow magnitude (compare tower off). The high velocity wake reattaching aft of the shoulder causes a strong recompression shock evidenced by the sudden pressure rise in the service module pressure distribution.

Service Module Loads

The existence of leeward pressures that are higher than the corresponding windward pressures suggest that regions of negative normal force exist over the service module. By examining the service module force characteristics it becomes evident that negative loadings exist over the service module. Figure 14 presents some typical service module normal force curves. One may see that with the escape system on the service module normal force is negative up to angles of attack of 6 or 7 degrees at transonic Mach numbers. As Mach number is increases supersonically the negative normal force regions

---

[1] The word "impingement" is used here to denote that the outer higher velocity region of the wake is impinging on and being deflected by the command module.

aft of the command module and forward of the flare diminish. Thus the service module normal force is positive at M = 2.5 and not much less than for the tower off configuration. When the angle of attack is increased the normal force curves for both configurations converge as they both are approaching complete leeward separation at high angles of attack. Figure 15 presents zero angle of attack service module characteristics tower on and tower off, and shows a comparison between supersonic tower off characteristics and analytical predictions. The zero angle of attack service module characteristics for the basic configuration dramatically illustrate the presence of the negative loading forward on the service module. The negative normal force derivative and the forward center of pressure location at transonic speeds indicate that the negative normal force induced by the tower wake is large. As Mach number is increased the negative forward loading decreases in magnitude and the center of pressure moves aft. At M = 1.9 the center of pressure becomes undefined. This is due to equal positive and negative normal force loadings, a pure force couple is acting on the service module. At Mach numbers greater than 1.9 the service module load is positive but less than that for attached flow and the center of pressure is forward of the attached flow (tower off) center of pressure indicating almost no negative loading forward on the service module. Therefore, the reduced normal force derivative is due to Type II shock-induced separation forward of the service module flare.

The tower off service module characteristics agreed reasonably well with theoretical and empirical results for supersonic attached flow. The deviations from second order shock predictions may seem surprising, but the data of Reference 15 indicates that such deviations exist for large nose angles such as the 33° Apollo cone angle.

EFFECTS OF ESCAPE SYSTEM CONFIGURATION

As indicated by the preceeding discussion the escape rocket drastically alters the aerodynamic characteristics of the forward body components. A discussion of the effects of various escape system configurations should be of benefit in understanding the flow phenomena involved and in predicting, at least qualitatively, the effects of possible future configuration changes in the escape system.

Command Module Characteristics

Addition of escape rocket and tower to the clean command module generally increases the command module normal force derivative, moves the center of pressure aft, and decreases the axial force. The escape rocket without the disk increases the command module normal force derivative as much as 150% transonically (Figure 16). This increase in normal force derivative tails off as Mach number is increased until at M = 2.5 the normal force derivative increment is only about 25% of the attached flow value. Corresponding reductions in the stability margin and axial force reduction at $\alpha = 0^\circ$ are experienced. The escape rocket with disk on increases the command

module normal force derivative as much as 375% over the clean command module value. Corresponding increases in the axial force reduction and the aft center of pressure movement, caused primarily by the stabilizing axial force moment, accompany this increase in normal force derivative. Again the separated flow effects are seen to diminish with increasing Mach number as the tower wake closes more with increasing Mach number.

The data presented in Figure 16 show a reduction in stability (forward center of pressure movement) at M = 1.1 to 1.2 for the open tower configurations. The incremental normal force derivative and the axial force reduction caused by adding the escape system also experience a reduction over this Mach number range. The data in References 16, 17, 18 and 19 show the same phenomenon for spiked blunt bodies[1]. The data of Reference 17 (Figure 17) indicates that the Mach number at which the axial force increases occurs is somewhat a function of spike length[2].

The monocoque tower produces some very interesting effects. Transonically the command module plus tower loads are low, but at M = 1.35 a sudden increase in normal force occurs with a corresponding rearward center of

---

[1] The data in Fig. 1, Ref. 16 has to be interpreted with some care. The low drag spike-off is realized because the blunt nose-tip causes the Type I nose-induced separation resulting in decreased drag on the following conical nose-section.

[2] It is unfortunate that the normal force and center of pressure data of Reference 17 are masked by separated flow effects on the aft body since this reference is the only one known to the authors that includes normal force data for spiked bodies over the transonic Mach number range.

pressure movement and a reduction in axial force. The flow over the command module and monocoque tower is attached subsonically but at supersonic Mach numbers a flare-induced separation occurs on the monocoque tower ahead of the command module producing the observed separated flow effects.

In general then, the addition of the escape rocket and open tower produces separated flow effects on the command module that are similar to the effects of a conventional flow separation spike. Removing the escape rocket disk is similar to shortening the spike and the separated flow effects are reduced. Replacing the open tower with a monocoque tower produces a new configuration. The configuration is no longer a spiked body but is similar to a cone-cylinder-flare body with a subcritical nose angle such that only Type II flare-induced separation occurs over the command module.

Service Module and Flare Characteristics

The zero angle of attack characteristics for the combined service module and flare (Figure 18) show that the negative cylinder loading over the service module has a dominating effect upon the normal force derivative for the basic configuration. Adding the escape rocket and tower to the clean configuration reduces the normal force derivative. The effect on the center of pressure can be explained by the combined effects of the negative cylinder loads, the separation-induced flare normal force and the axial force moment. As for the command module characteristics discussed earlier, the disk off configuration represents an intermediate case between the clean and basic

configurations. Removing the disk reduces the forward negative loading on the service module (as is illustrated in Figure 15[1]) as well as the wake-triggered flare-induced separation. At supersonic speed the monocoque tower does not change the spike-characteristics of the escape-rocket (Figure 18). At subsonic speeds, however, the flow is attached over the command module for the monocoque tower. Thus the nose-induced Type I separation occurs at the command module shoulder, and the subsonic characteristics are similar to the tower-off characteristics.

An important effect of geometry is demonstrated in Figure 15, viz. the difference between the interstage flare of an ascent vehicle and the terminating flare of a re-entry body. The cylindrical afterbody at the interstage flare causes a substantial reduction in the separation-induced flare load. This effect was also indicated by the pressure data in Figure 12.

How the various tower and escape rocket configurations affect the angle of attack characteristics of the combined service module and flare is shown in Figure 19. In addition to confirming the results just discussed (Figure 18), Figure 19 shows that the effect of the various escape rocket

---

[1] This effect at supersonic Mach numbers suggests that a similar reduction in loads should be achieved transonically by removing the disk.

configurations decreases with increasing angle of attack and disappears at high α[1]. The hysteresis loops at $M = 1.0$ for the tower off configuration are the same as those obtained on re-entry bodies (Reference 20).

In general then, the addition of the escape rocket and open tower reduces the normal force and moves the center of pressure aft on the combined service module and flare. When the disk is removed the effects of the escape rocket are reduced. Shrouding the escape rocket tower does not have any appreciable effects on the supersonic characteristics. At subsonic speeds, however, the shrouding produces close to tower off characteristics.

EFFECT OF SERVICE MODULE LENGTH

One would expect that increasing the service module length would have no effect on the tower induced command module and forward service module loadings; however, the aft service module and flare loadings would be changed since the longer service module would allow a thicker boundary layer to develop forward of the flare thereby increasing the effects of flare induced separation. Figure 20 compares the disk on normal force distributions at $\alpha = 2^{\circ}$ and $M = 1.0$ and 1.2 for the two service module lengths, (1.134 and 1.387 calibers respectively). The forward service module loading is plotted relative to the command module while the aft

---

[1] The flow over the service module and flare is then completely attached on the windward side and completely separated on the leeward side irrespective of the escape rocket configuration.

service module load is plotted relative to the flare. There is no change in the forward service module loading due to cylinder length as expected since this loading is purely a function of the escape system geometry. The aft service module and flare loadings show the following effects caused by lengthening the service module:

1. The flare induced negative loading occurs further forward of the flare,
2. Increased positive service module loading just forward of the flare,
3. Increased flare loading.

All three effects are consistent with the additional boundary layer growth caused by lengthening the service module. However, when disk off normal force derivatives are compared, as in Figure 21, one sees some peculiar results.

Figure 21a shows the combined service module and flare characteristics for a number of configurations. For the disk on configurations the longer service module produces similar C_{N_α} versus Mach number characteristics of only slightly larger magnitudes than those for the short service module. Figures 21b and c indicate that this increased loading is caused by an increased flare loading which is consistent with the thicker boundary layer on the longer service module. The disk off service module and flare characteristics are approximately the same subsonically for both cylinder lengths while supersonically the longer service module produces a much lower normal force derivative than the short service module. Examining Figure 21c one sees that subsonically the long service module flare force follows the

disk on trend while supersonically it follows the tower off trend. It appears then that disk off the boundary layer forward of the flare is stronger on the longer (1.387 caliber) service module and the flare induced separation is reduced. Since this trend does not appear disk on it is obviously intimately related to the extent of the tower wake. Disk off the longer cylinder allows the service module boundary layer to become completely reattached before it encounters the flare thereby reducing the flare induced separation. Disk on the longer wake produces a transitional service module boundary layer which is not completely reattached forward of the flare and lengthening the service module promotes flare induced separation. Subsonically the local normal shocks aft of the command module shoulder fix reseparation relative to the nose and disk on and disk off characteristics are similar differing only in magnitude.

There exists then, at supersonic speeds, a critical cylinder length for each escape configuration. For greater than critical (supercritical) cylinder lengths the boundary layer forward of the flare becomes completely reattached. For the short service module (1.138 calibers) the cylinder length is subcritical both disk on and disk off. The long service module length (1.387 calibers) is supercritical disk off and the boundary layer is completely attached forward of the flare while disk on the long service module length is still subcritical.

NORMAL FORCE DERIVATIVE DISTRIBUTION

The preceding discussion has been presented in an attempt to provide some insight into how separated flow affects the Saturn I - Apollo configuration. The complete normal force derivative distribution will be discussed in this section, and the separated flow effects will be shown to dominate the load distribution.

Obviously the total normal force derivatives of the command module, service module, and service module flare can be obtained directly from the data of References 3 and 4. The pressure data of Reference 5 was used to obtain the longitudinal distribution of the normal force derivative. Since the data of Reference 5 was somewhat scanty in regard to peripheral pressure distribution it was necessary to use an empirical integration technique to obtain the integrated normal force at each station as discussed in Appendix A.

The longitudinal normal force distribution was thus calculated at $\alpha = 2^{\circ}$ and 4°. The longitudinal data point density was insufficient to determine the various service module positive and negative load peaks, and it was necessary to adjust the normal force distribution until agreement with the force data of References 3 and 4 was obtained. The various positive and negative service module normal force regions were integrated and replaced by discrete force vectors as shown in Sketch 2 on the following page.

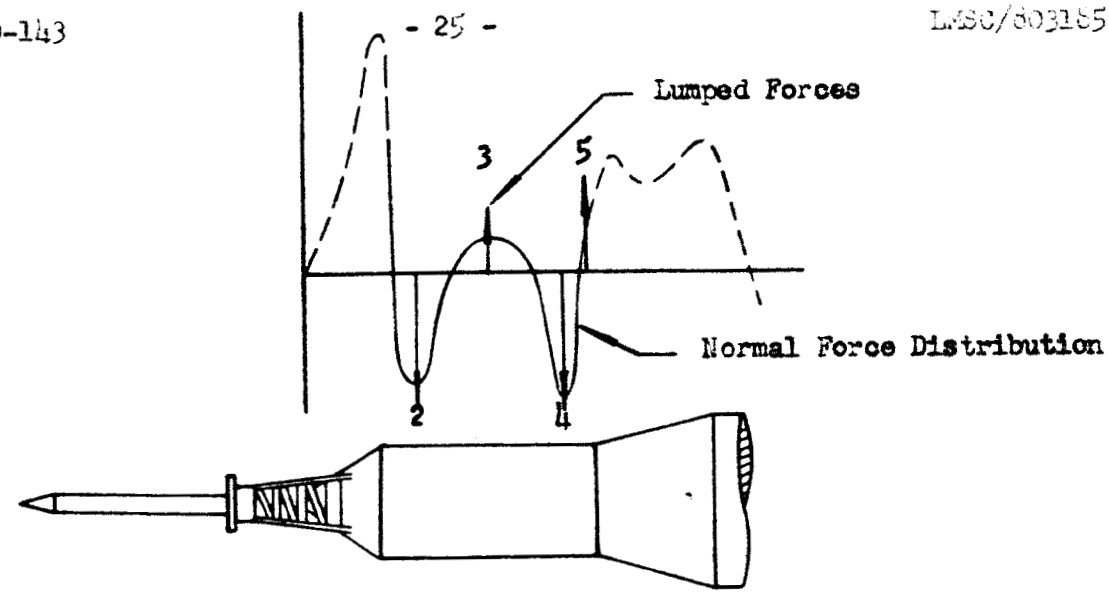

Sketch 2

The lumped force vectors for α = 2° and 4° were faired through α =0° assuming symmetry for positive and negative angles of attack to obtain the values of $C_{N\alpha_2}$, $C_{N\alpha_3}$, $C_{N\alpha_4}$, and $C_{N\alpha_5}$ at α = 0°. The same procedure was followed with the lumped pitching moments. Since the lumped forces are highly nonlinear with angle of attack it was necessary to adjust the α-fairing until sufficient agreement was obtained with the service module derivative and center of pressure data of References 3 and 4. Figure 15 illustrates the degree of agreement thus obtained. The lumped force vectors, $C_{N\alpha_2}$, $C_{N\alpha_3}$, $C_{N\alpha_4}$, and $C_{N\alpha_5}$ were then distributed using the general shape of the α = 2° distribution as a guide.

The data of Reference 8 were used to obtain the normal force derivative distribution over the flight configuration, disk off and long service module, for the Mach number range .8 to 1.28. These data were also used to obtain the normal force derivative distributions over the basic configuration, disk

on and short service module, aft of the service module flare. This is more reasonable than it might seem at first. The only aft body loadings that would be affected by forebody configuration is the loading on the second stage just aft of the service module flare. It was found that there was very little difference even in that loading between disk on and disk off for the flight configuration. Therefore, it was reasoned that the effect of service module length on the aft body loading would be even less and could be neglected.

The data of Reference 6 were used to obtain the higher Mach number (M = 1.42 and 1.93) normal force derivative distributions for both the flight configuration, disk off and long service module, and the basic configuration, disk on and short service module. At these high Mach numbers reattachment occurs on the service module flare and forebody geometry has negligible effect on the aft body loads.

Basic Configuration

The effect of adding the basic escape system configuration to the clean command module is illustrated in Figures 22a and b. The effect on the normal force derivative distribution is quite drastic particularly on the forward portion of the vehicle. The command module loading is increased and large negative loads are generated forward on the service module by adding the escape system. Due to its spike effect the escape system eliminates the Type I separation and reduces the separation-induced loadings aft on the service module, flare, and forward portion of the second stage.

Large negative loadings forward of the various body flares appear supersonically as a result of the flare-induced Type II separations (Figures 22c and d). As the Mach number is increased the flare-induced loads decrease. The wake-induced command module load remains relatively constant when the Mach number is increased but the forward negative service module load diminishes due to the reduced size of the escape rocket wake. That the deviations between the separated flow characteristics and the loading one would compute using attached flow methods are large is vividly demonstrated.

Flight Configuration

The normal force distribution with the disk added to the flight configuration is compared to the disk off distribution in Figure 23. The disk produces increased command module loading, greater negative loadings on the forward service module and increased flare loading. The aft body loading (aft of the service module flare) can be seen to vary only slightly between disk on and disk off.

The loading on the second stage immediately aft of the service module flare should be sensitive to forebody configuration. It appears, however, that subsonically the greater part of the negative loading forward on the second stage is caused by the normal shocks which occur at reattachment (Figures 23a and b). Therefore, this loading is, for all practical purposes, constant for both configurations and the subsequent aft body loading differences are within the accuracy of the data. Supersonically reattachment occurs on the service module flare and the subsequent aft body loadings can be seen to be practically identical for both configurations (Figures 23c and d).

CONCLUSIONS

The flow field over the Saturn I-Apollo vehicle is dominated by numerous regions of separated flow which have a drastic effect on the static load distribution. The following conclusions can be drawn from the static load analysis:

1. The various open tower configurations produce a wake which causes an increased command module loading and may produce a negative forward service module load depending on the wake size.
2. Due to its thickening effect upon the service module boundary layer, the tower wake also promotes flare induced separation at the service module flare.
3. Removal of the escape rocket causes complete (nose-induced) separation to occur at the command module shoulder at high subsonic Mach numbers.
4. A critical service module length exists for each escape configuration such that for subcritical lengths the service module boundary layer is transitional or not completely attached forward of the flare; whereas for longer than critical service module lengths the boundary layer becomes completely attached forward of the flare. The transitional boundary layer for subcritical cylinder lengths promotes the flare induced separation.

5. The loadings aft of the service module flare are relatively insensitive to changes in the escape system configuration and the service module length.

The major sources of flow separation over the Saturn I-Apollo vehicle are: the tower mounted escape system, the blunt nose cone, and the steep interstage flares. One may expect similar static force irregularities for other vehicle configurations which exhibit similar geometric properties.

REFERENCES

1. AeroSpace Engineering, Vol. 21, pg. 42-51, "Aeroelastic Considerations in a Slender, Blunt-Nose, Multistage Rocket", by P. S. Woods and L. E. Ericsson, LMSC, May 1962.

2. "Final Report on Saturn-I-Apollo Unsteady Aerodynamic Study", by L. E. Ericsson and J. P. Reding, to be published.

3. TM 53-40-122 (LMSC/802367), "Preliminary Data Release for the Transonic Wind Tunnel Tests of the Saturn-Apollo 5% Model", by J. P. Reding, November 1962.

4. TM 53-40-123 (LMSC/802393), "Preliminary Data Release for the Supersonic Wind Tunnel Tests of the Saturn-Apollo 5% Model", by J. P. Reding, December 1962.

5. Preliminary unpublished Static Pressure Distribution Data on a 5.5% Saturn-Apollo Model (PSTL-1), obtained from the Experimental Aerodynamics Branch, Aeroballistics Division, George C. Marshall Space Flight Center.

6. MSFC Memo NR: M-AERO-E-110-62, "Results of a Wind Tunnel Investigation to Determine Pressure and Load Distribution Over the Saturn C-1, Block II Vehicle", by John O. Windman and Ann C. Seiber, September 21, 1962.

7. Preliminary unpublished Static Force Data on a 1.75% Saturn-Apollo Model (P-25), obtained from the Experimental Aerodynamic Branch, Aeroballistics Division, George C. Marshall Space Flight Center.

REFERENCES (Continued)

8. Cornell Aeronautical Laboratory Report No. HM-1510-V-8, "Transonic Wind Tunnel Tests of a .0175 Scale Pressure Model of the Saturn C-1, Block II Launch Vehicle", by D. L. Millikan, July 1, 1963.

9. TM 53-40-121 (LMSC/A312114), "Steady Loads on Spiked Blunt Bodies of Revolution", by Lars-Eric Ericsson, 30 November 1962, CONFIDENTIAL.

10. TM 53-40-119 (LMSC/802336), "Separated Flow Effects on the Static Stability of Cone-Cylinder-Flare Bodies", (U), by J. P. Reding, CONFIDENTIAL.

11. NASA TR R-117, "Turbulent Boundary-Layer Separation Induced by Flares on Cylinders at Zero Angle of Attack", by Donald M. Kuehn, 1961.

12. NAA ATS/60-159, "Stability and Control Manual", by D. C. Olsen, 1960.

13. NACA Report 1328, "A Second-Order Shock-Expansion Method Applicable to Bodies of Revolution Near Zero Lift", by Clarence A. Syverson and David H. Dennis, 1957.

14. TM 57-11-54, (LMSC/656461), "Second-Order Shock Program", by R. L. Bowlby, M. A. Chisholm, and N. L. Davis, 4 April 1962.

15. ARGMA TN 106N, "Comparison of Second-Order Shock-Expansion Theory with Data for Cone-Cylinder-Frustum Bodies of Revolution at Supersonic Mach Numbers", (U), by Joseph C. Craft, 31 December 1959, CONFIDENTIAL.

REFERENCES (Continued)

16. NACA RM L54A23, "Zero-Lift Drag of Several Conical and Blunt Nose Shapes obtained in Free Flight at Mach Numbers of 0.7 to 1.3", by Robert O. Piland and Leonard W. Putland, March 23, 1954.

17. NASA TM X-574, "Effects of Spike-Mounted Flow Deflectors on the Transonic Aerodynamic Characteristics of a Blunt-Nosed Body of Revolution having a Cylindrical or Flared Afterbody", (U), by Stuart L. Treon, Roy M. Wakefield, and Earl D. Knechtel, October 1961, CONFIDENTIAL

18. NASA Memo 5-17-59A, "The Effect of Nose Shapes on the Static Aerodynamic Characteristics of Ballistic-Type Missile Models at Mach Numbers from 0.6 to 1.4", (U), by Stuart L. Treon, May 1959, CONFIDENTIAL.

19. NACA RM L6K08A, "Results of Tests to Determine the Effect of a Conical Windshield on the Drag of a Bluff Body at Supersonic Speeds", by Sidney R. Alexander, January 14, 1947.

20. TM 53-14-100 (LMSD 800415), "Relation Between Static and Dynamic Characteristics for a Slowly Oscillating Blunt Re-Entry Body with Non-Linear Amplitude Effects. Part I, Pitch Oscillations around a Fixed Axis", by L. E. Ericsson, April 1961, CONFIDENTIAL.

21. George C. Marshall Space Flight Center, MPT-AERO-61-38, "Aerodynamic Characteristics of Spherically Blunted Cones at Mach Numbers from 0.5 to 5.0", May 2, 1962

SATURN I - APOLLO
BASIC CONFIGURATION SKETCH

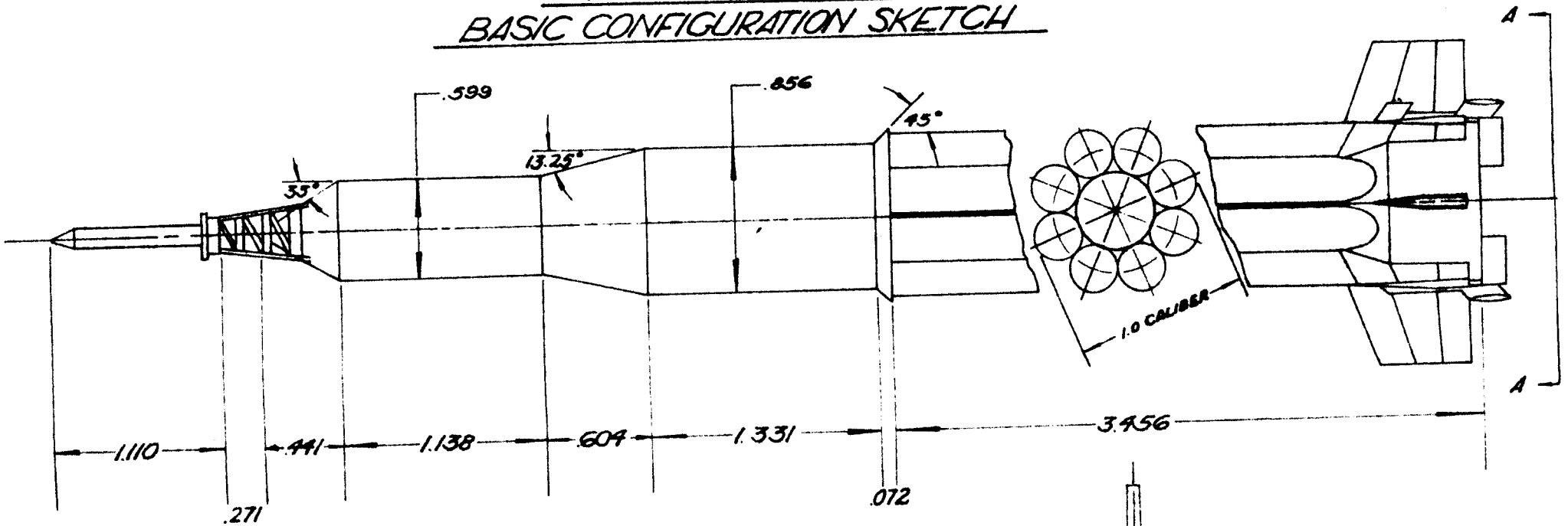

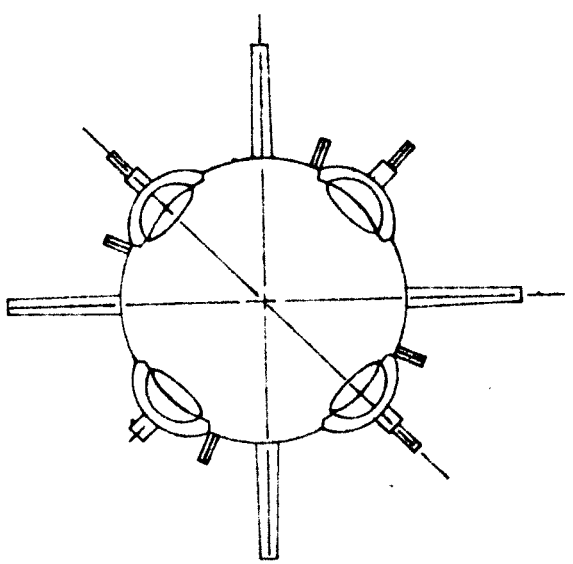

VIEW A-A

NOTE: ALL LINEAR DIMENSIONS IN CALIBERS.
1 CALIBER = 257.0 INCHES

FIGURE 1
PAGE 33

SATURN I-APOLLO
FOREBODY CONFIGURATIONS TESTED

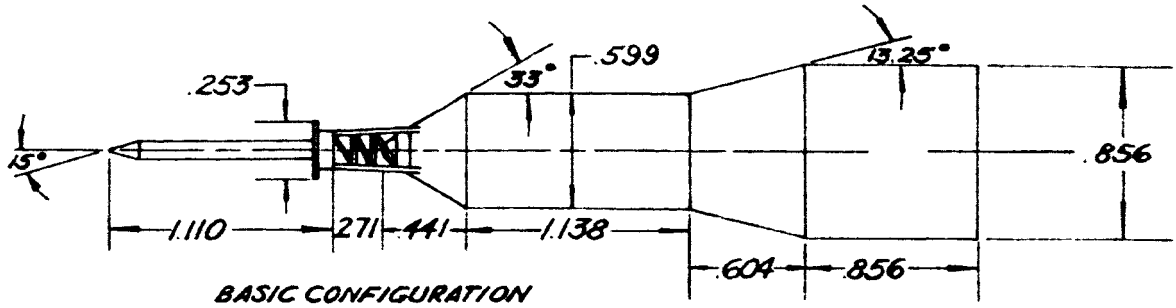

BASIC CONFIGURATION

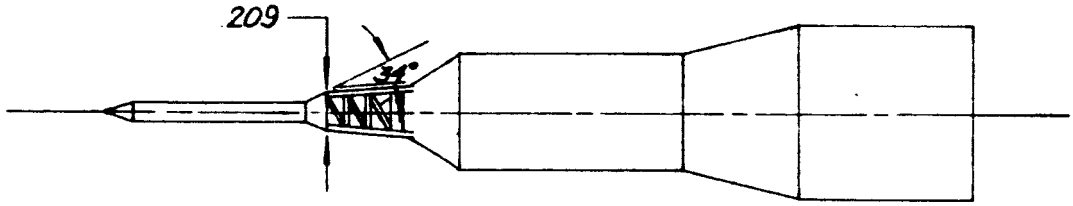

ESCAPE ROCKET DISK REMOVED

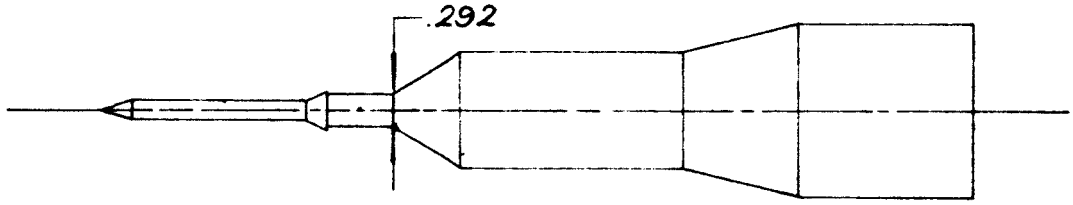

MONOCQUE TOWER

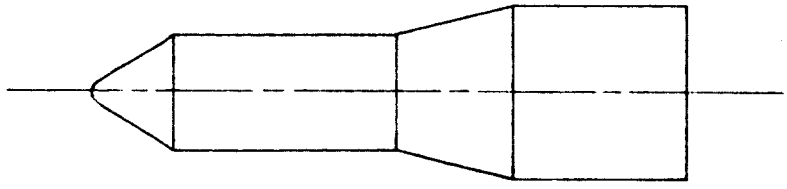

ESCAPE ROCKET AND TOWER REMOVED

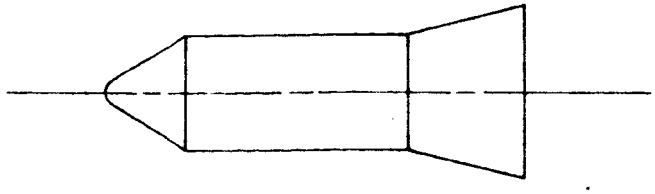

ESCAPE ROCKET, TOWER, AND SLEEVE REMOVED

NOTE: ALL LINEAR DIMENSIONS IN CALIBERS.

SATURN I - APOLLO
FLIGHT CONFIGURATION SKETCH

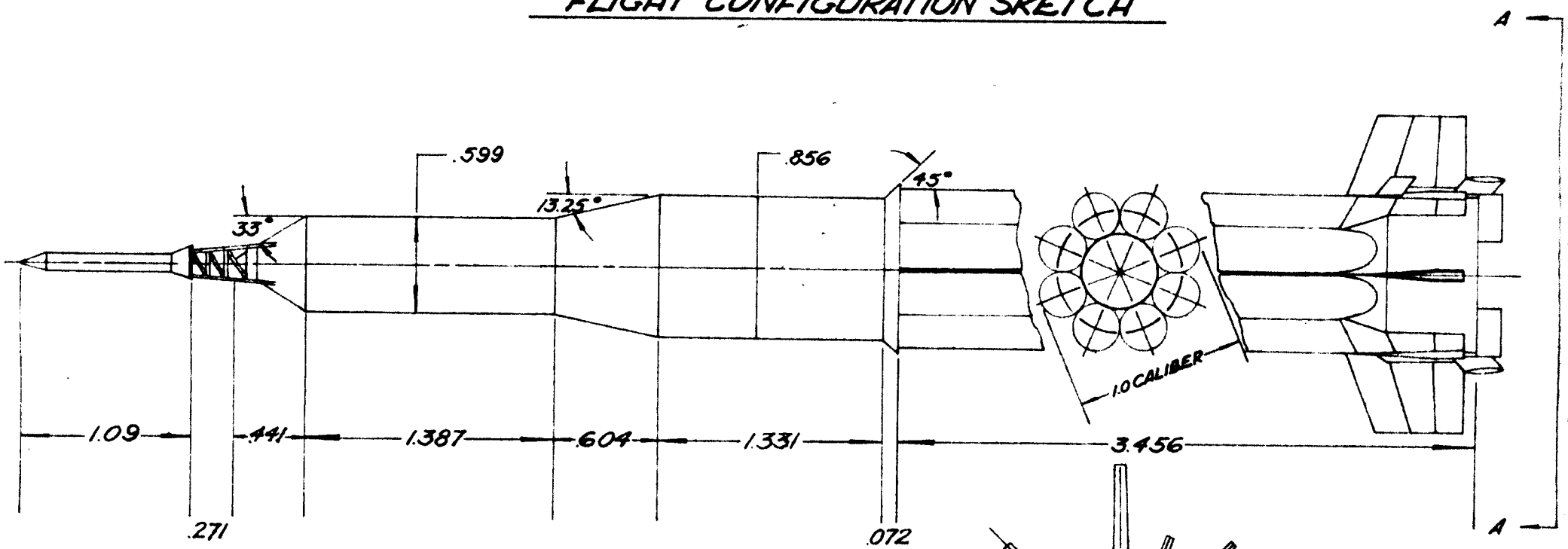

NOTE: ALL LINEAR DIMENSIONS IN CALIBERS.
1 CALIBER = 257.0 INCHES

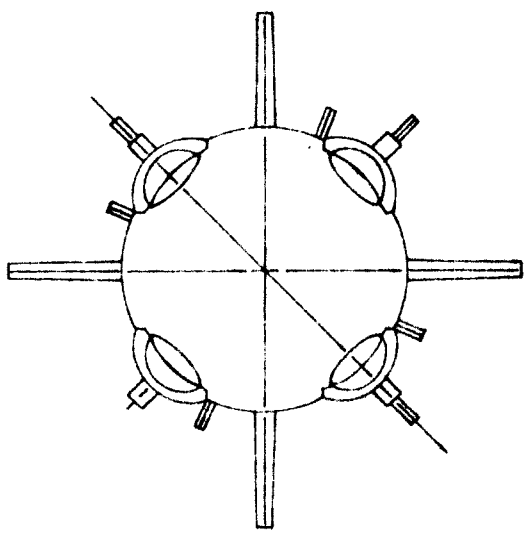

VIEW A—A

FIGURE 3
PAGE 35

SATURNI-APOLLO FLOW FIELD

MACH = 1.35
NOTE: FINS REMOVED FOR CLARITY

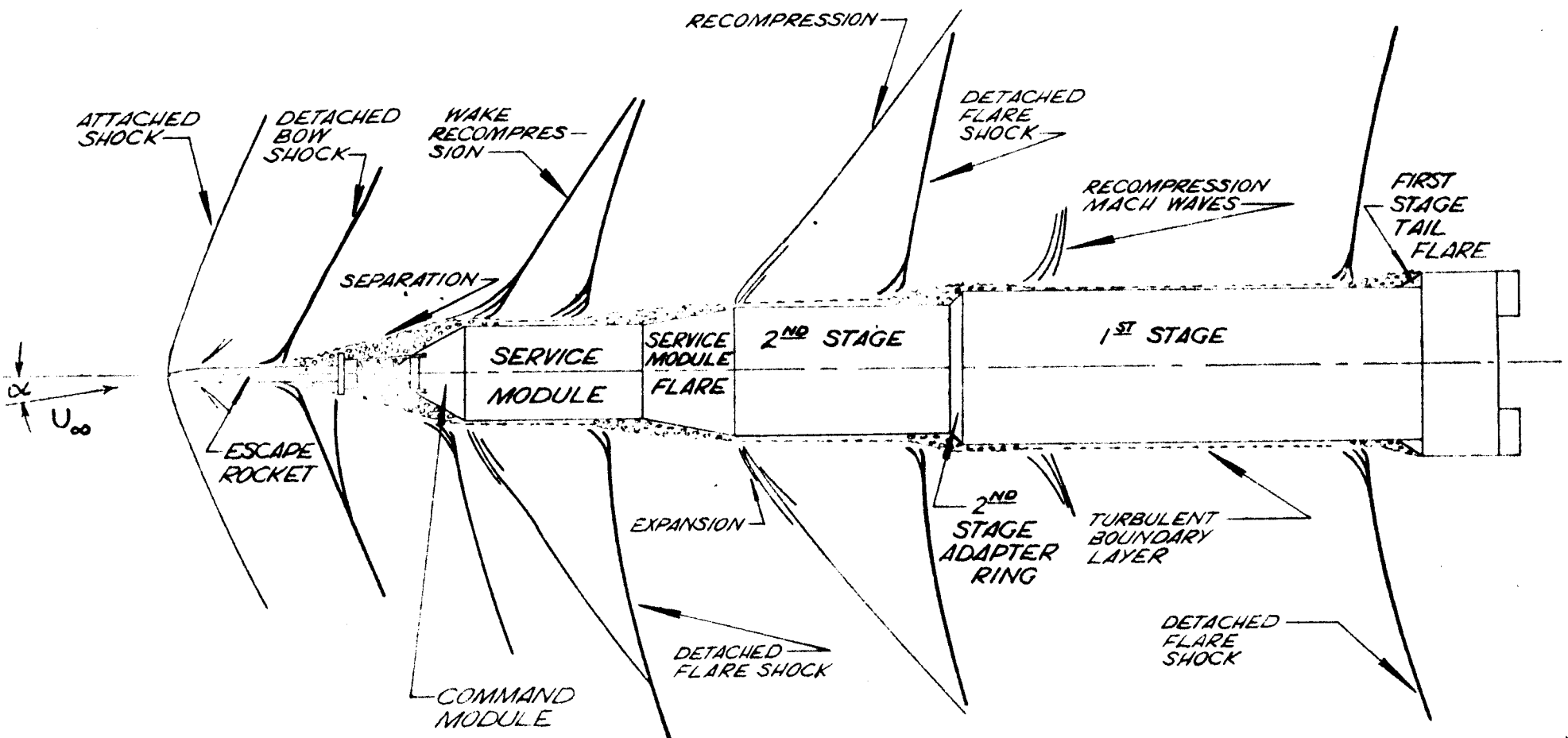

FIGURE 4
PAGE 36

SPIKE EFFECTS ON THE AERODYNAMIC CHARACTERISTICS OF A LOW FINENESS RATIO CONICAL WINDSHIELD

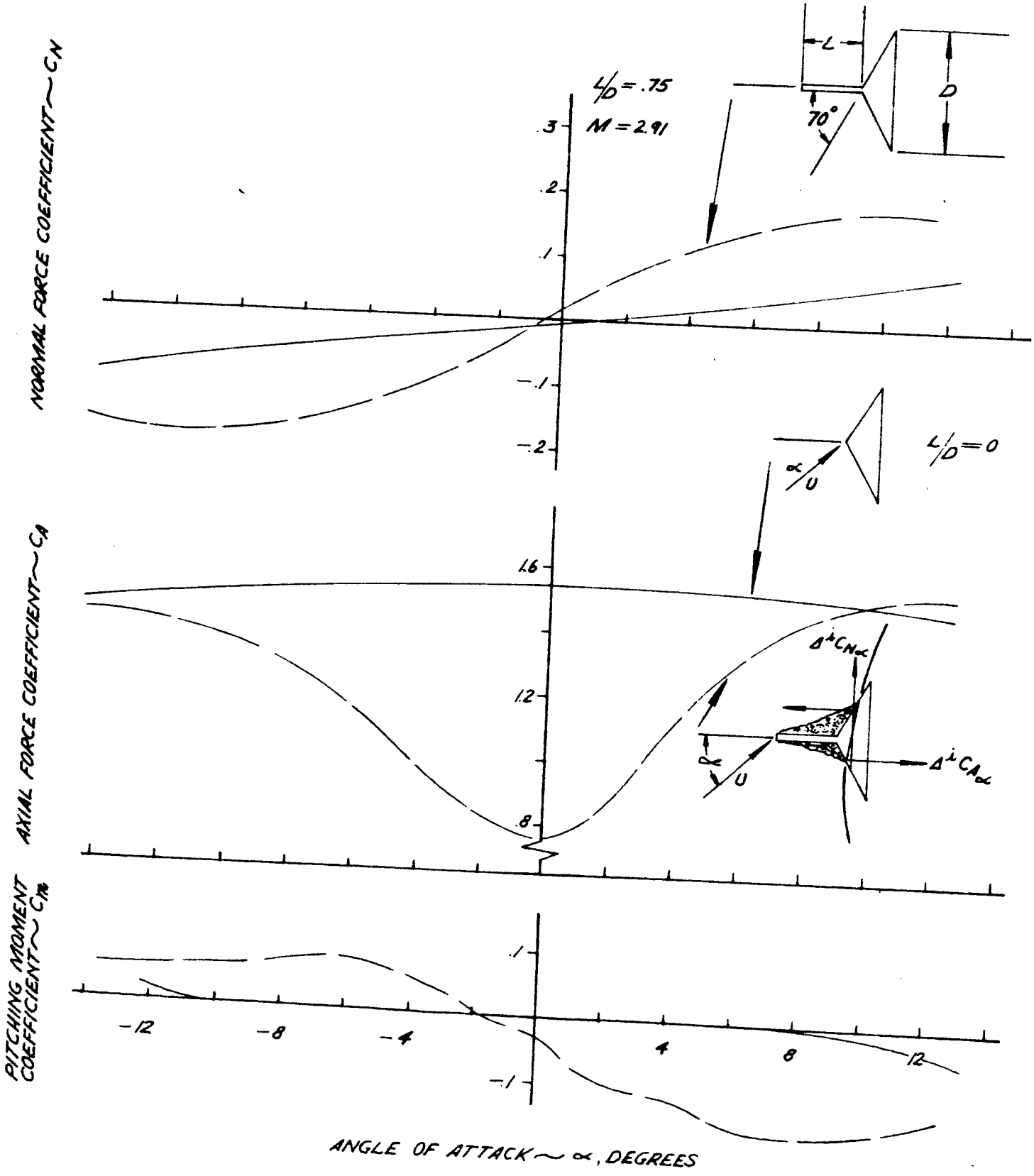

EFFECT OF ESCAPE ROCKET ON COMMAND MODULE NORMAL AND AXIAL FORCE CHARACTERISTICS

$M_\infty = 1.0$

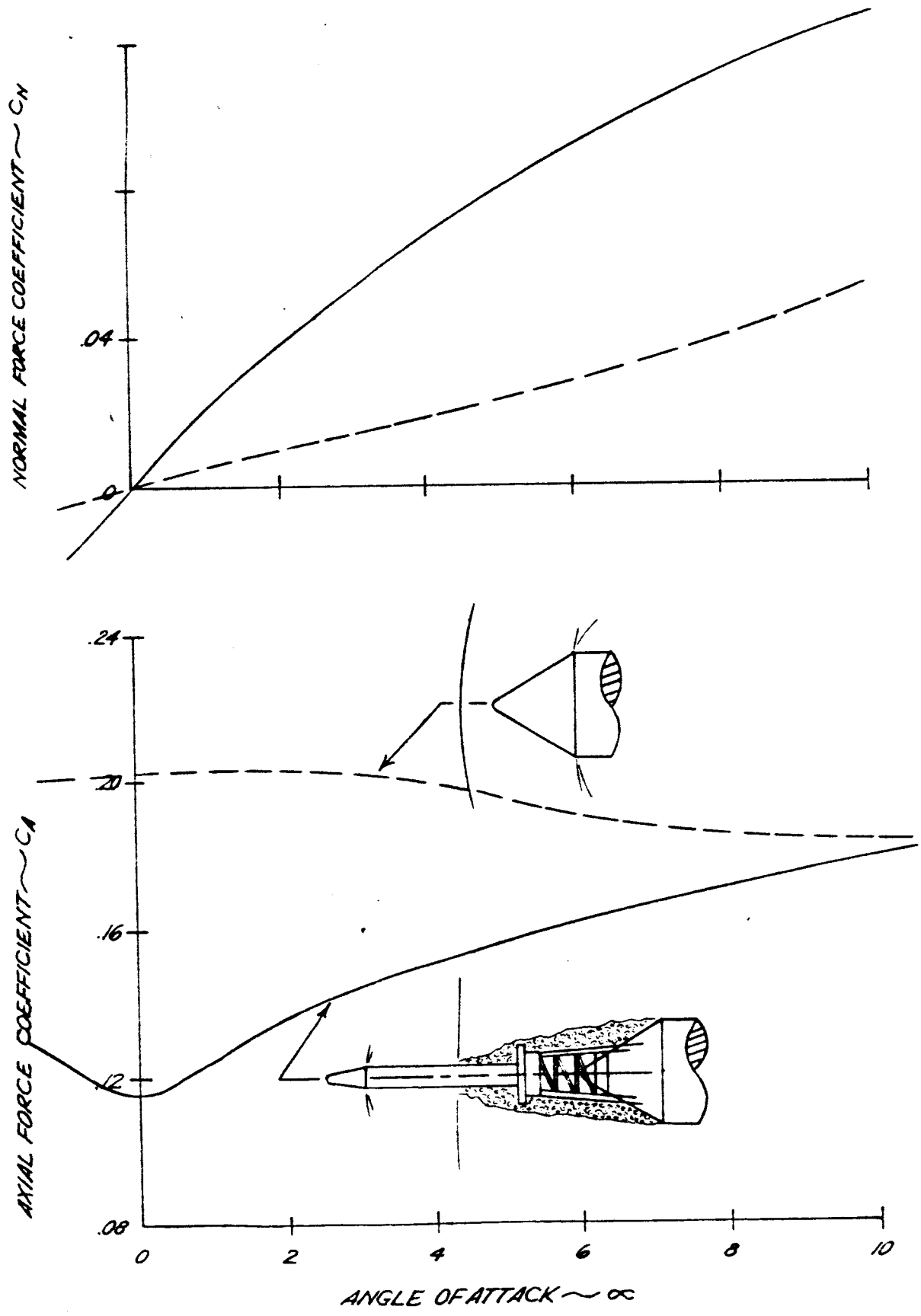

TYPES OF FLOW CONE-CYLINDER-FLARE SEPARATION

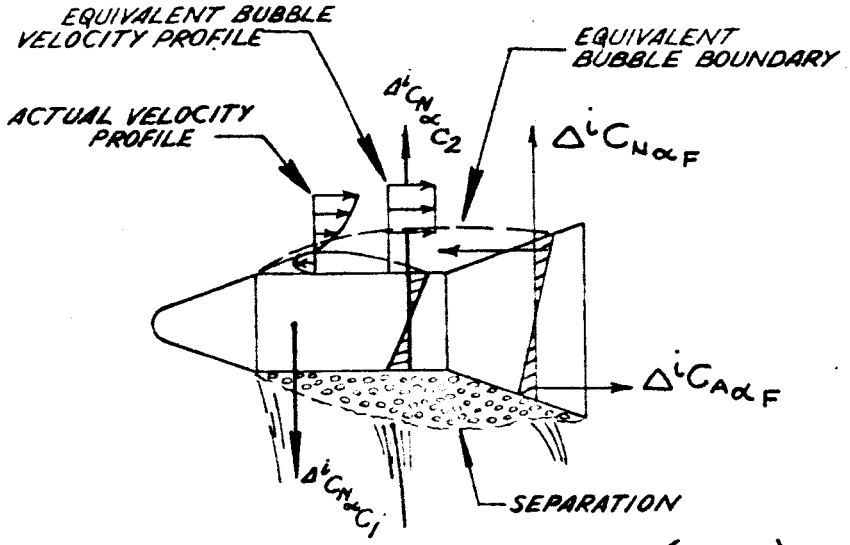

TYPE I - NOSE INDUCED SEPARATION ($M < 1.0$)

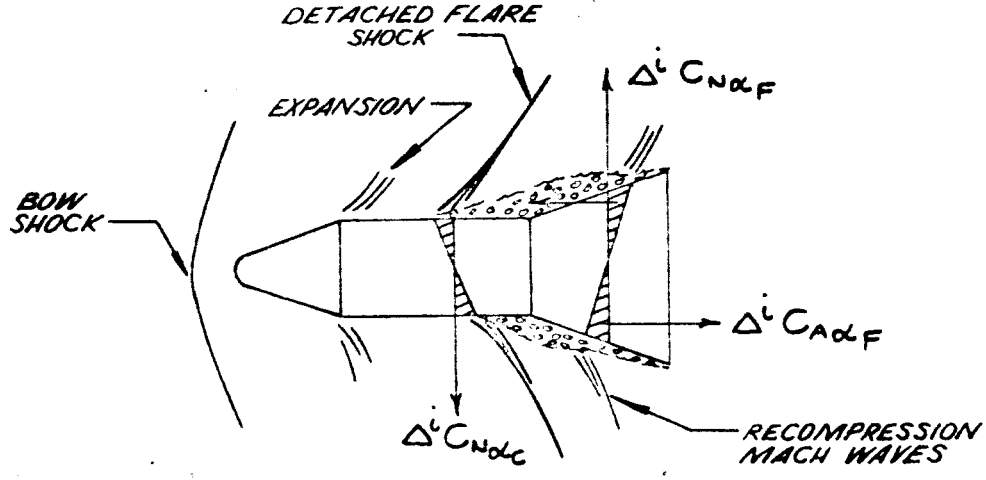

TYPE II - SUPERSONIC FLARE INDUCED SEPARATION ($M > 1.0$)

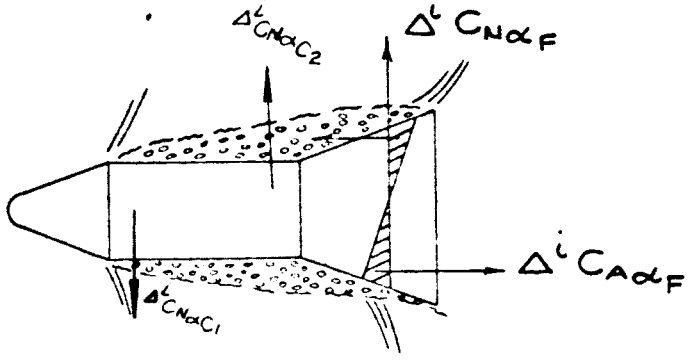

TYPE III - TRANSONIC FLARE INDUCED SEPARATION ($M \approx 1.0$)

SEPARATED FLOW FLARE CHARACTERISTICS

TYPE I AND III SEPARATION
TRANSONIC MACH NUMBERS

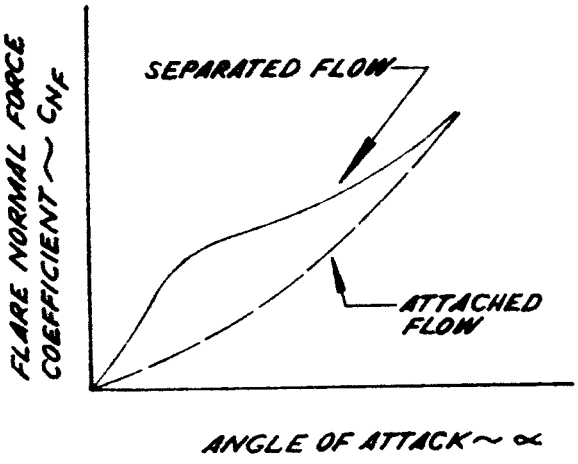

TYPE II SEPARATION
SUPERSONIC MACH NUMBERS

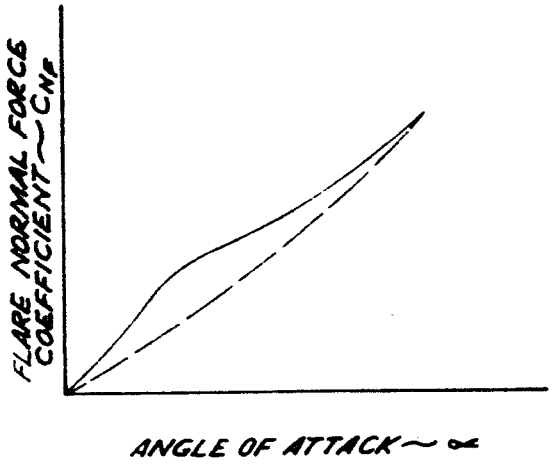

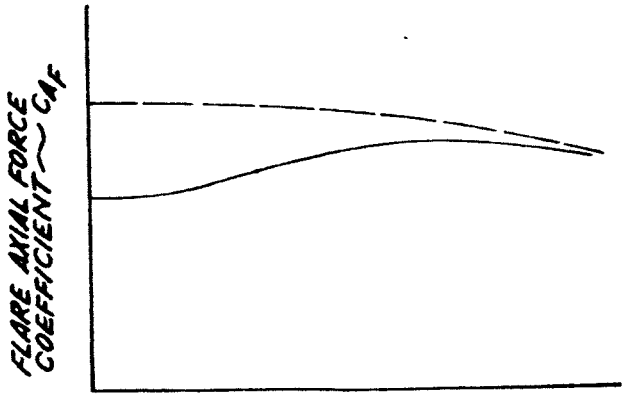

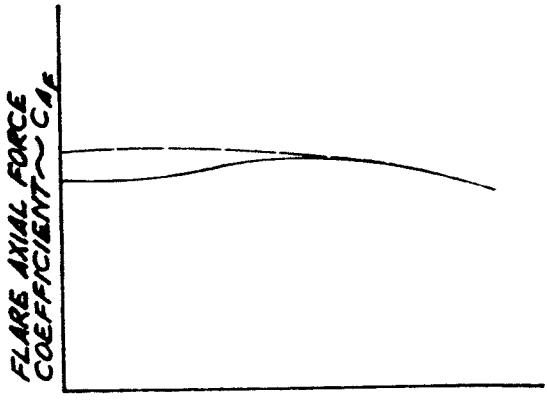

EFFECT OF ESCAPE ROCKET ON SERVICE MODULE FLARE NORMAL FORCE CHARACTERISTICS

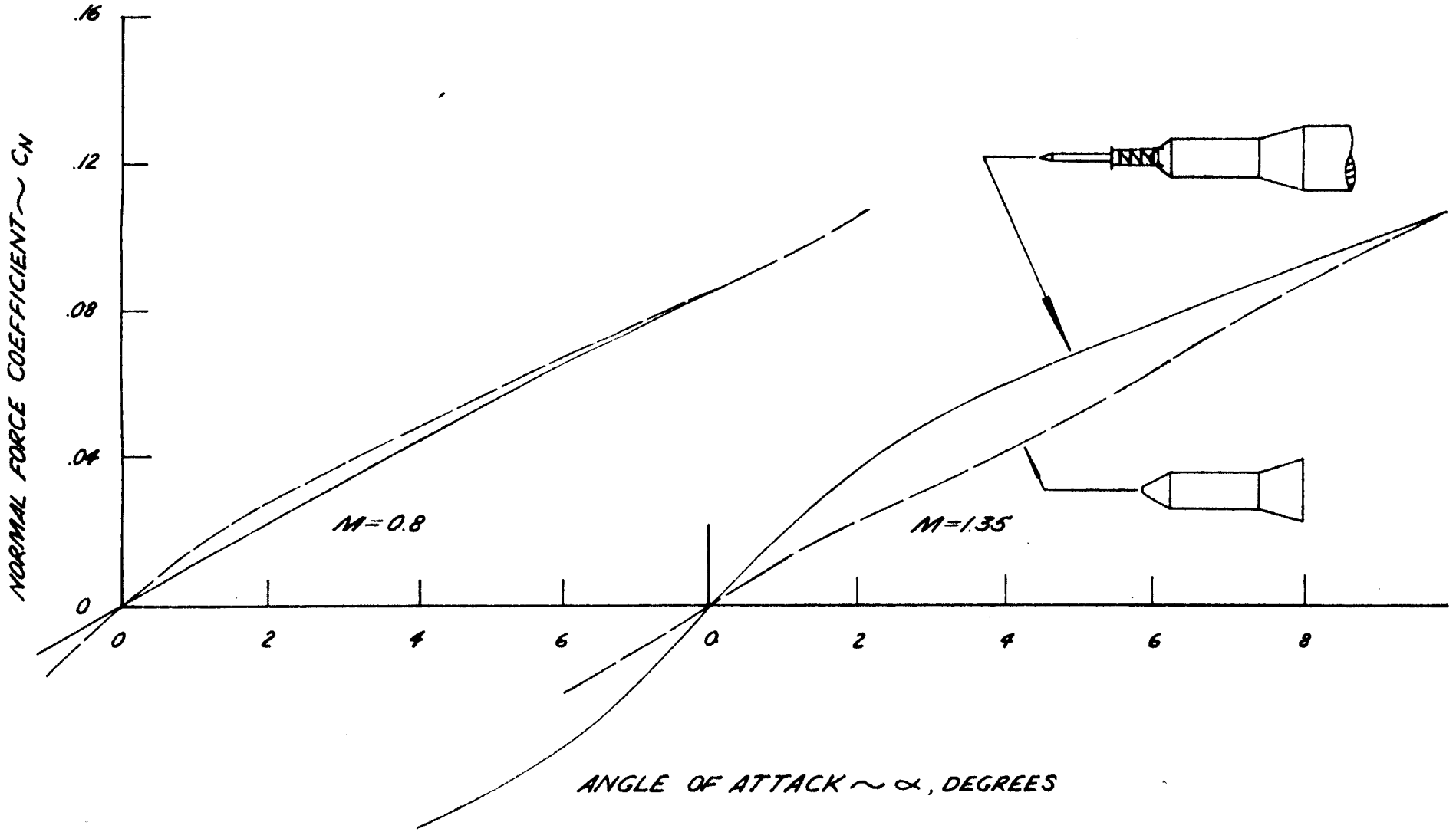

FIGURE 9
PAGE 41

EFFECT OF ESCAPE ROCKET ON FLARE AXIAL FORCE CHARACTERISTICS

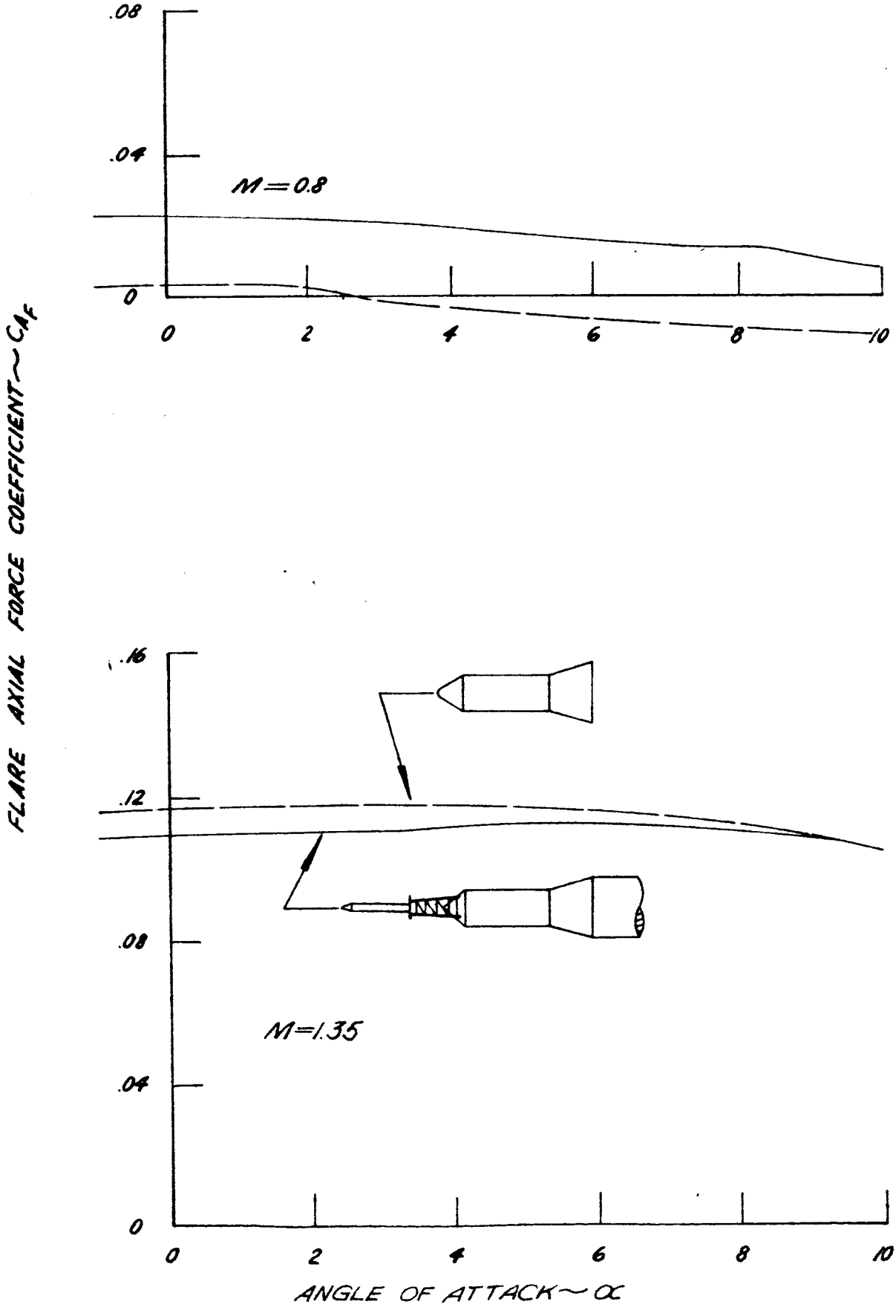

EFFECT OF ESCAPE ROCKET ON SERVICE MODULE FLARE $\alpha=0$ AERODYNAMIC CHARACTERISTICS

SERVICE MODULE FLARE NORMAL FORCE DERIVATIVE $\sim C_{N_\alpha}$, PER DEGREE

.03
.02
.01
0

.8 1.0 1.2 1.4 1.6 1.8 2.0 2.2 2.4

MACH NUMBER $\sim M$

SERVICE MODULE FLARE $\alpha=0$ CENTER OF PRESSURE $\sim X_{c.p.}{}_{\alpha=0}$ (CALIBERS FROM FLARE BASE)

1.0
0.5
0

.8 1.0 1.2 1.4 1.6 1.8 2.0 2.2 2.4

MACH NUMBER $\sim M$

- ⊙ BASIC CONFIGURATION ~ REFERENCES 3 AND 4
- △ ESCAPE ROCKET, TOWER, AND SECOND STAGE REMOVED ~ REFERENCES 3 AND 4
- ——— COMPUTED FROM REFERENCE 12
- —·— SECOND ORDER SHOCK ~ REFERENCE 14
- △ EXTRAPOLATED FROM M=1.0 DATA ~ REFERENCE 3

SERVICE MODULE FLARE $\alpha=0$ AXIAL FORCE COEFFICIENT $\sim C_{A_{\alpha=0}}$

2
1
0

.8 1.0 1.2 1.4 1.6 1.8 2.0 2.2 2.4

MACH NUMBER $\sim M$

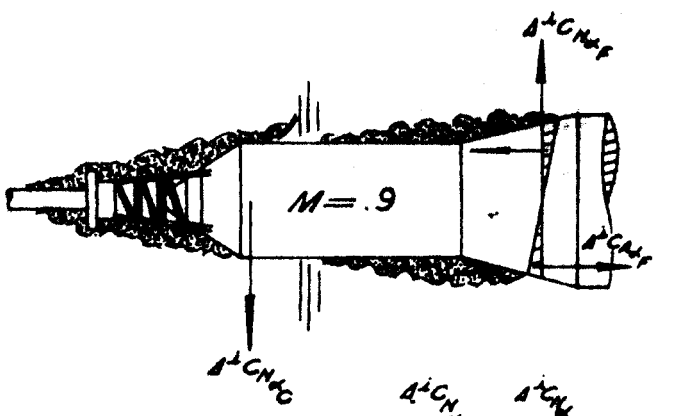

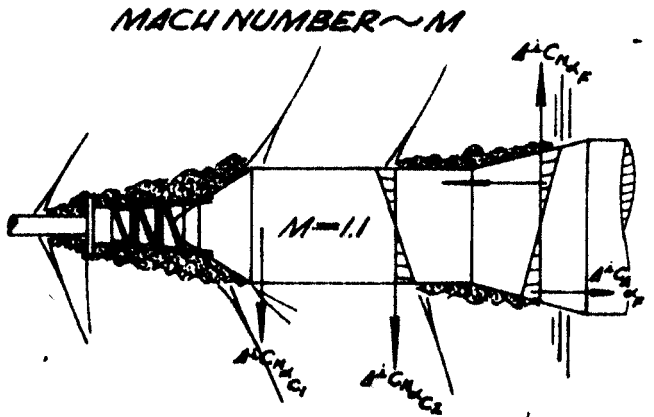

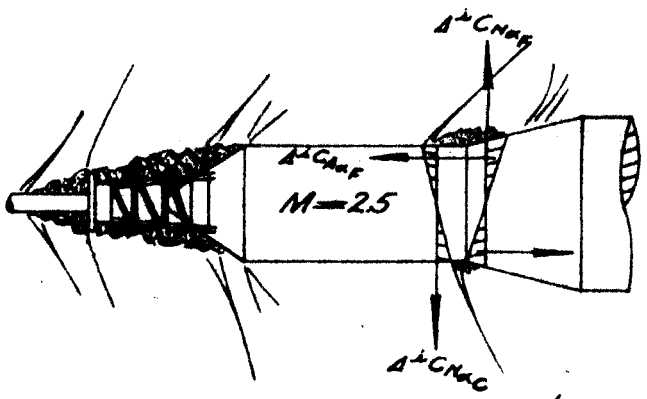

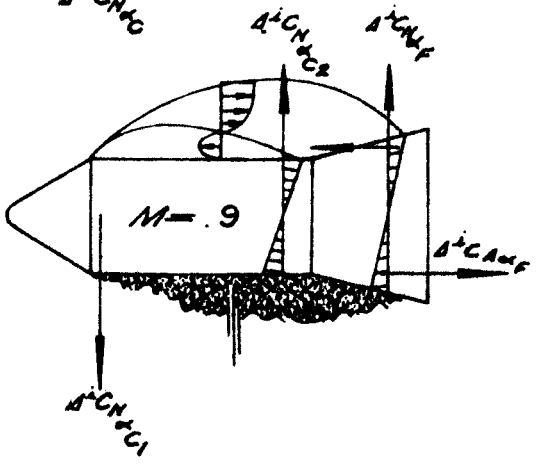

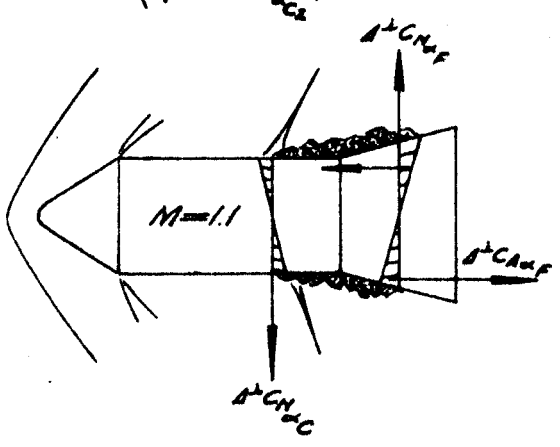

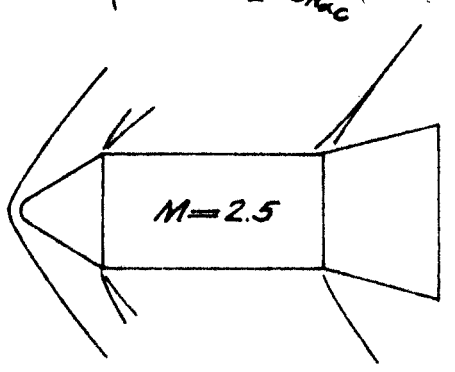

FIGURE 11
PAGE 43

EFFECT OF ESCAPE ROCKET AND TOWER ON THE COMMAND AND SERVICE MODULE PRESSURE DISTRIBUTION AT M=0.9

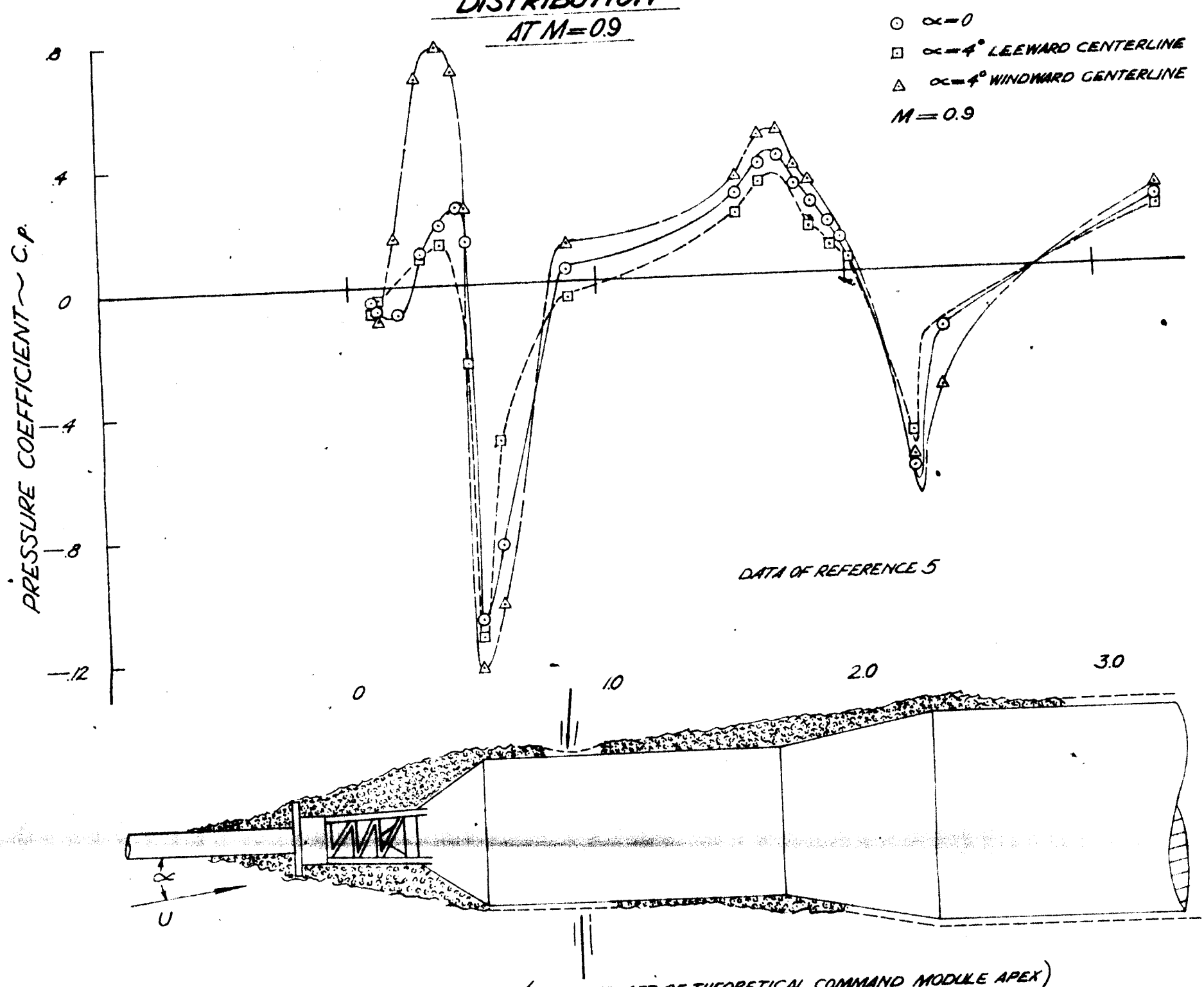

EFFECT OF ESCAPE ROCKET AND TOWER ON THE COMMAND AND SERVICE MODULE MODEL PRESSURE DISTRIBUTION AT $M \approx 1.5$

○ $\alpha = 0$
□ $\alpha = 4°$ LEEWARD CENTERLINE
△ $\alpha = 4°$ WINDWARD CENTERLINE

DATA OF REFERENCE 5
MACH = 1.5

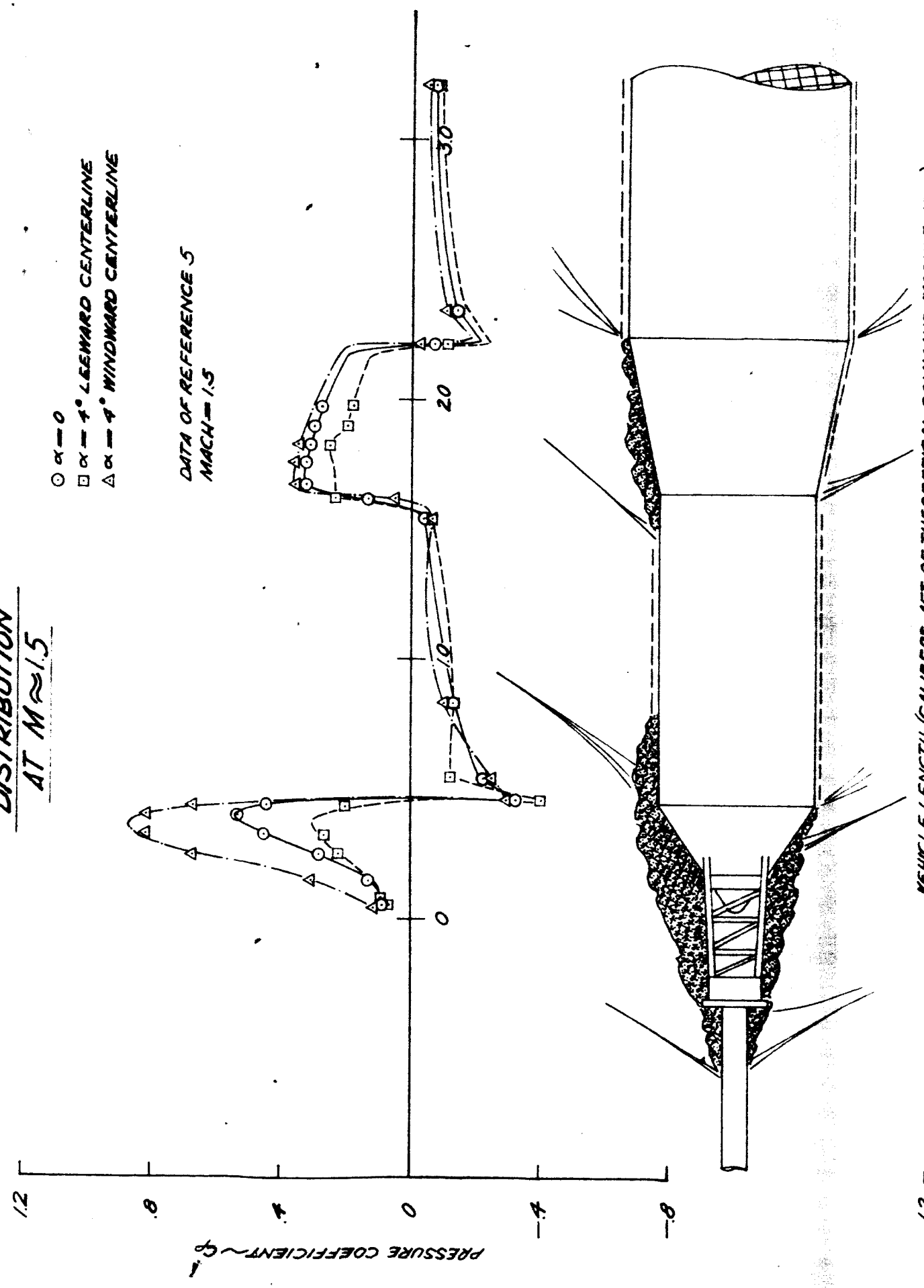

DATA OF REFERENCE 6
MACH = 1.45

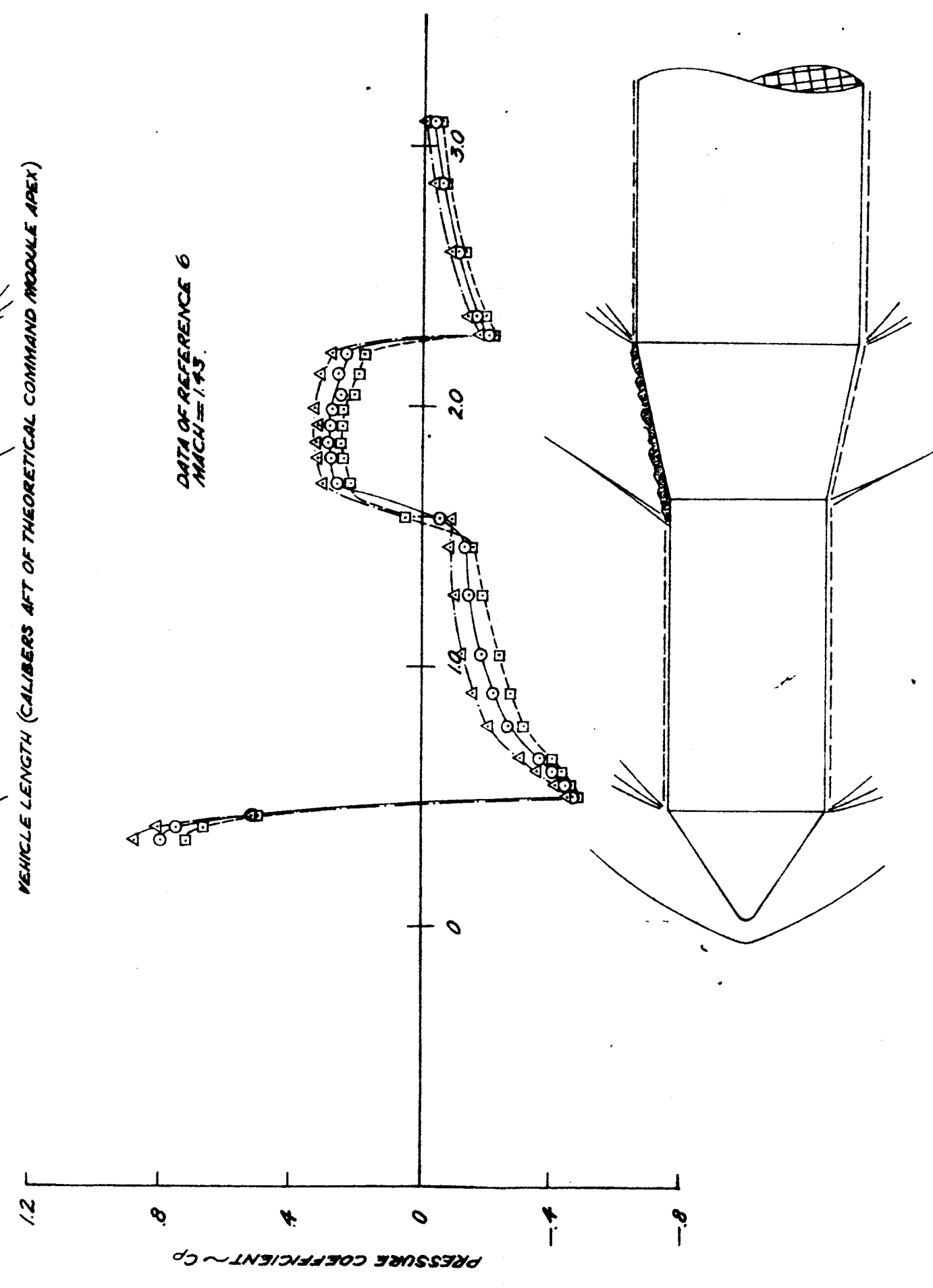

EFFECT OF ESCAPE ROCKET ON SERVICE MODULE NORMAL FORCE CHARACTERISTICS

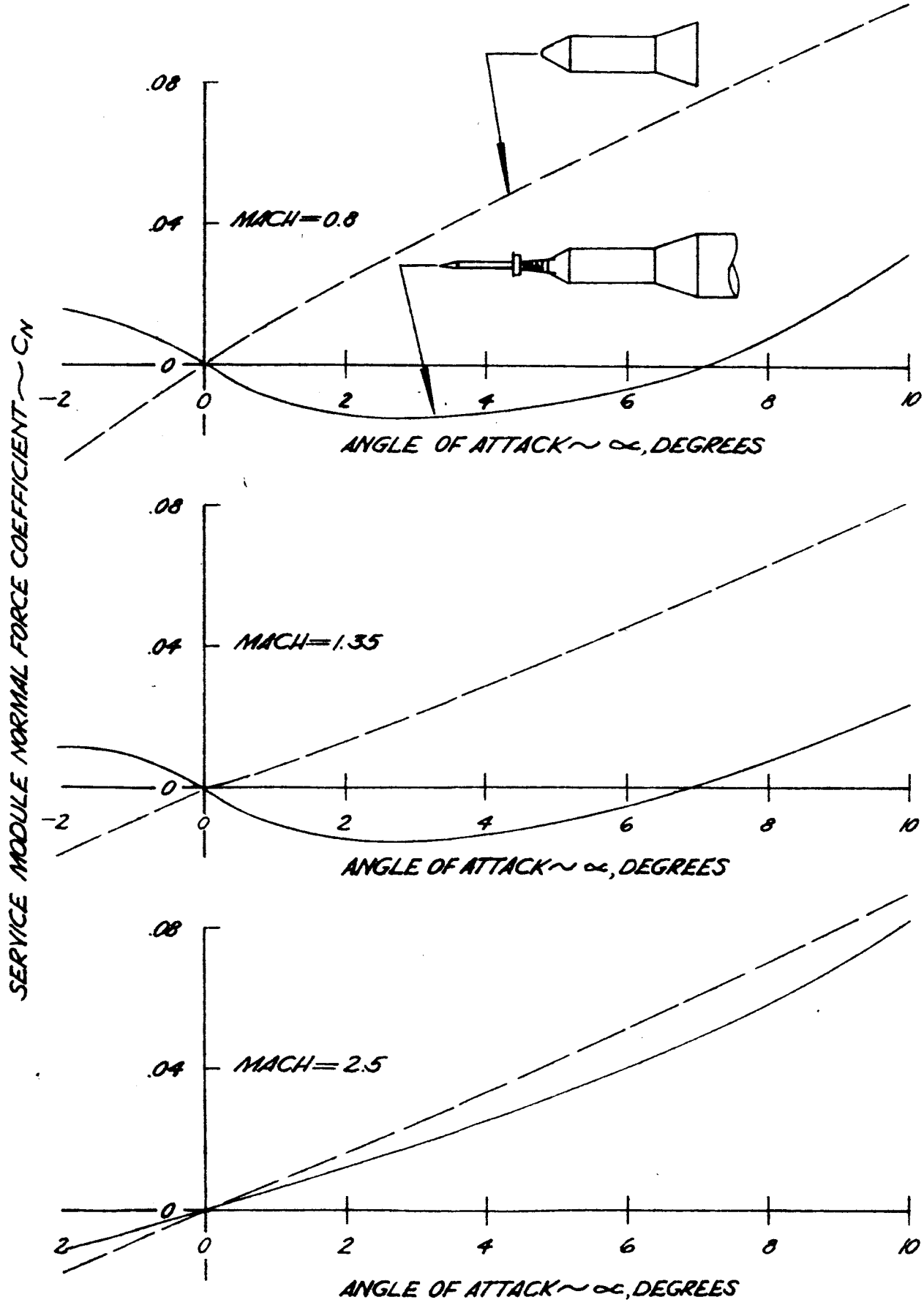

COMPARISON OF SERVICE MODULE $\alpha=0$ AERODYNAMIC CHARACTERISTICS

SERVICE MODULE NORMAL FORCE DERIVATIVE ~ C_{N_α}, PER DEGREE

.02
.01
0
-.01
-.02

.8 1.0 1.2 1.4 1.6 1.8 2.0 2.2 2.4 2.6

- ⊙ BASIC CONFIGURATION – REFERENCES 3 AND 4
- ⊡ ESCAPE ROCKET DISK REMOVED – REFERENCES 3 AND 4
- △ ESCAPE ROCKET, TOWER, AND 2ND STAGE REMOVED – REFERENCES 3 AND 4
- ⚐△ EXTRAPOLATED FROM M=1.0 DATA – REFERENCE 3
- —·— 2ND ORDER SHOCK – REFERENCE 14
- — — — COMPUTED FROM REFERENCE 12
- ⚐ INTEGRATED PRESSURE DATA – REFERENCE 5

SERVICE MODULE $\alpha=0$ CENTER OF PRESSURE ~ $X_{C.P.}$ (CALIBERS FORWARD OF SERVICE MODULE FLARE BASE) $_{\alpha=0}$

3.0
2.0
1.0
0
-1.0

.8 1.0 1.2 1.4 1.6 1.8 2.0 2.2 2.4 2.6

MACH NUMBER ~ M

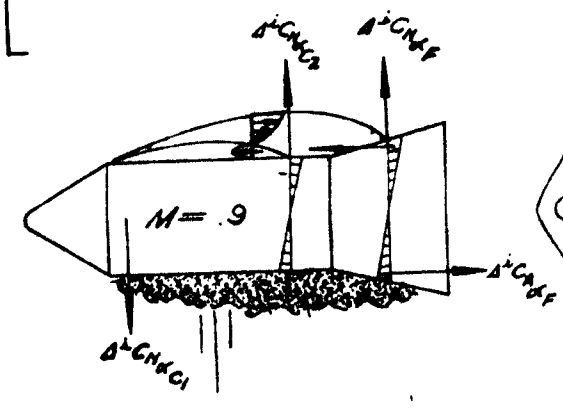

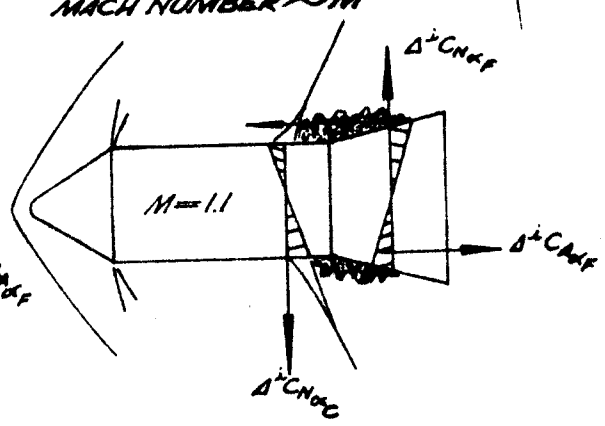

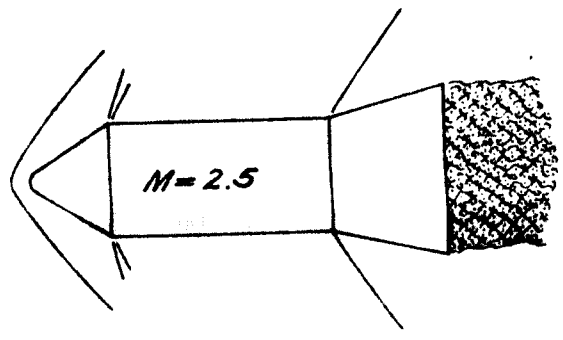

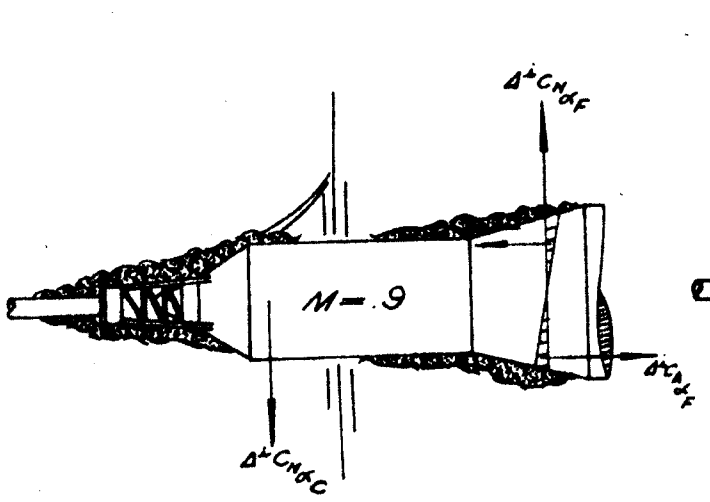

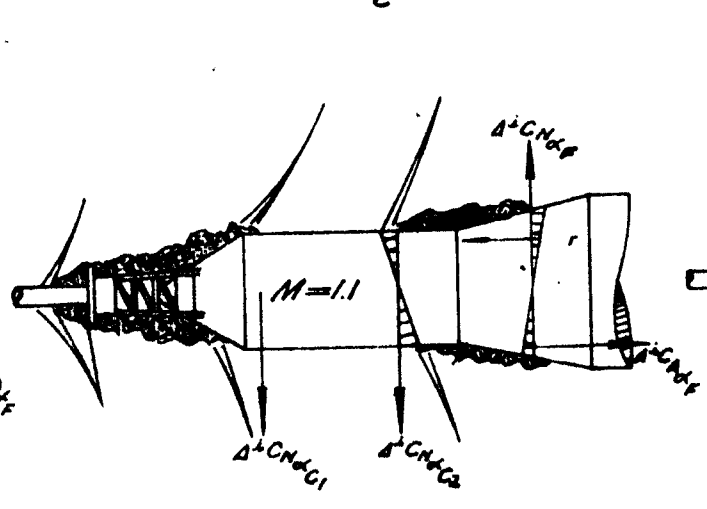

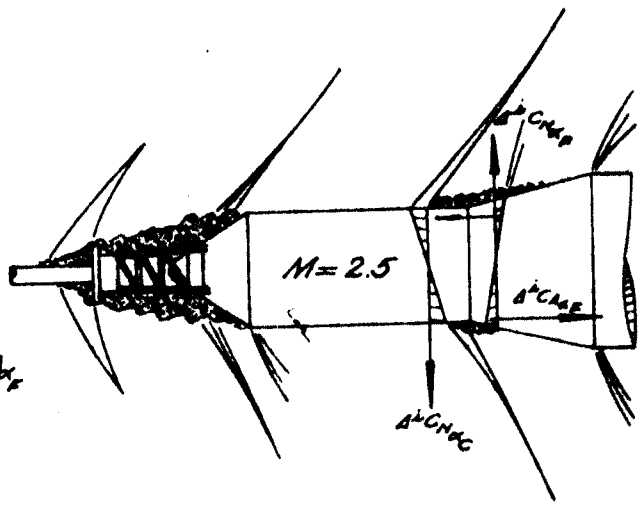

FIGURE 15
PAGE 47

EFFECT OF ESCAPE ROCKET TOWER CONFIGURATION ON COMMAND MODULE $\alpha=0°$ AERODYNAMIC CHARACTERISTICS

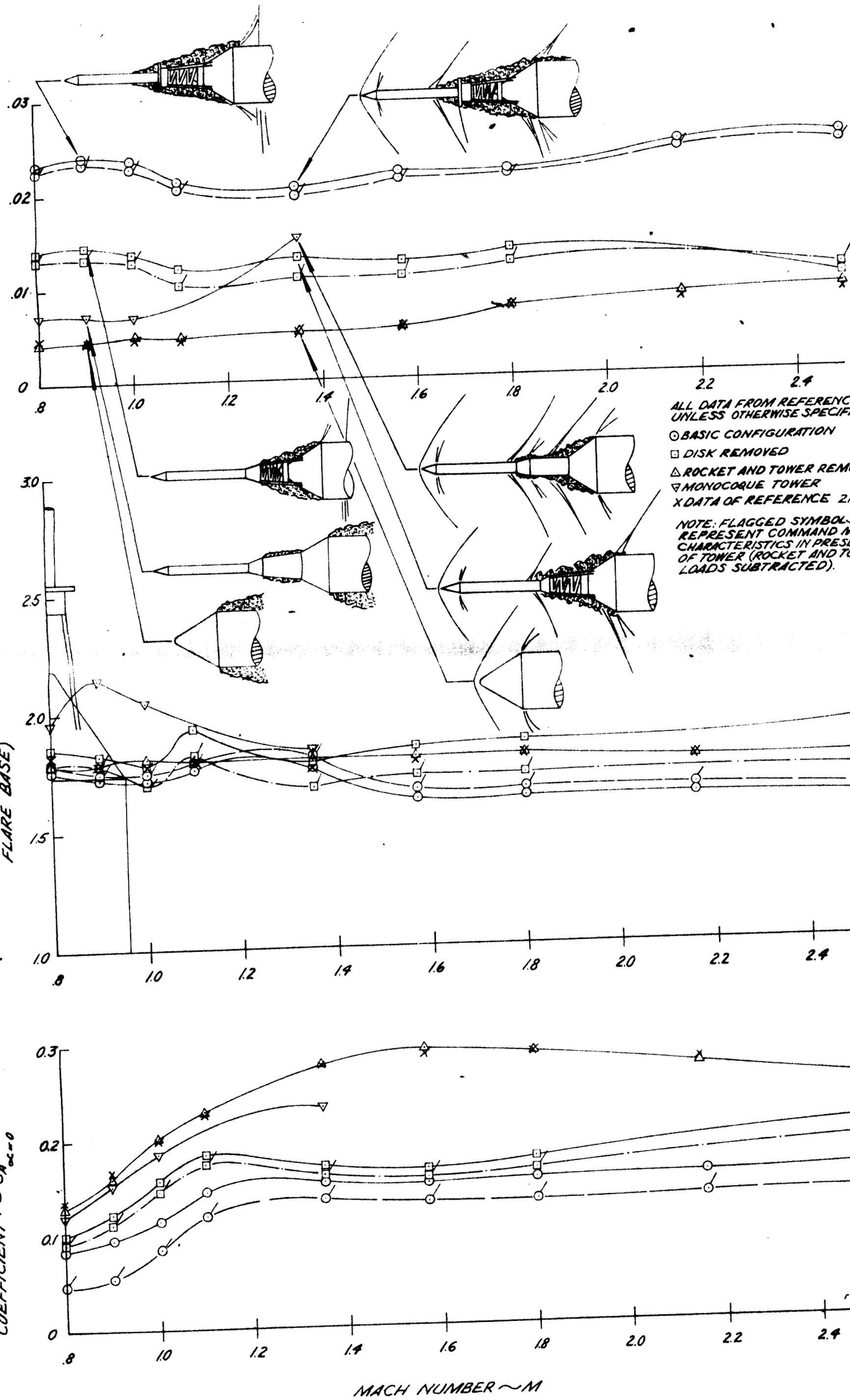

FIGURE 16
PAGE 49

TRANSONIC SPIKED BODY AXIAL FORCE CHARACTERISTICS

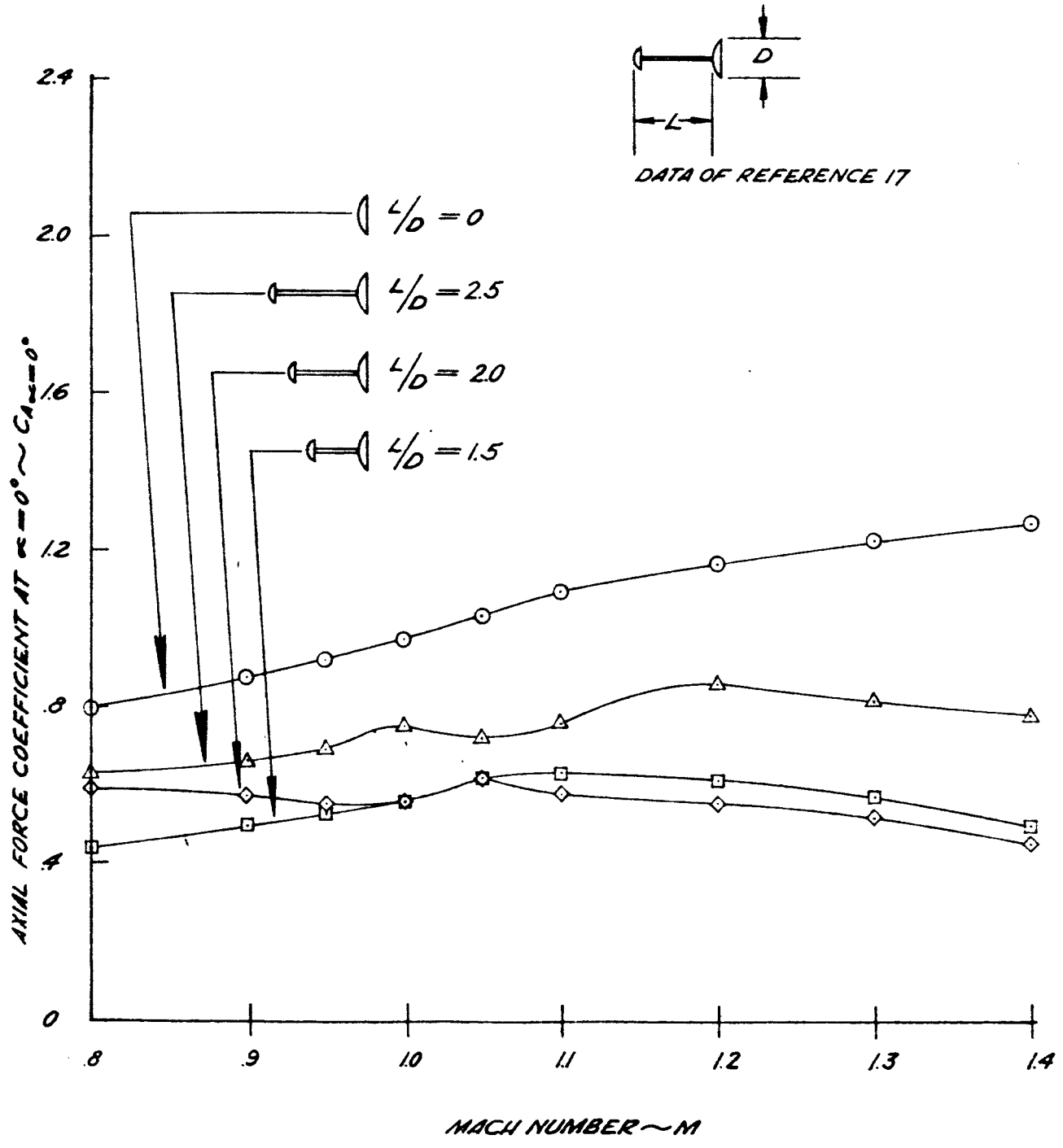

SECRET OF ESCAPE ROCKET AND TOWER CONFIGURATION ON SERVICE MODULE AND SERVICE MODULE FLARE AERODYNAMIC CHARACTERISTICS AT $\alpha = 0°$

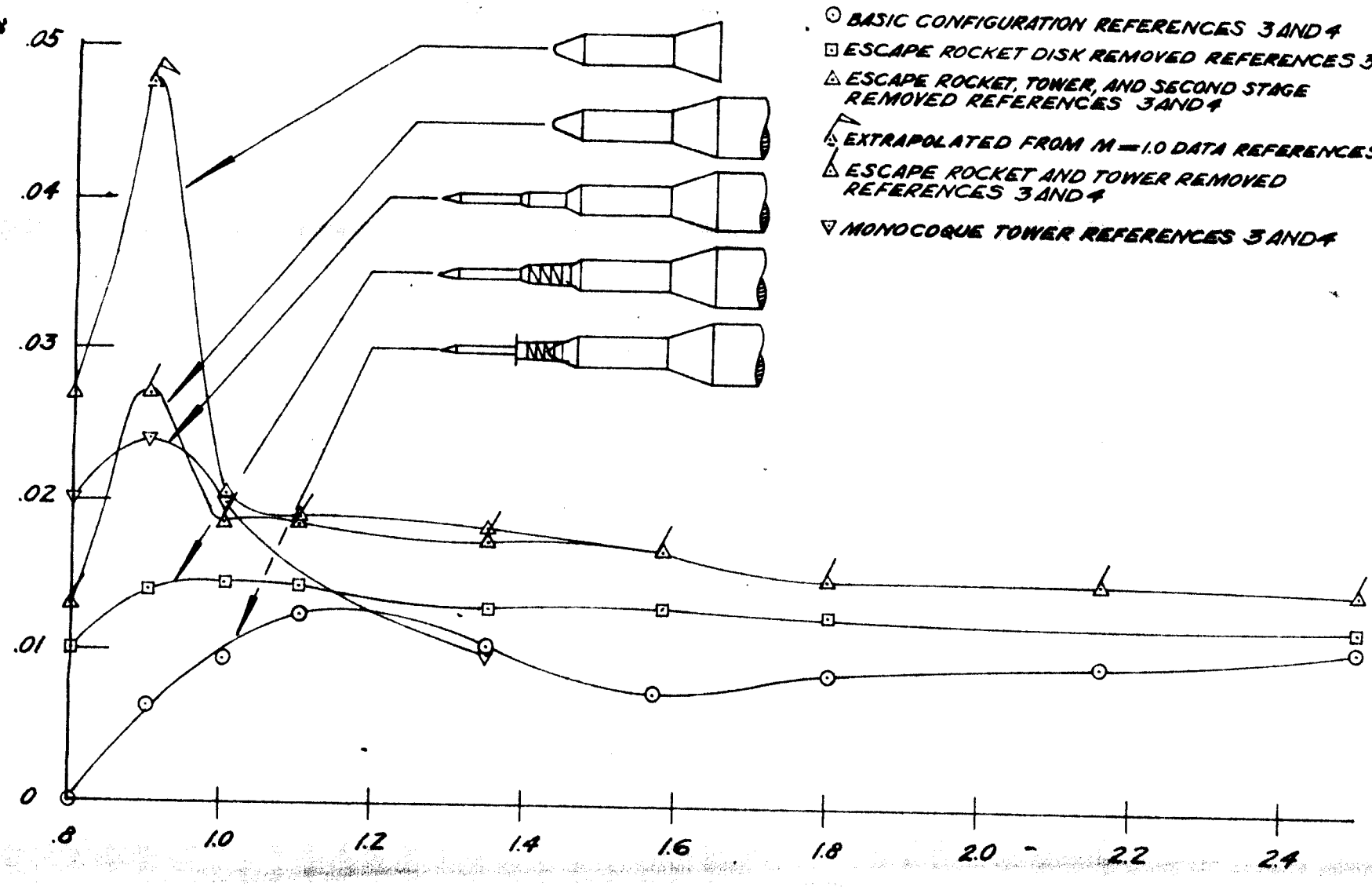

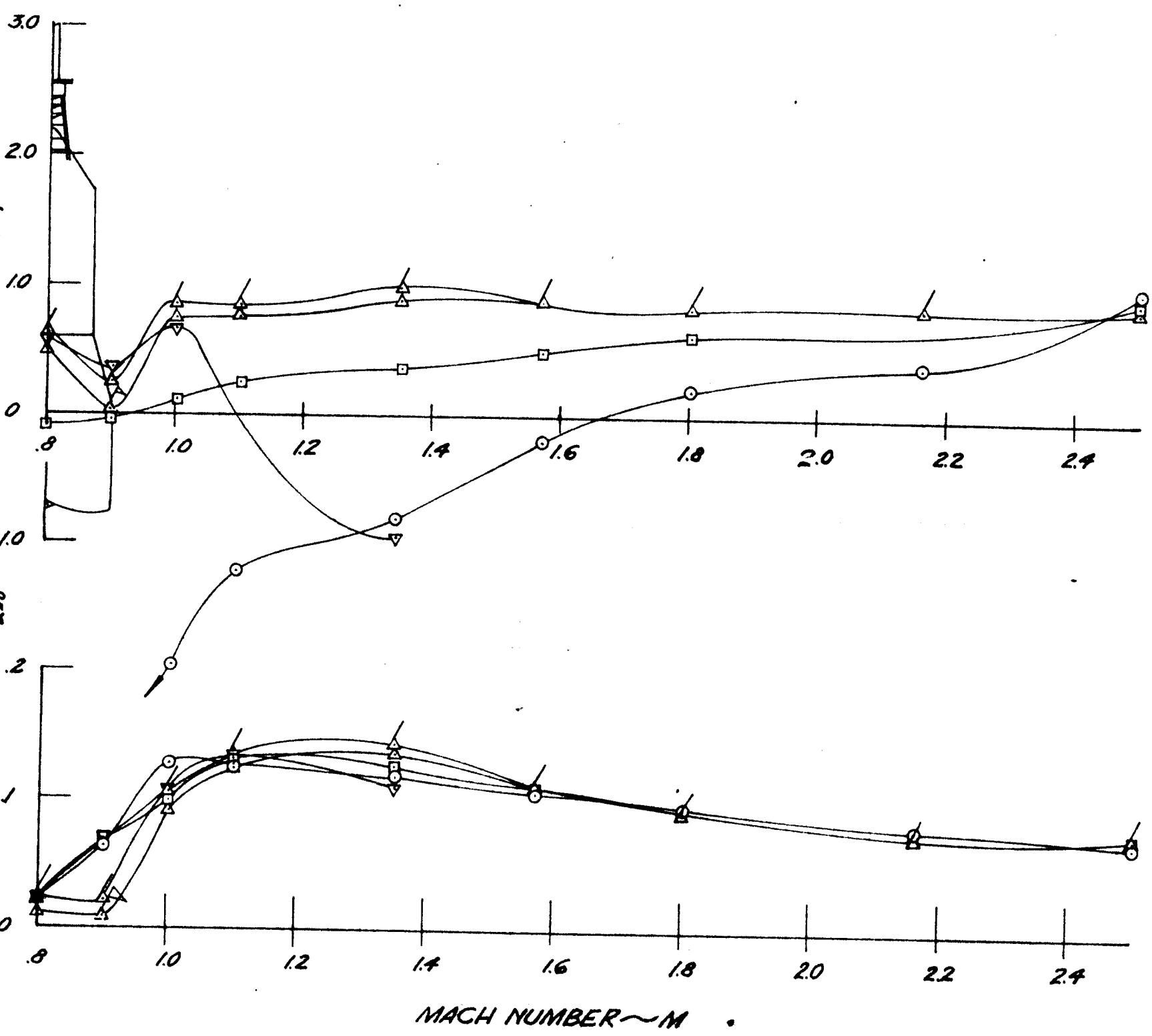

FIGURE 18
PAGE 50

EFFECT OF ESCAPE ROCKET AND ESCAPE ROCKET TOWER CONFIGURATION ON SERVICE MODULE–SERVICE MODULE FLARE NORMAL FORCE CHARACTERISTICS

NOTE: DATA FROM REFERENCES 3 AND 4

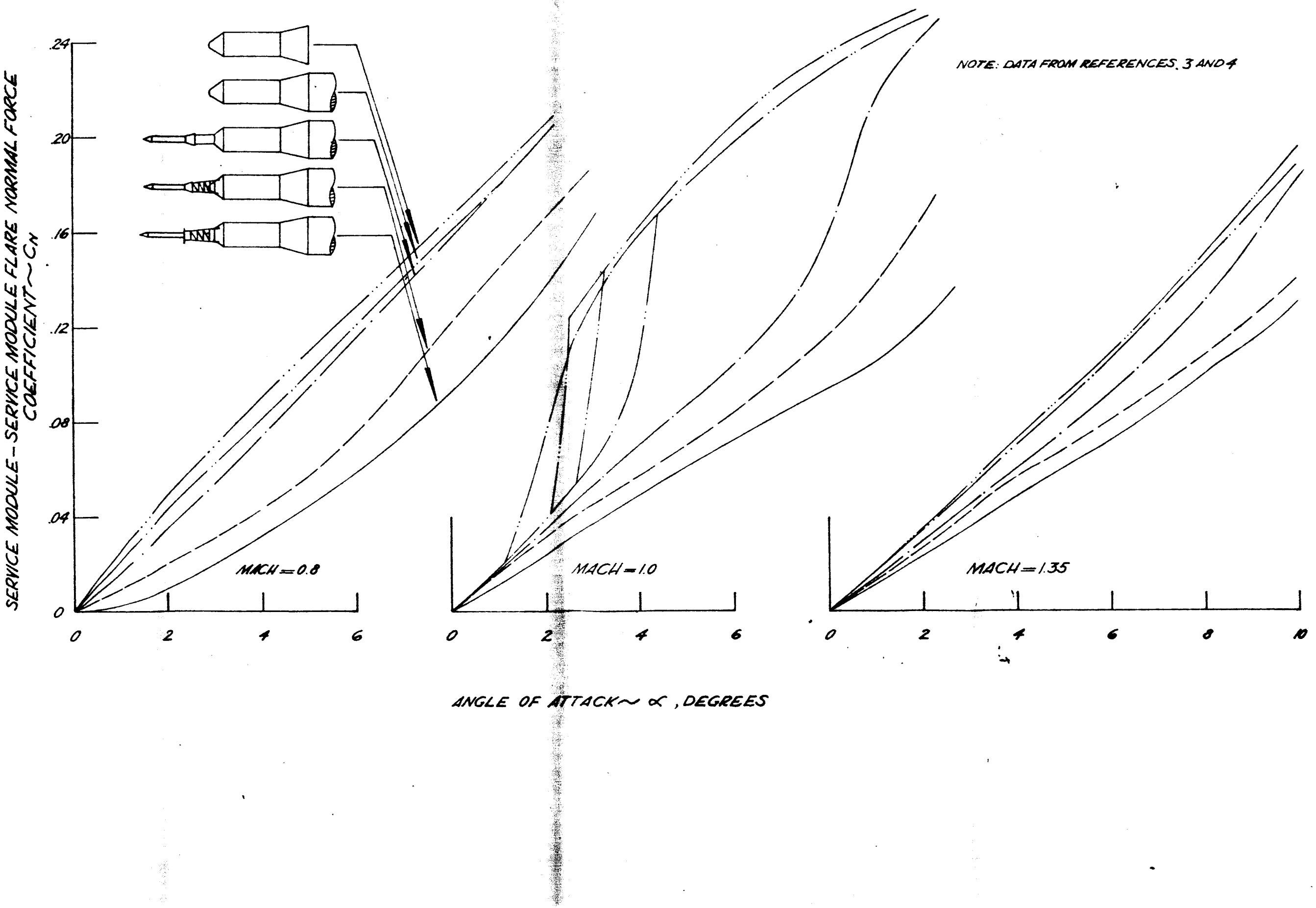

EFFECT OF SERVICE MODULE ON FOREBODY NORMAL FORCE DISTRIBUTION

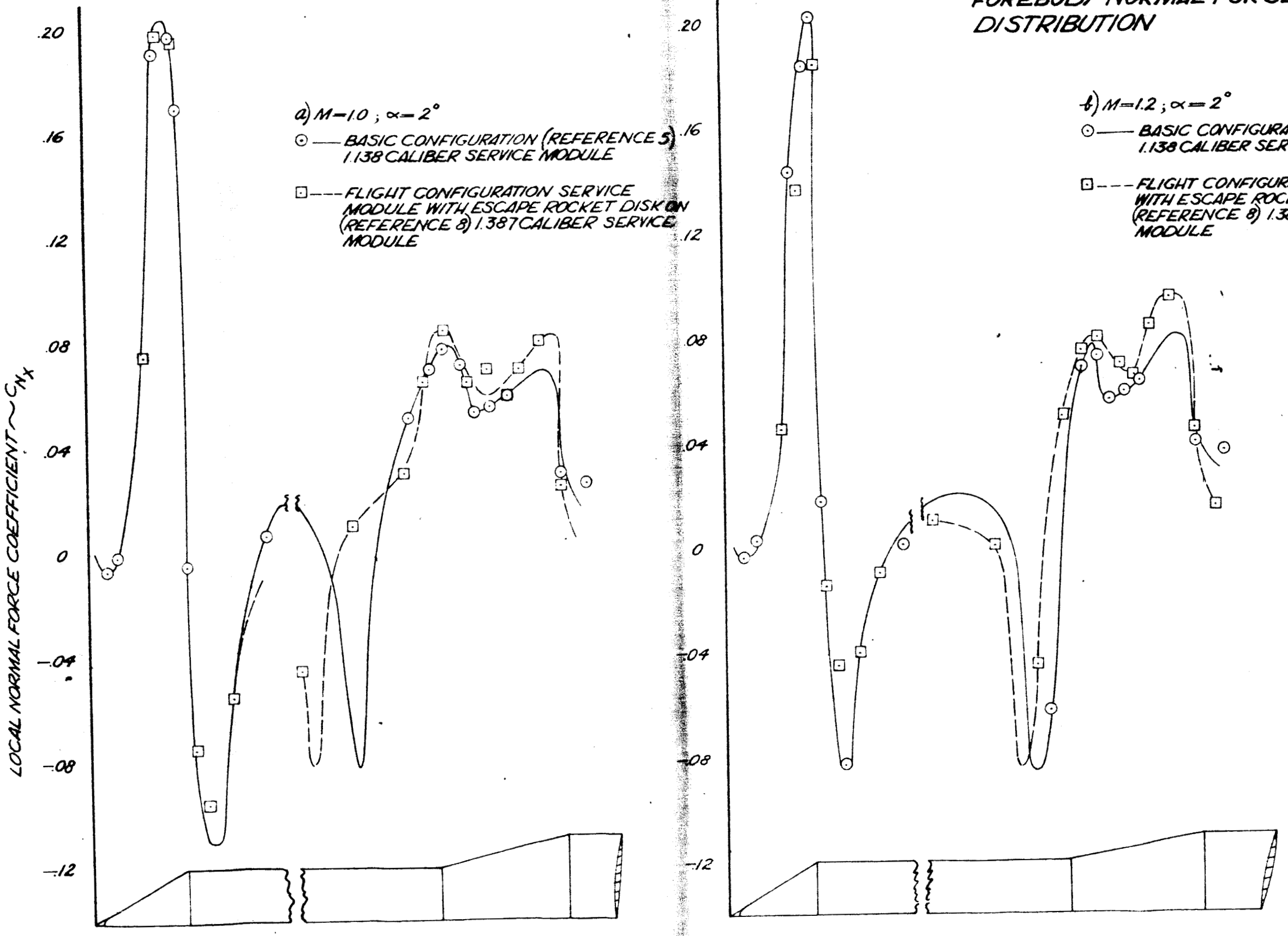

EFFECT OF SERVICE MODULE LENGTH ON NORMAL FORCE DERIVATIVES

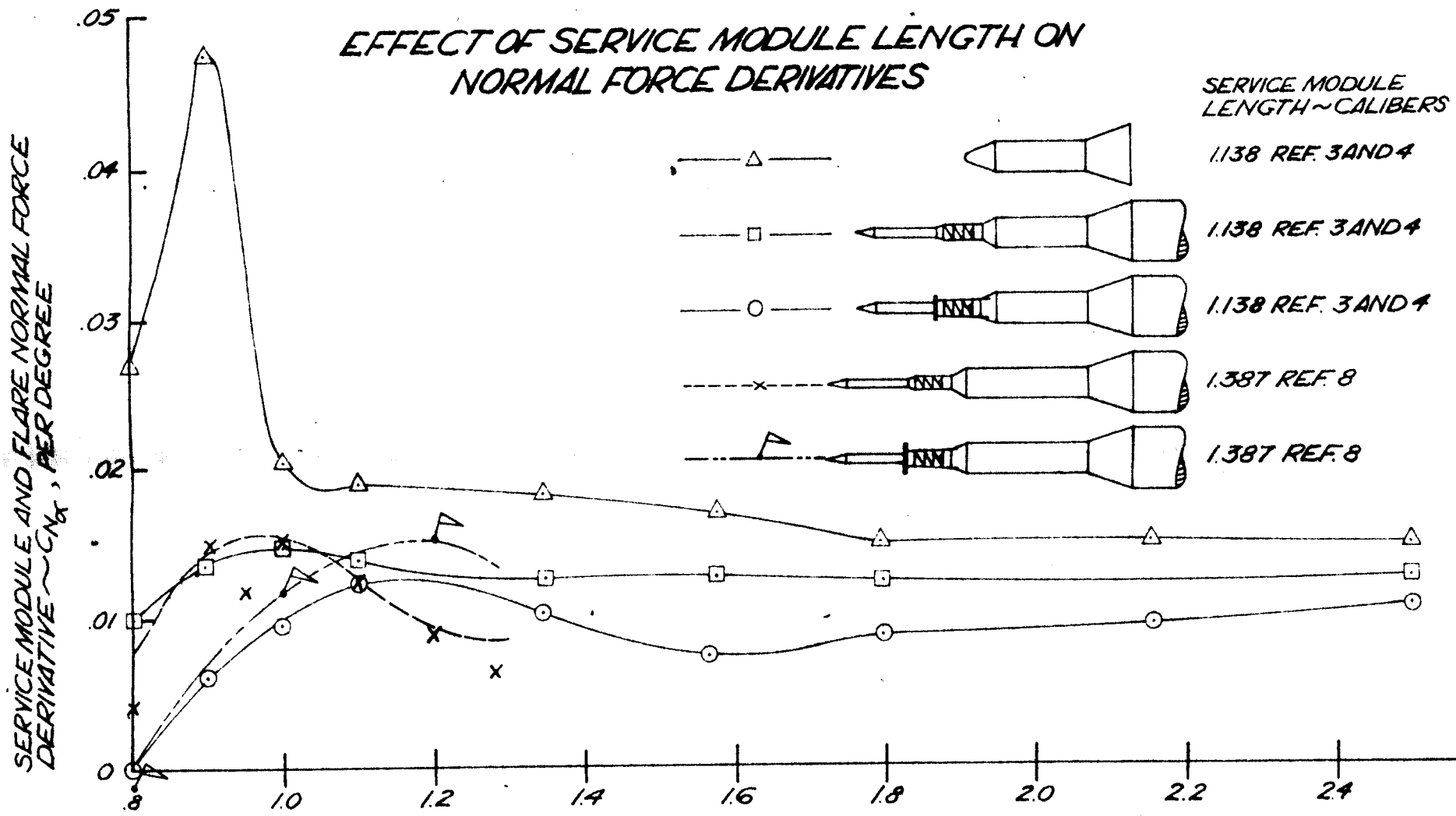

a) SERVICE MODULE — SERVICE MODULE FLARE LOADS

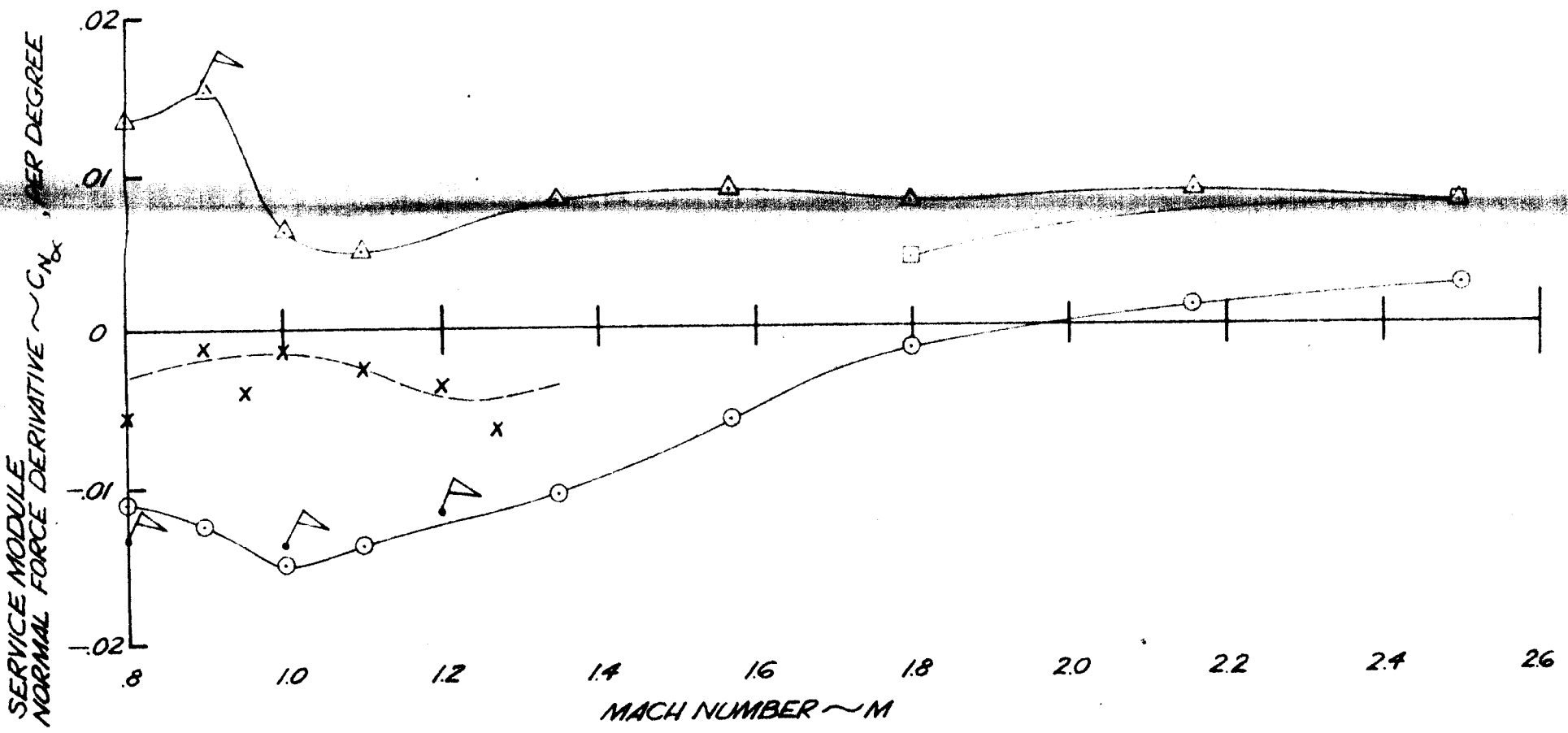

b) SERVICE MODULE LOADS

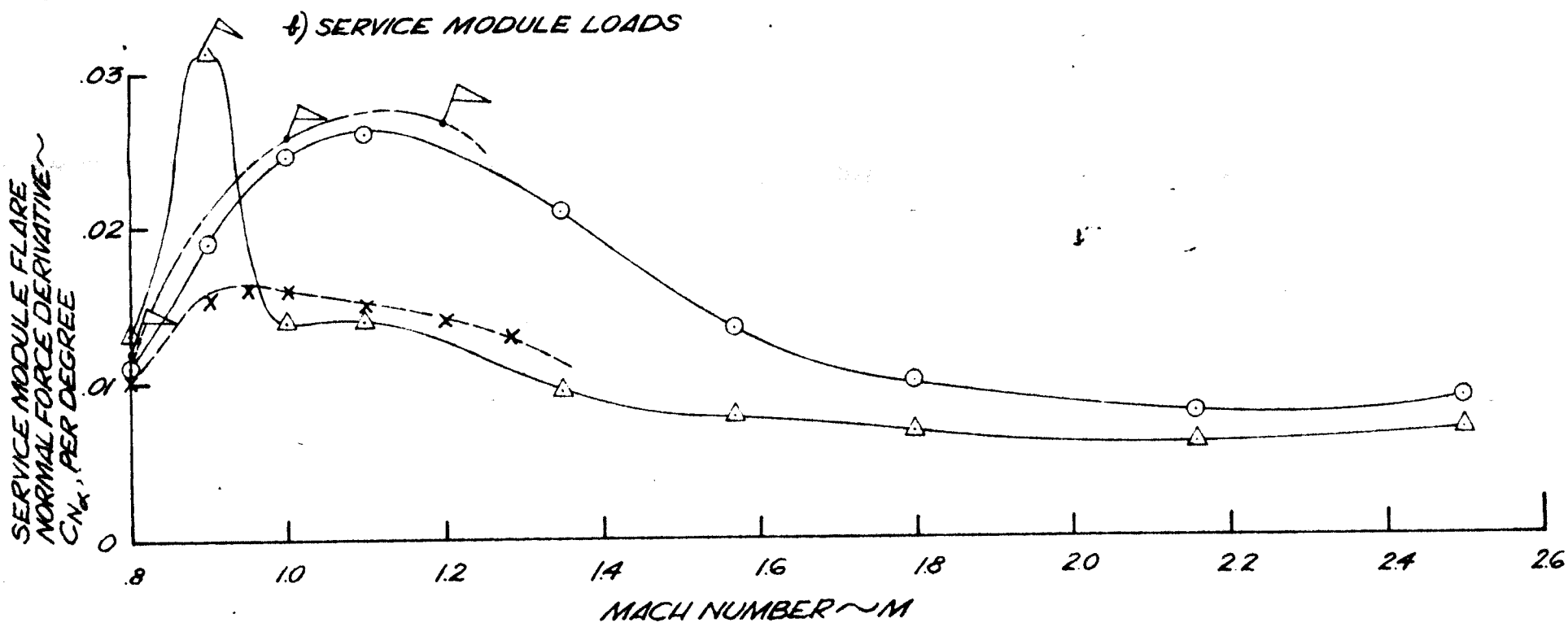

c) SERVICE MODULE FLARE LOADS

FIGURE 21
PAGE 53

SATURNI-APOLLO BASIC CONFIGURATION NORMAL FORCE DERIVATIVE DISTRIBUTION

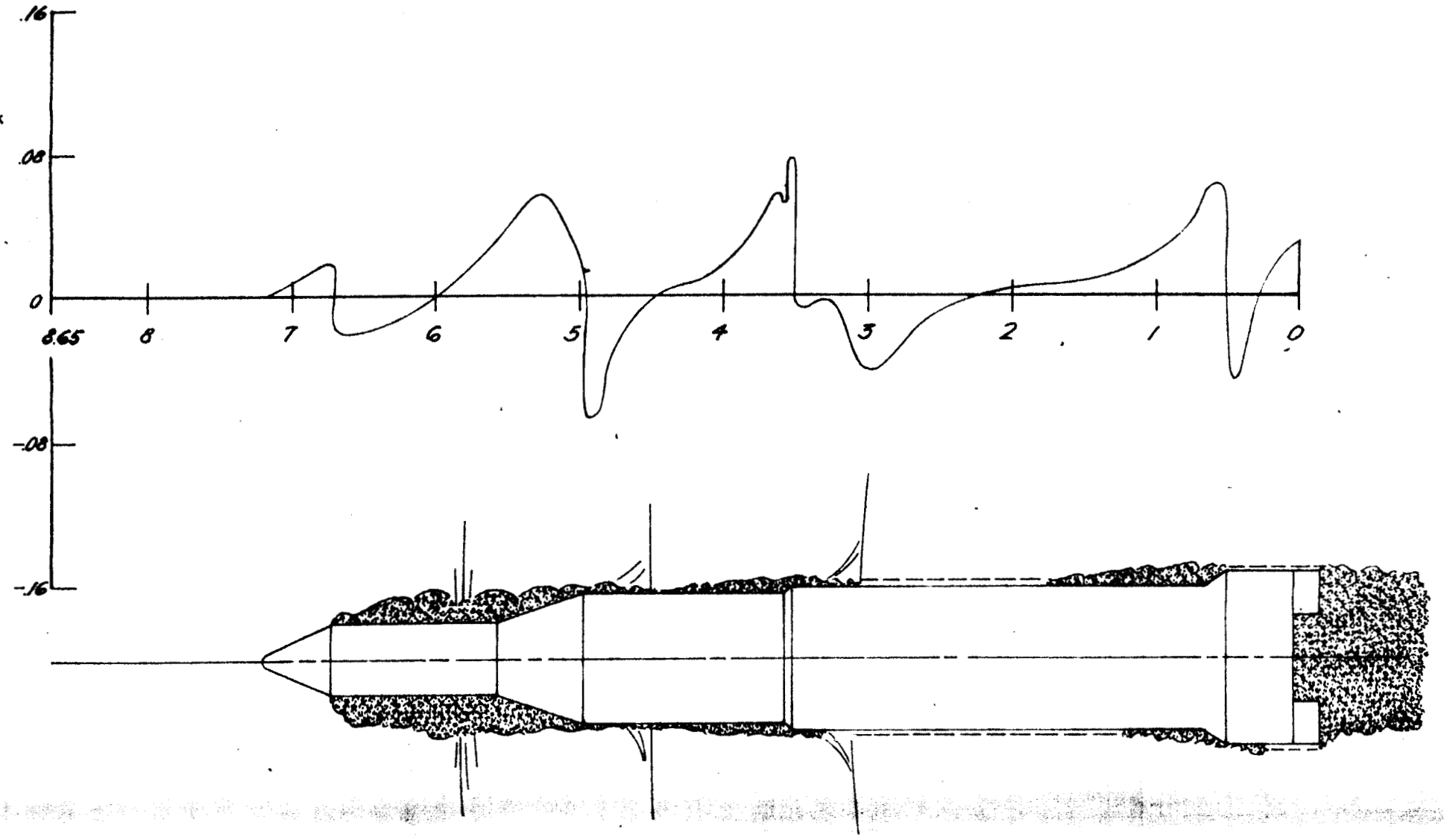

a) CLEAN CONFIGURATION
MACH = 0.9

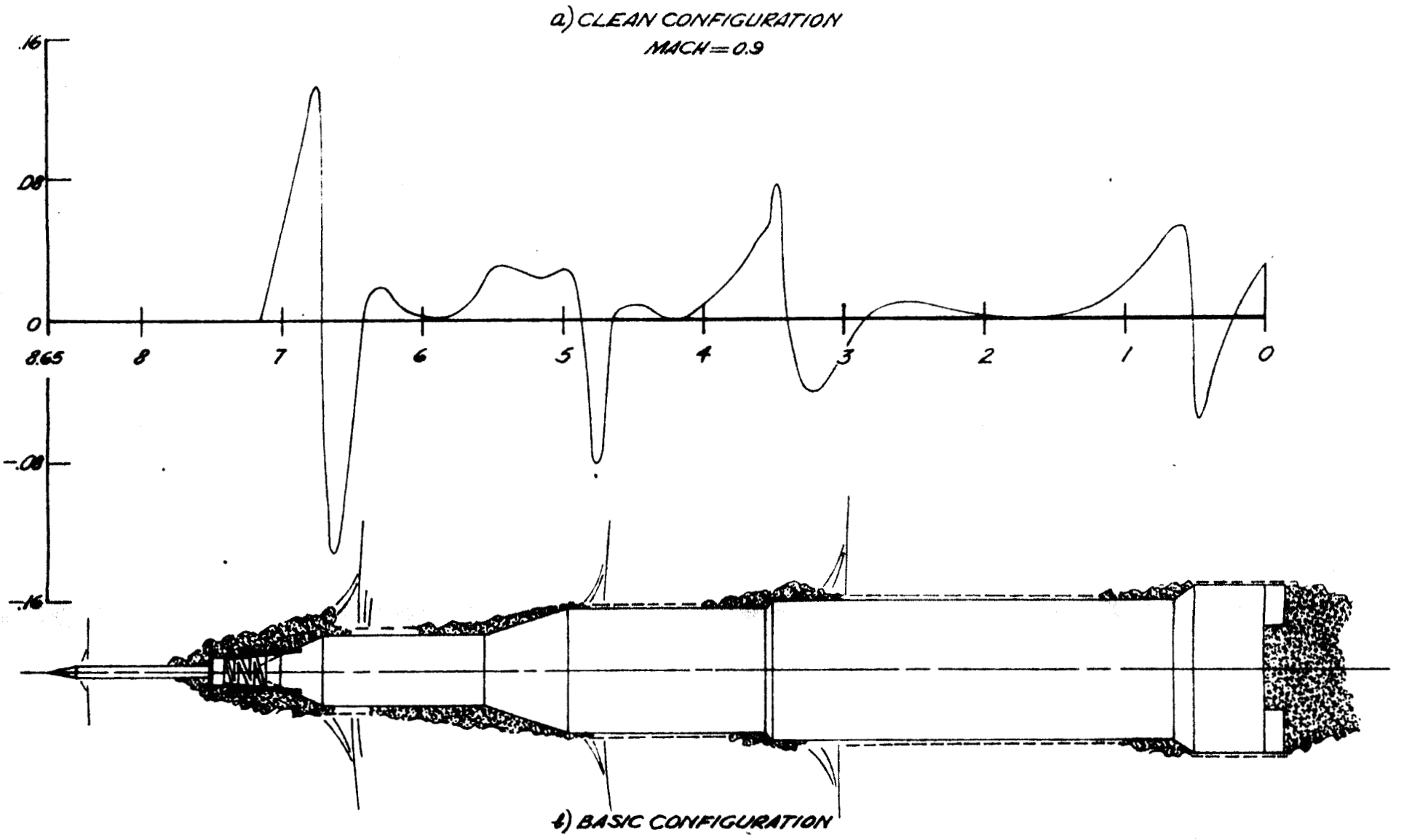

b) BASIC CONFIGURATION
MACH = 0.9

VEHICLE LENGTH ~ CALIBERS

FIGURE 22a
PAGE 54

SATURN I–APOLLO BASIC CONFIGURATION LOCAL NORMAL FORCE DERIVATIVE DISTRIBUTION

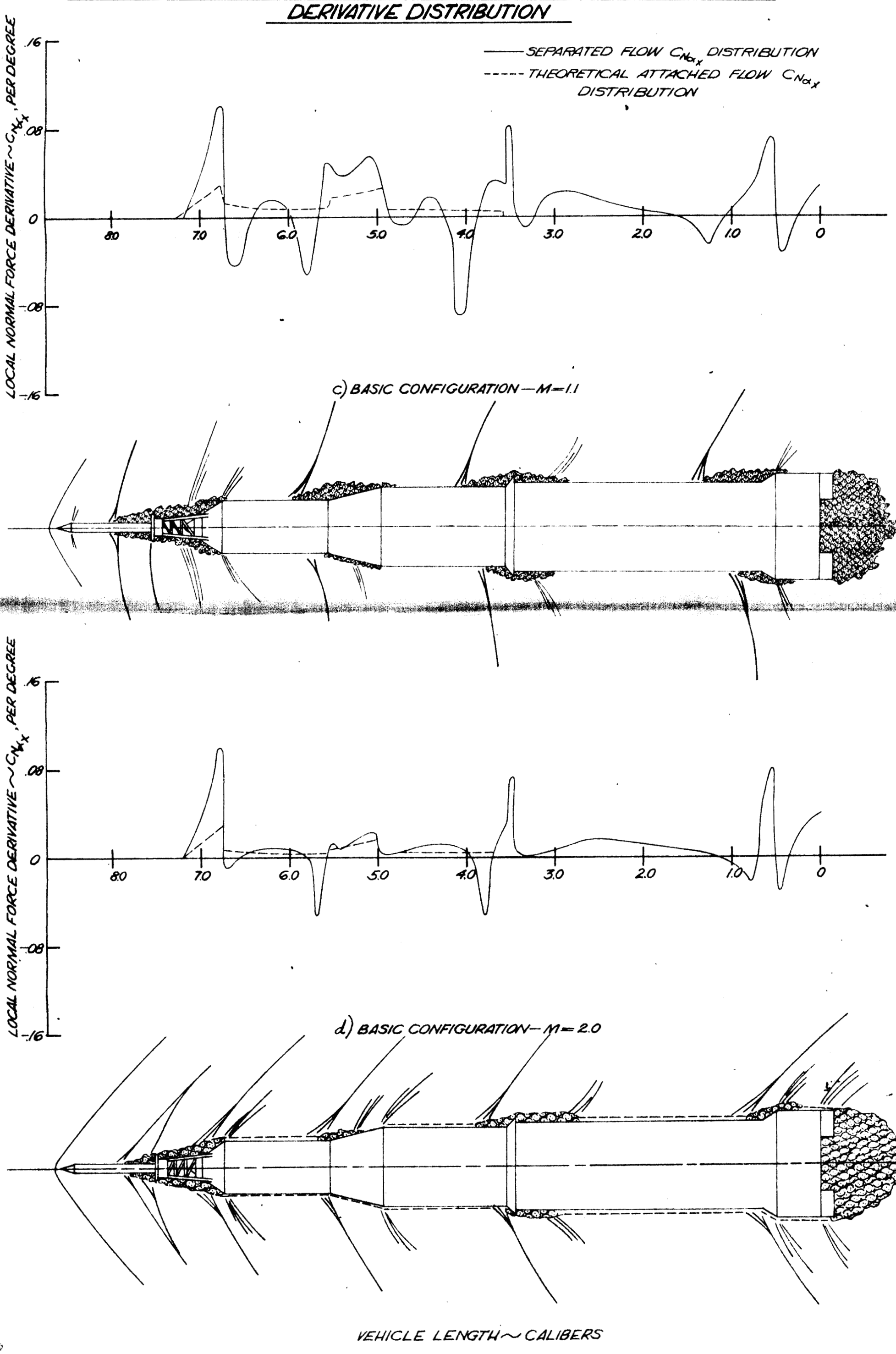

FIGURE 226
PAGE 55

SATURN I – APOLLO FLIGHT CONFIGURATION
NORMAL FORCE DERIVATIVE DISTRIBUTION

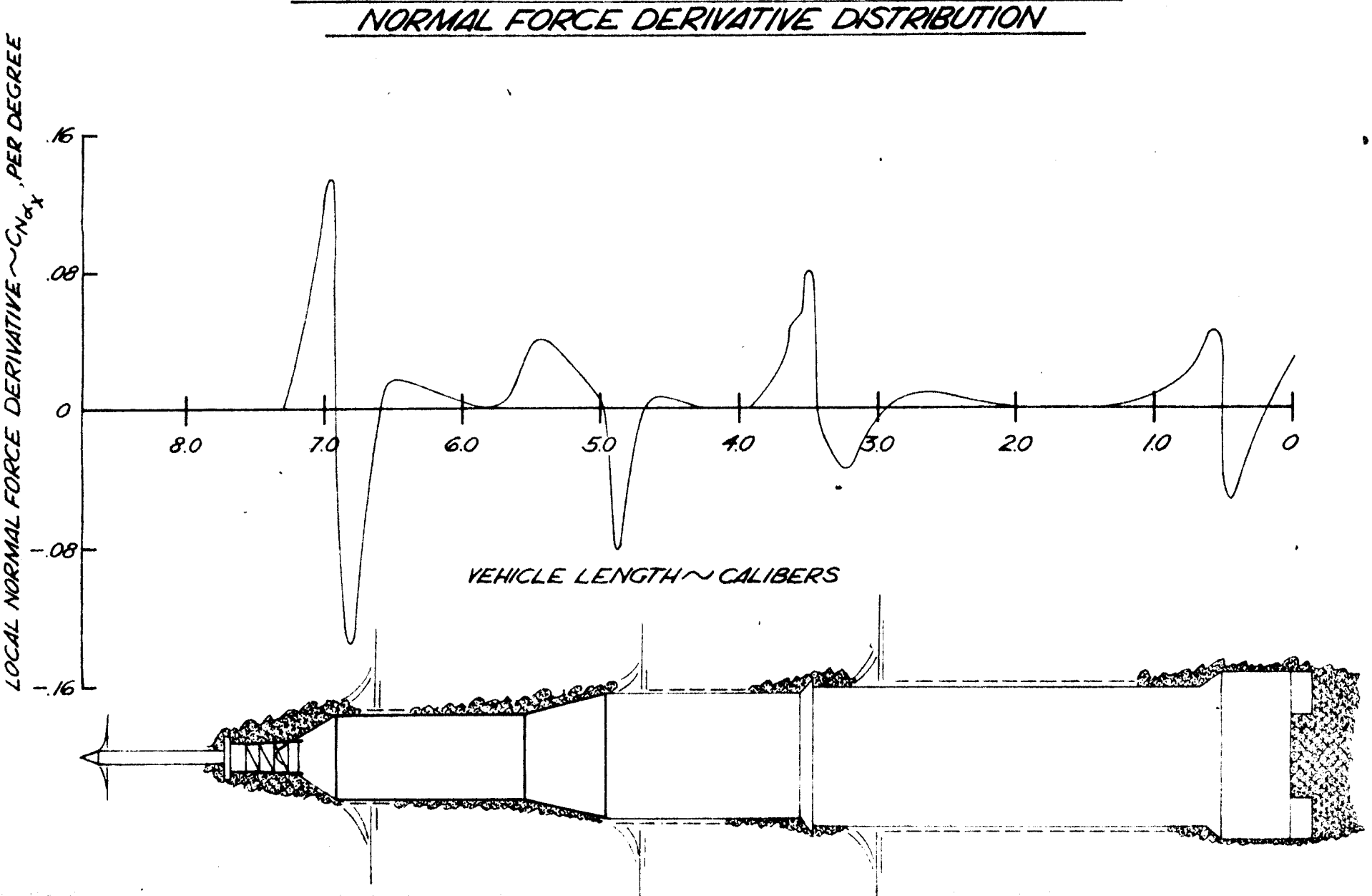

a) FLIGHT CONFIGURATION WITH DISK
MACH = 0.8

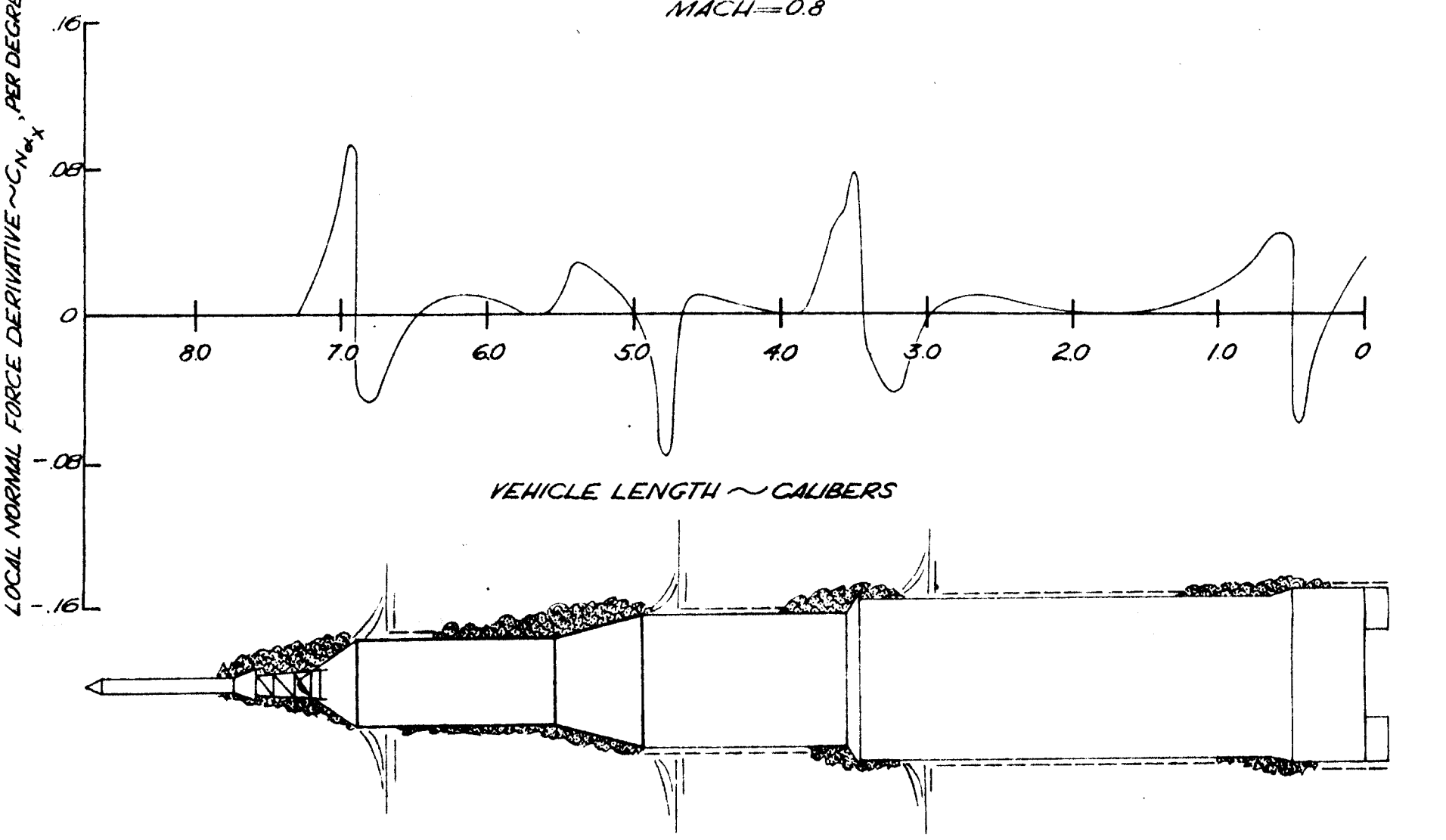

b) FLIGHT CONFIGURATION
MACH = 0.8

FIGURE 23a
PAGE 56

SATURN I-APOLLO FLIGHT CONFIGURATION
NORMAL FORCE DERIVATIVE DISTRIBUTION

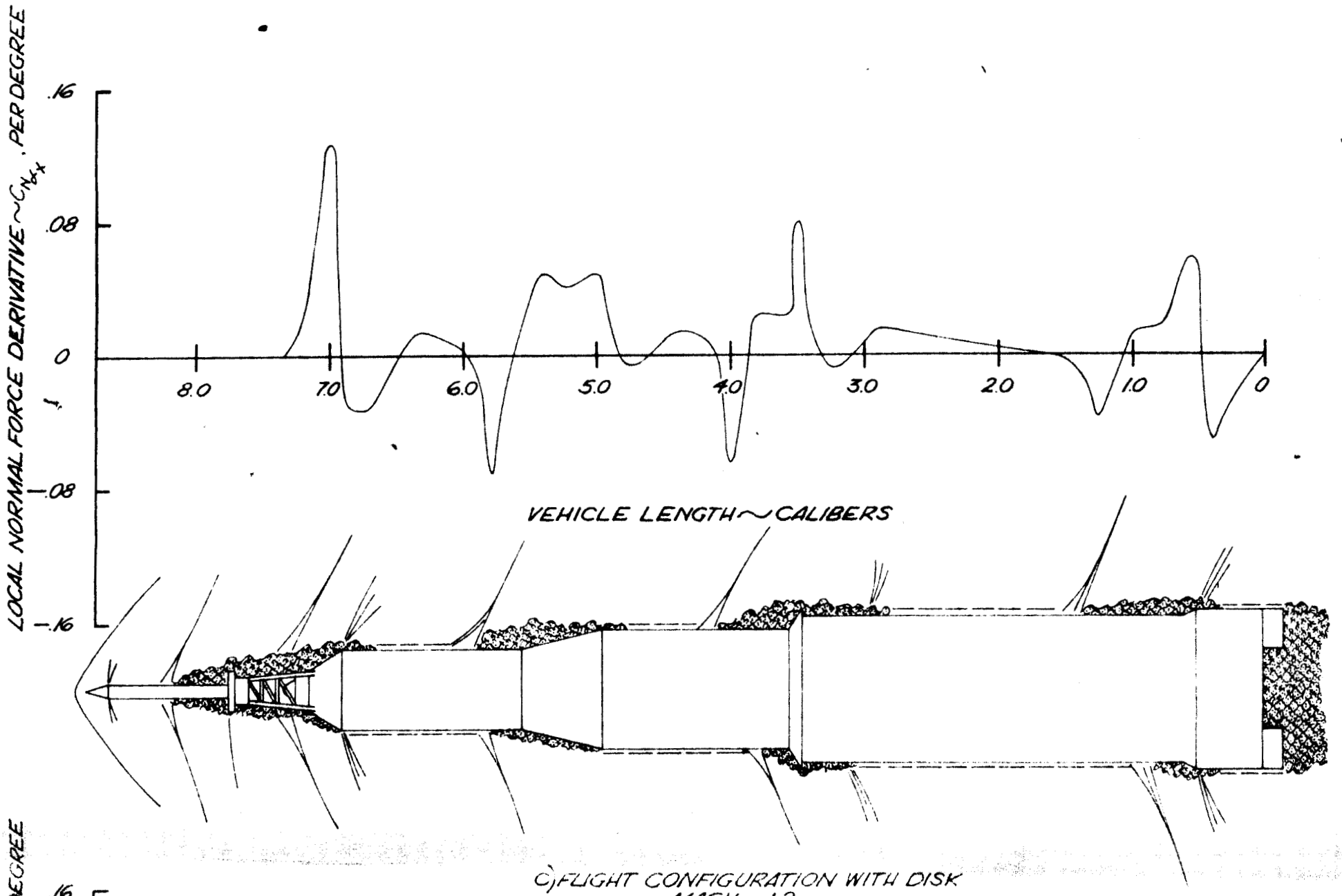

c) FLIGHT CONFIGURATION WITH DISK
MACH = 1.2

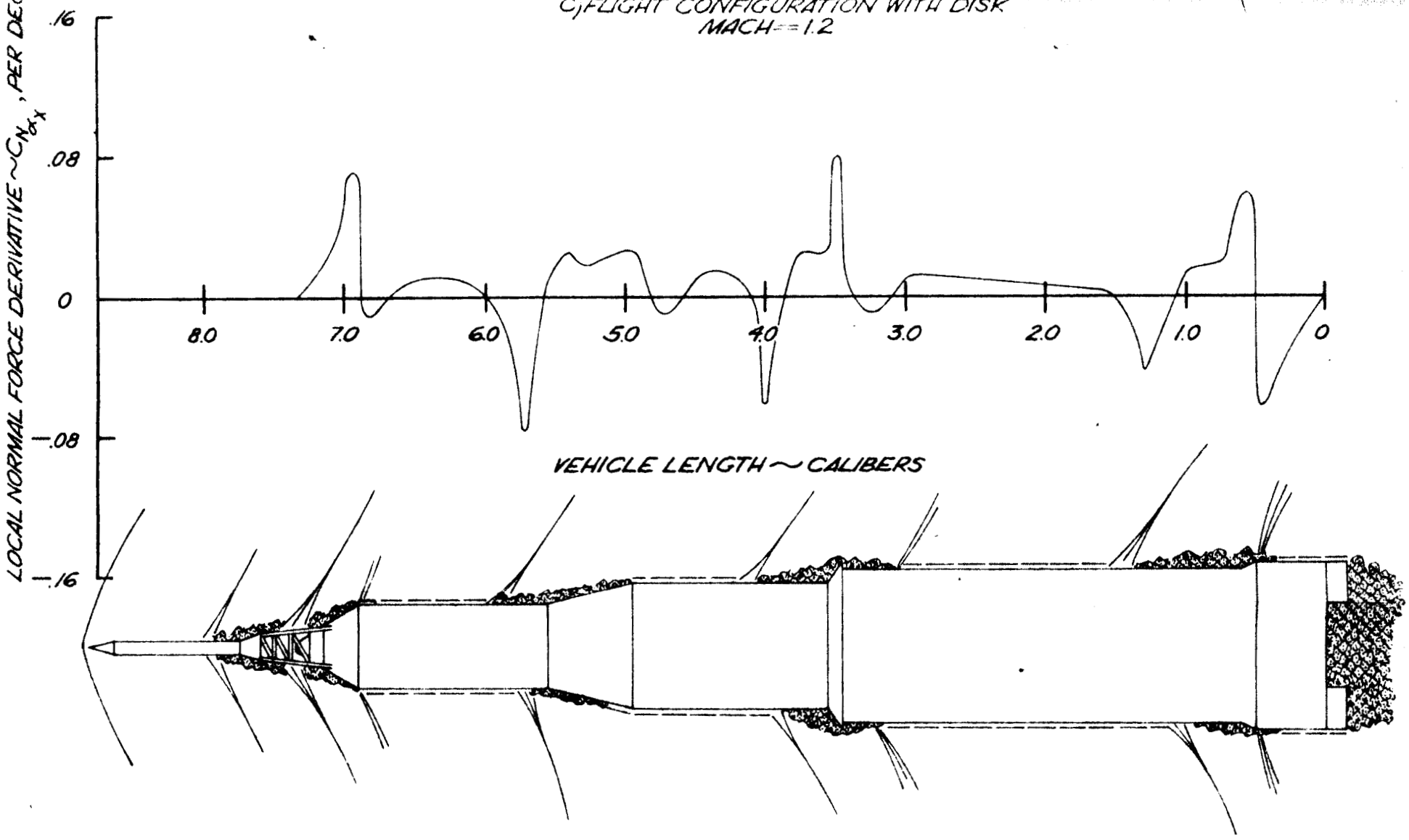

d) FLIGHT CONFIGURATION
MACH = 1.2

FIGURE 23b
PAGE 57

APPENDIX A

DETERMINATION OF THE SERVICE MODULE LOAD DISTRIBUTION

As discussed in the body of this report the normal force distribution over the service module is altered drastically by separated flow. In order to obtain a detailed load distribution it was necessary to make use of the somewhat scanty pressure distribution data of Reference 5. In this appendix the method of integration used to obtain the service module force distribution will be discussed.

Radial Pressure Distribution

Figures A-1a, b, and c present three typical radial pressure distributions obtained from the data of Reference 5. The data are plotted as $C_{p\phi} - C_{p\ \phi = 90^o}$ versus $|\sin \alpha|$,

where $C_{p\phi}$ is the pressure coefficient at any radial station and $C_{p.\ \phi = 90^o}$ is the pressure coefficient at $\phi = 90^o$.

By plotting the data in such a manner angle of attack trends are readily discernible. The radial pressure distribution over the command module is nearly elliptical (Figure A-1a). The cylinder data is, however, rather irregular (Figures A-1b and c). The distribution at Station 13 (Figure A-1c) resembles the pressure distribution obtained on a cylinder at high angles of attack and shows the effects of flow separation. The fact that the leeward pressures are higher than the windward pressures should not be too disconcerting since Station 13 is in a region of shock induced separation. What is disconcerting is the fact that the data point density

(every 45°) is insufficient for any routine type of integration. A purely emperical integration technique was therefore devised. This integration method was adjusted to agree with the graphic integration of the radial pressure distributions for a number of cases.

In brief, the emperical technique used amounted to fitting a rectangle and two ellipses to the data as shown in sketch A-1 below:

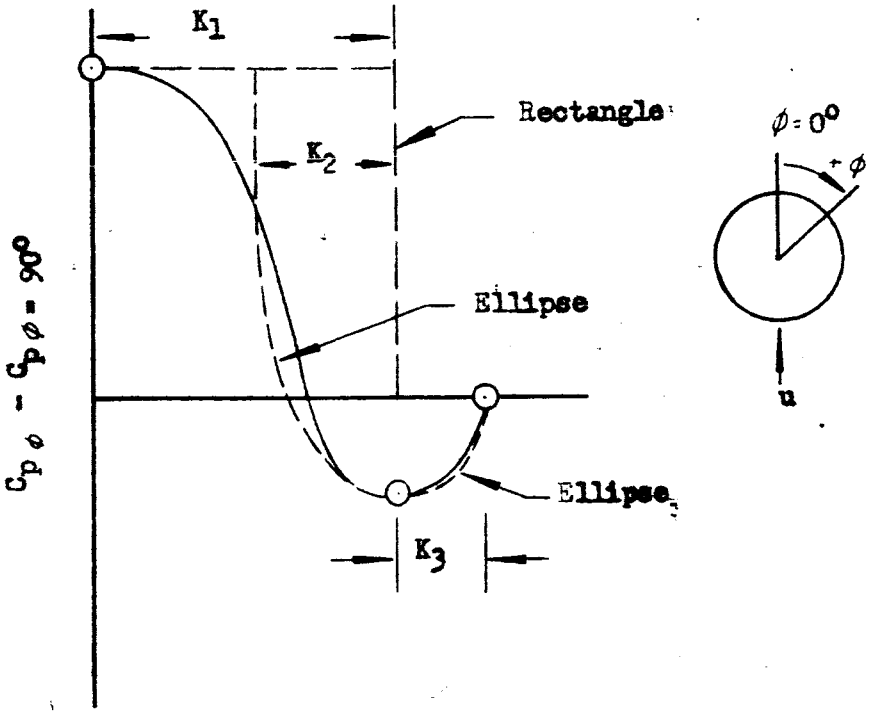

EMPERICAL CURVE FIT - SKETCH A-1

Using the same fit to both windward and leeward side pressure distribution data one obtains the following expression for the local normal force coefficient, C_{N_I}:

$$C_{N_I} = \frac{4d}{C}\left[K_1\left\{(C_{p\phi=180^\circ} - C_{p\phi=90^\circ}) - (C_{p\phi=0^\circ} - C_{p\phi=90^\circ})\right.\right. \quad \text{(A-1)}$$
$$\frac{-K_2\pi}{4}\left\{(C_{p\phi=180^\circ} - C_{p\phi=135^\circ}) - (C_{p\phi=0^\circ} - C_{p\phi=45^\circ})\right\}$$
$$\left.\left.\frac{+K_3\pi}{4}\left\{(C_{p\phi=135^\circ} - C_{p\phi=90^\circ}) - (C_{p\phi=45^\circ} - C_{p\phi=90^\circ})\right\}\right]$$

where C_p = Pressure coefficient, $\frac{P - P_\infty}{\frac{1}{2}\rho U^2}$

d = Local diameter at Station X

c = Reference length

ϕ = Radial position as defined in Sketch A-1

and the constants are:

$K_1 = .707$

$K_2 = .337$

$K_3 = .293$

The constants K_1, K_2, and K_3 were obtained by trial and error comparison with graphically integrated data.

Simplifying equation A-1 one obtains:

$$C_{N_X} = \frac{4d}{\pi c} .443 (C_p\phi = 180^o - C_p\ \phi = 0^o) + .494(C_p\ \phi = 135^o - C_p\ \phi = 45^o) \quad (A-2)$$

which is the expression used in integrating the radial pressure distributions.

Longitudinal Normal Force Distribution

The normal force distributions obtained from the radial pressure integration described in the preceding section were plotted and integrated graphically. The plots in Figure 20 in the body of the report show the excellent agreement obtained with the normal force distribution data of Reference 8 over the command module and forward service module. The difference in the aft service module and flare distributions are the result of a difference in service module length for the two sets of data as explained earlier.

The longitudinal force distribution data is sparce. However, by utilizing force data a reasonable fairing was obtained. Figures 2a and b show the degree of agreement obtained with the service module force data at $\alpha = 2$ and 4 degrees respectively. As explained in the body of the report the various cylinder positive and negative load regions were replaced by lumped force vectors, faired through $\alpha = 0^{o}$, and the lumped force derivatives were obtained. Again adjustments to the force data were necessary until the good agreement shown in Figure 15 was obtained.

TYPICAL RADIAL PRESSURE DISTRIBUTION DATA

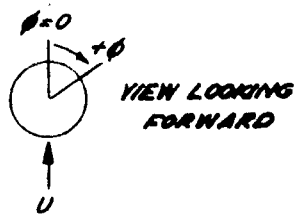

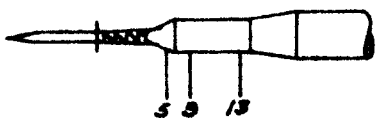

BASIC CONFIGURATION
M=1.5

——— WINDWARD SIDE

- - - - LEEWARD SIDE

FIG. A-1a STATION 5

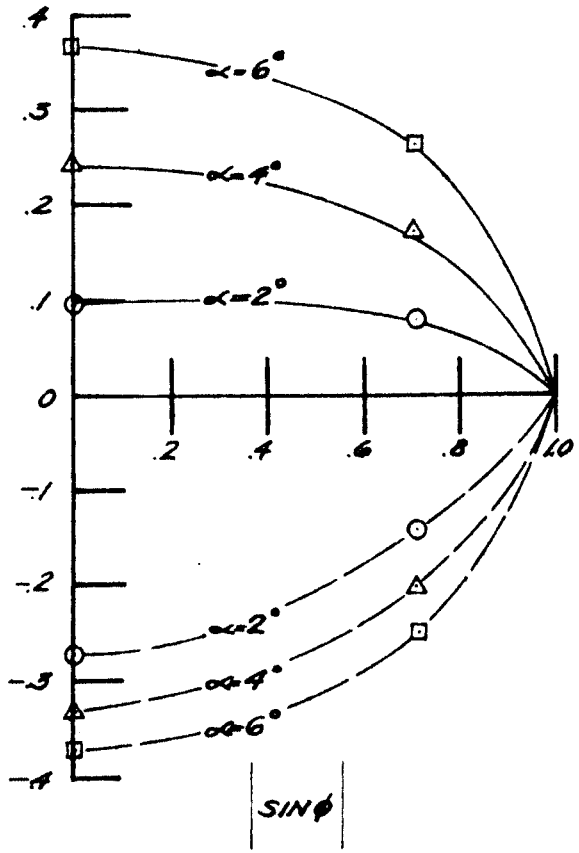

FIG. A-1b STATION 9

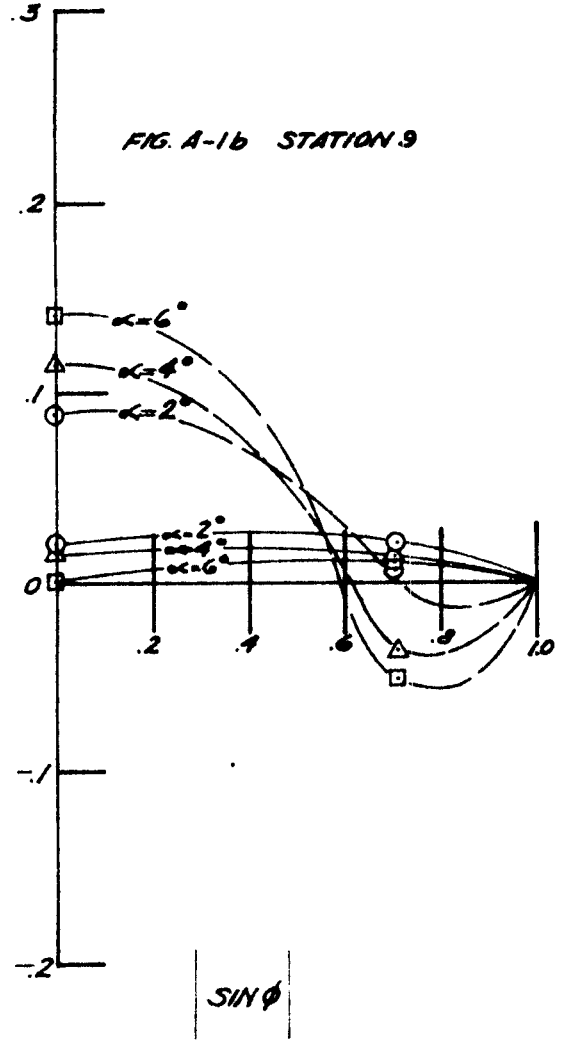

FIG. A-1c STATION 13

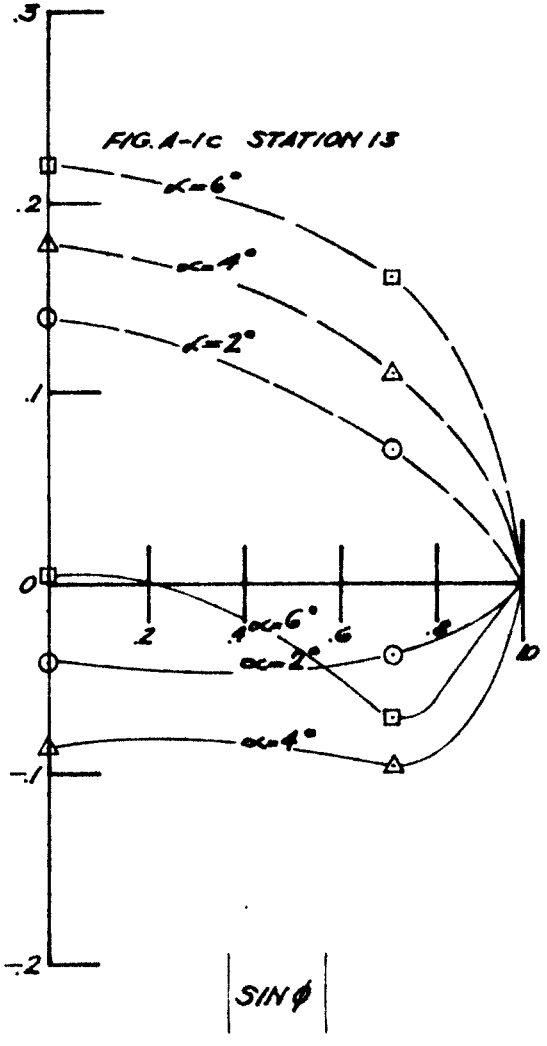

FIGURE A-1
PAGE A-5

SERVICE MODULE LOADS

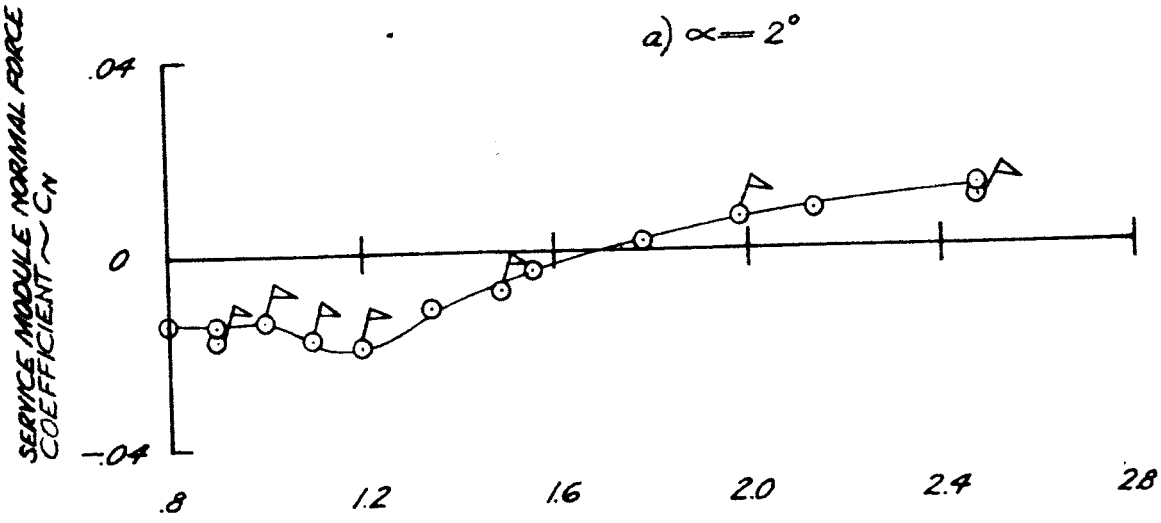

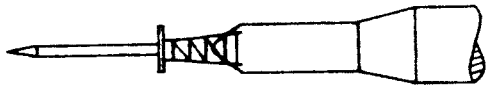

BASIC CONFIGURATION

⊙ FORCE DATA REFERENCE 3 AND 4

⊙ PRESSURE DATA REFERENCE 5

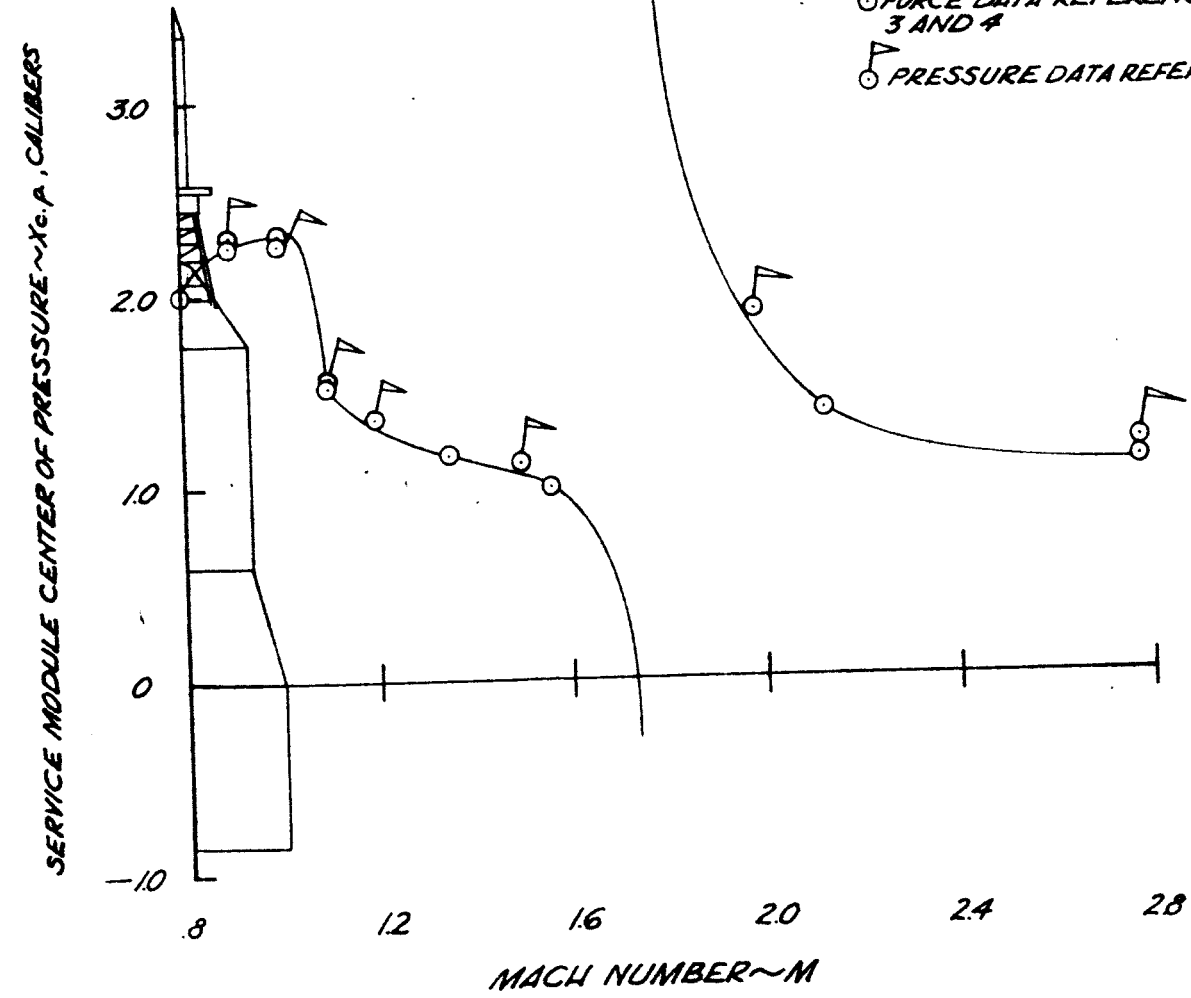

SERVICE MODULE LOADS

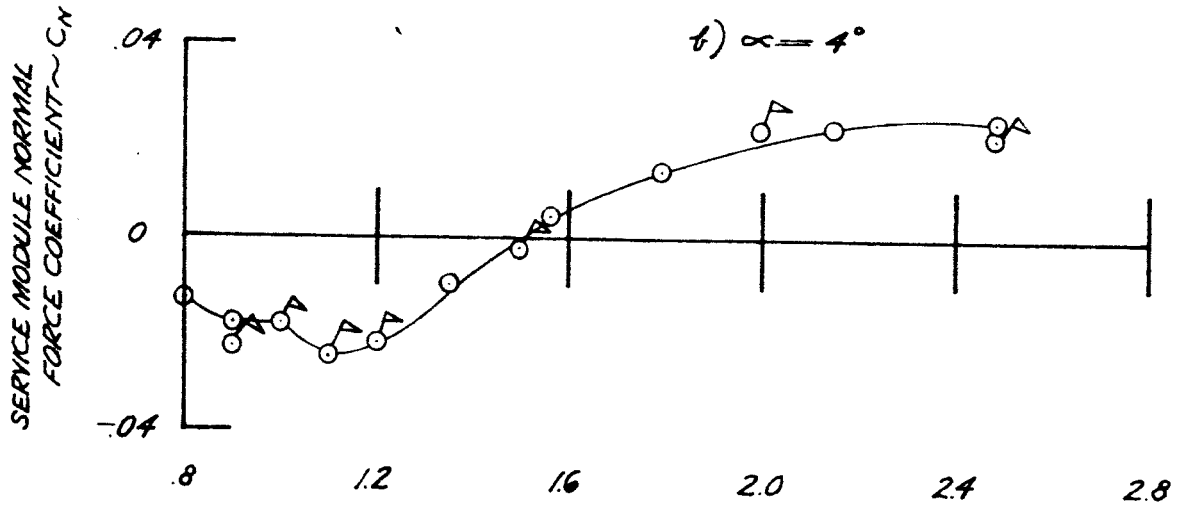

BASIC CONFIGURATION

⊙ FORCE DATA REFERENCE 3 AND 4

⊙ PRESSURE DATA REFERENCE 5

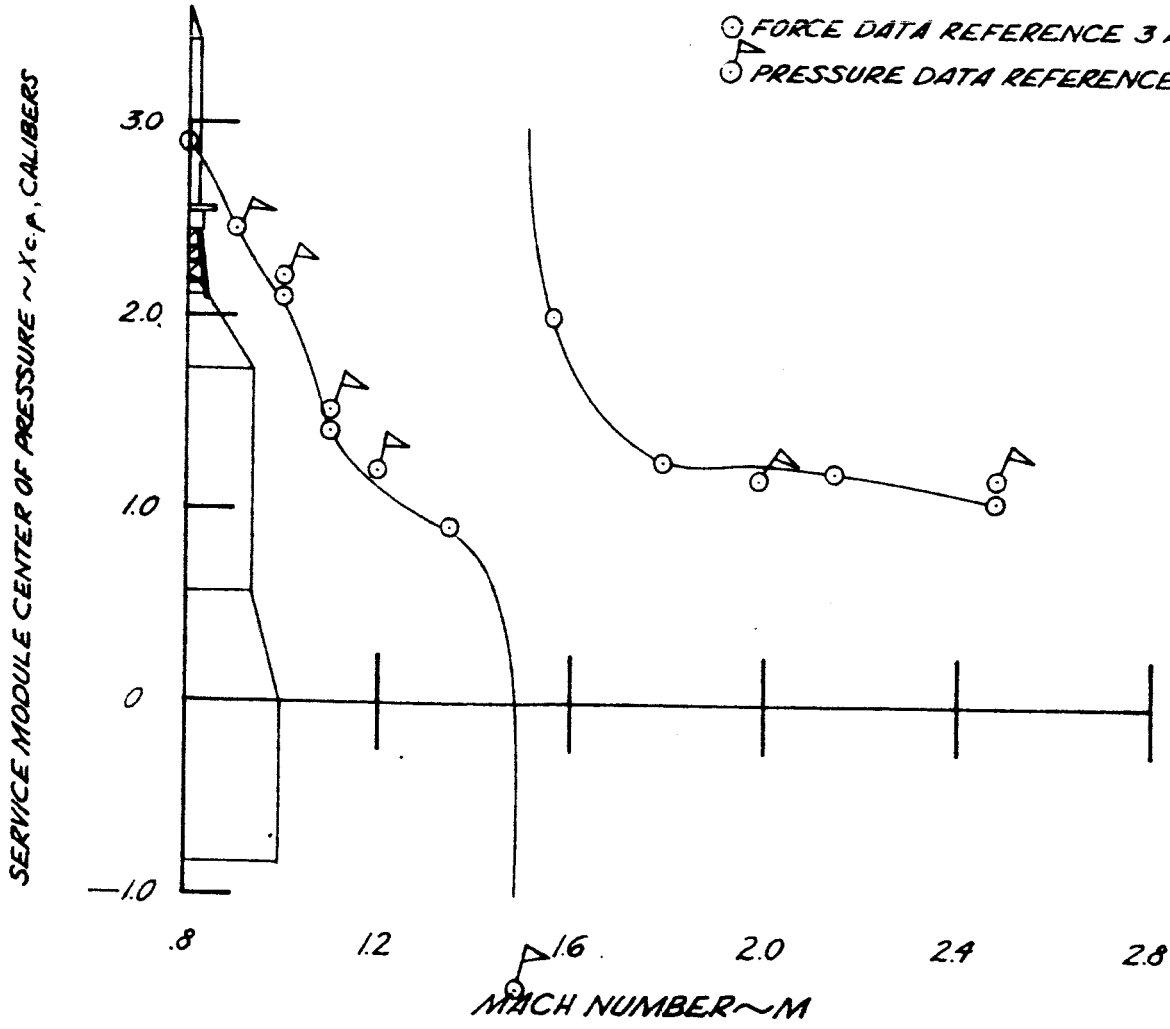

APPENDIX B

LUMPED FORCE APPROXIMATION TO THE LOAD DISTRIBUTION

As discussed in the body of the report, the various regions of positive and negative loading may be replaced by discrete force vectors. The load distribution changes with Mach number and some loadings merge while others may disappear or change sign. Figure B-1 defines the general load distribution and the 19 lumped forces (18 body forces plus the fin loading) used to approximate the loading.

Various references were used to obtain an estimate of the load distribution for the various configurations. Table B-I below lists the configurations and the sources used to obtain the load distributions.

TABLE B-I

SOURCE OF DATA USED IN ESTIMATING LOAD DISTRIBUTION

Configuration		
Basic (Short service module, disk on)	Forebody	Ref. 3, 4 and 5
	Aft Body	Ref. 6 and 8
	Fins	Ref. 7
Basic with escape rocket disk removed (Short service module, disk off)	Forebody	Ref. 3, 4, 7 plus extrapolation
	Aft Body	Ref. 6 and 8
	Fins	Ref. 7
Flight (Long service module, disk off)	Forebody	Ref. 8 plus extrapolation
	Aft Body	Ref. 6 and 8
	Fins	Ref. 7
Flight with escape rocket disk on (Long service module, disk on)	Forebody	Ref. 8 plus extrapolation
	Aft Body	Ref. 6 and 8
	Fins	Ref. 7

Forebody: Body forward of service module flare - 2nd stage juncture

Aftbody: Body aft of service module flare - 2nd stage juncture

Fins: Includes total fin increment from force data (fins plus body carry over)

The method of obtaining the forebody loads on the basic configuration using force and pressure data has been discussed previously in the body of the report (section entitled "Normal Force Derivative Distribution")as has the justification for using the data of References 6 and 8 to obtain the aft body loading for all configurations. The fin increments were obtained directly from Reference 7. The forebody loading over the flight configuration was obtained directly from Reference 8 after the data had been zero shifted. These data covered the Mach number range .8 to 1.28. The zero angle of attack distribution was extrapolated using basic configuration data as a guide. The forebody data for the short service module, disk off was obtained by assuming that the flight configuration (long service module) loading applied over the service module. The service module flare loading was then obtained by computing the flare loading necessary to produce the proper service module - service module flare normal force derivative.

Figures B-2 and B-3 present the $\alpha = 0^{\circ}$ lumped force derivative loads and centers of pressure for the flight configuration (long service module) disk on and disk off. Figure B-4 presents the $\alpha = 0^{\circ}$ lumped force derivative loads and centers of pressure for the basic configuration (short service module) disk off and disk on.

A triple slope approximation to the lumped force angle of attack characteristics is presented in Table B-II. Sketch B-1 below defines the triple slope approximation.

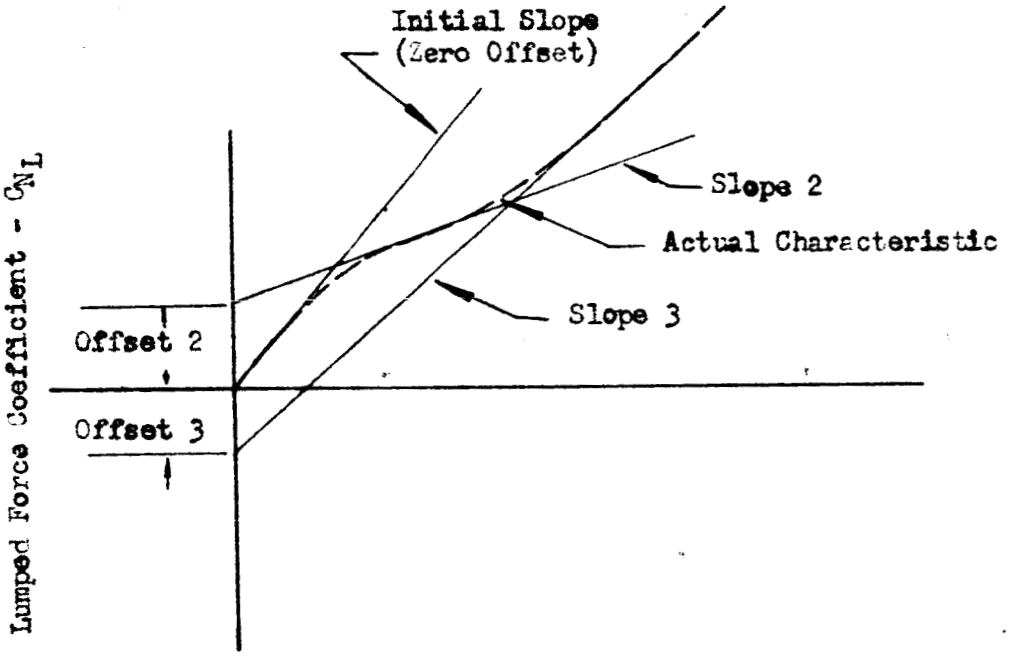

TRIPLE SLOPE APPROXIMATION

Sketch B-1

The slopes, zero offsets, applicable angle of attack range, and centers of pressures of the force vectors are given in the table. In some cases the same slope may apply over the complete angle range (0 to 8.0 degrees). There are other cases where a double slope approximation yields sufficient accuracy. Where these singularities occur the value of the applicable slope is repeated in the table for completeness. There are cases, however, where the slope may remain constant but the center of pressure changes as indicated in the table. Data are presented for a Mach number range .8 to 1.28, due to the absence of higher Mach number data for the flight configuration. These data should not be used beyond an angle of attack of 8°.

TABLE B-II

FLIGHT CONFIGURATION TRIPLE SLOPE LUMPED FORCE APPROXIMATION

MACH NUMBER = 0.8

Lumped Force	C_N (α = 0°)	Offset	α Range, Degrees	X_{cp} Calibers	$C_{N\alpha_2}$	Offset	α Range, Degrees	X_{cp} Calibers	$C_{N\alpha_3}$	Offset	α Range, Degrees	X_{cp} Calibers
1	.013	0	0-1.1	6.94	.0095	.012	1.1-1.6	7.0	.0065	.0215	1.6-8.0	7.1
2	-.013	0	0-1.1	6.75	-.0035	-.011	1.1-1.6	6.7	-.001	-.0175	1.6-8.0	6.8
3	.0035	0	0-1.9	6.25	.0017	.0025	1.9-8.0	6.35	.0017	.0025	1.9-8.0	6.35
4	—	-	-	-	—	—	-	-	—	—	-	-
5	.004	0	0-3.0	5.55	.0035	.001	3.0-8.0	5.65	.0035	.001	3.0-8.0	5.65
6	.01	0	0-8.0	5.3	.01	0	0-8.0	5.3	.01	0	0-8.0	5.3
7	-.012	0	0-1.6	4.8	-.002	-.012	1.6-4.8	4.85	-.005	-.002	4.8-8.0	4.8
8	.00125	0	0-4.0	4.6	.0005	.0035	4.0-8.0	4.6	.0005	.0035	4.0-8.0	4.6
9	—	-	-	-	—	—	-	-	—	—	-	-
10	.0145	0	0-1.4	3.65	.0085	.0115	1.4-3.6	3.75	.006	.018	3.6-8.0	3.75
11	.003	0	0-3.9	3.5	.002	.0045	3.9-8.0	3.5	.002	.0045	3.9-8.0	3.5
12	-.012	0	0-1.6	3.2	-.0085	-.0055	1.6-3.8	3.2	-.0035	-.0245	3.8-8.0	3.2
13	.011	0	0-8.0	2.4	.011	0	0-8.0	2.45	.011	0	0-8.0	2.45
14	—	-	-	-	—	—	-	-	—	—	-	-
15	.0125	0	0-2.0	.95	.006	.012	2.0-4.9	1.0	.055	-.016	4.9-8.0	1.0
16	.01	0	0-1.6	.6	.005	.0075	1.6-5.6	.6	.0075	-.0035	5.6-8.0	.6
17	-.0035	0	0-1.6	4.5	-.0095	.008	1.6-4.0	.45	.001	-.0025	4.0-8.0	.45
18	.0035	0	0-1.2	.1	0	.006	1.2-5.5	.1	.0005	.002	5.5-8.0	.1
Fins	.059	0	0-4.8	.6	.1	-1.75	4.8-8.0	.6	.1	-1.75	4.8-8.0	.6

MACH NUMBER = 0.9

Lumped Force	C_N ($\alpha = 0$)	Offset	α Range, Degrees	X_{c_p} Calibers	$C_{N\alpha_2}$	Offset	α Range, Degrees	X_{c_p} Calibers	$C_{N\alpha_3}$	Offset	α Range, Degrees	X_{c_p} Calibers
1	.0155	0	0-2.8	6.9	.008	.0185	2.8-4.1	7.1	.005	.0315	4.1-8.0	7.1
2	-.0067	0	0-3.4	6.75	-.0035	-.011	3.4-5.1	6.7	-.0016	-.02	5.1-8.0	6.8
3	.003	0	0-4.7	6.35	.0018	.007	4.7-8.0	6.4	.0018	.007	4.7-8.0	6.4
4	--	-	-	-	--	--	-	-	--	--	-	-
5	.0027	0	0-4.0	5.6	.002	.0025	4.0-8.0	5.6	.002	.0025	4.0-8.0	5.6
6	.017	0	0-2.0	5.25	.0085	.034	2.0-5.0	5.25	.0055	.05	5.0-8.0	5.25
7	-.019	0	0-2.3	4.7	-.0045	-.0345	2.3-3.7	4.75	-.0015	-.045	3.7-8.0	4.75
8	.0016	0	0-1.9	4.35	.003	-.0025	1.9-8.0	4.35	.003	-.0025	1.9-8.0	4.35
9	--	-	-	-	--	--	-	-	--	--	-	-
10	.017	0	0-2.6	3.65	.01	.0135	2.6-3.7	4.7	.0046	.032	3.7-8.0	4.75
11	.004	0	0-2.4	3.5	.0025	.004	2.4-8.0	3.5	.0025	.004	2.4-8.0	3.5
12	-.019	0	0-1.3	3.15	-.006	-.0165	1.3-2.0	3.25	-.0035	-.026	2.0-8.0	3.3
13	.012	0	0-1.4	2.25	.0065	.008	1.4-3.6	2.35	.0045	.016	3.6-8.0	2.4
14	--	-	-	-	--	--	-	-	--	--	-	-
15	.0135	0	0-2.7	.95	.0075	.015	2.7-5.2	1.0	.0035	.0255	5.2-8.0	1.05
16	.01	0	0-2.8	.6	.0067	.008	2.8-8.0	.6	.0067	.008	2.8-8.0	.6
17	-.0085	0	0-3.8	.4	0	-.0335	3.8-5.3	.42	.008	-.075	5.3-8.0	4.5
18	.0015	0	0-3.0	.075	.003	-.004	3.0-6.5	.08	.004	-.011	6.5-8.0	.13
Fins	.06	0	0-4.2	.6	.1	-.175	4.2-8.0	.6	.1	-.175	4.2-8.0	.6

MACH NUMBER = .95

Lumped Force	C_N ($\alpha = 0$)	Offset	α Range, Degrees	X_{c_p} Calibers	$C_{N\alpha_2}$	Offset	α Range, Degrees	X_{c_p} Calibers	$C_{N\alpha_3}$	Offset	α Range, Degrees	X_{c_p} Calibers
1	.0135	0	0-2.4	6.88	.005	.016	2.4-8.0	7.1	.005	.016	2.2-8.0	7.1
2	-.0055	0	0-1.6	6.8	0	-.0085	1.6-5.5	6.8	.003	-.024	5.5-8.0	6.9
3	.0025	0	0-5.5	6.6	.01	-.05	5.5-8.0	6.6	.01	-.05	5.5-8.0	6.7
4	-.003	0	0-3.0	6.4	-.002	-.0025	3.0-8.0	6.4	-.002	-.0025	3.0-8.0	6.4
5	.004	0	0-3.0	5.85	.0017	.007	3.0-5.2	5.75	.00025	.014	5.2-8.0	5.7
6	.016	0	0-2.1	5.3	.0095	.0125	2.1-3.8	5.25	.007	.0235	3.8-8.0	5.2
7	—	-	-	-	—	—	-	-	—	—	-	-
8	0	0	0-3.6	0	0	0	0-3.6	0	.003	-.01	3.6-8.0	4.8
9	-.016	0	0-1.6	4.6	-.006	-.0165	1.6-3.8	4.6	-.0045	-.0225	3.8-8.0	4.35
10	.02	0	0-1.4	3.75	.0075	.0165	1.4-3.9	3.75	.004	.031	3.9-8.0	3.75
11	.00525	0	0-2.7	3.5	.0035	.0045	2.7-5.0	3.5	.002	.0115	5.0-8.0	3.5
12	-.0145	0	0-2.5	3.15	-.0045	-.0295	2.5-4.6	3.3	-.0015	-.0044	4.6-8.0	3.3
13	.012	0	0-3.1	2.4	.007	.014	3.1-4.0	2.45	.007	.014	4.0-8.0	2.55
14	—	-	-	-	—	—	-	-	—	—	-	-
15	.0185	0	0-2.2	.95	.0085	.0225	2.2-3.5	1.0	.005	.0355	3.5-8.0	1.05
16	.0135	0	0-2.6	.6	.0095	.015	2.6-4.5	.6	.007	.027	4.5-8.0	.6
17	-.0225	0	0-1.5	.4	-.0095	-.021	1.5-2.0	.4	-.005	-.0305	2.0-8.0	.35
18	.001	0	0-2.0	.05	0	.002	2.0-4.3	.05	-.0005	.0045	4.3-8.0	.05
Fins	.06175	0	0-2.4	.6	.1	-.12	2.4-8.0	.6	.1	-.12	2.4-8.0	.6

TABLE B-II (Continued)

MACH NUMBER = 1.0

Lumped Force	C_N (α = 0)	Offset	α Range, Degrees	X_{c_p} Calibers	$C_{N\alpha_2}$	Offset	α Range, Degrees	X_{c_p} Calibers	$C_{N\alpha_3}$	Offset	α Range, Degrees	X_{c_p} Calibers
1	.0125	0	0-4.0	6.86	.006	.0255	4.0-8.0	7.1	.006	.0255	4.0-8.0	7.1
2	-.0040	0	0-1.7	6.8	.0005	-.0075	1.7-5.6	6.85	.002	-.0175	5.6-8.0	6.85
3	.0037	0	0-4.5	6.5	.0075	-.0095	4.5-6.3	6.5	.015	-.06	6.3-8.0	6.5
4	-.005	0	0-1.2	5.25	-.0025	-.003	1.2-8.0	6.1	-.0025	-.003	1.2-8.0	6.1
5	.004	0	0-1.6	5.65	.00125	.045	1.6-8.0	5.6	.00125	.045	1.6-8.0	5.6
6	.016	0	0-3.5	5.25	.0075	.031	3.5-4.6	5.25	.004	.0485	4.6-8.0	5.25
7	—	-	-	-	—	—	-	-	—	—	-	-
8	0	0	0-2.2	-	.005	-.0115	2.2-8.0	4.8	.005	-.0115	2.2-8.0	4.8
9	-.0288	0	0-1.4	4.5	-.00325	-.0355	1.4-5.5	4.45	-.0045	-.029	5.5-8.0	4.35
10	.0195	0	0-1.7	3.75	.010	.015	1.7-3.3	3.75	.006	.028	3.3-8.0	3.75
11	.006	0	0-2.5	3.5	.0035	.0065	2.5-8.0	3.5	.0035	.0065	2.5-8.0	3.5
12	-.0085	0	0-1.3	3.2	-.0015	-.009	1.3-4.0	3.25	-.0015	-.009	4.0-8.0	3.3
13	.0045	0	0-3.7	2.55	.0055	.0115	3.7-5.9	2.65	.008	-.031	5.9-8.0	2.85
14	-.0015	0	0-4.0	1.6	-.0035	.006	4.0-6.0	2.0	-.0035	.006	6.0-8.0	2.05
15	.016	0	0-1.9	.95	.0095	.0115	1.9-3.9	1.05	.005	.029	3.9-8.0	1.05
16	.01625	0	0-1.8	.6	.0065	.0165	1.8-3.6	.6	.005	.025	3.6-8.0	.6
17	-.025	0	0-2.2	.35	0	-.055	2.2-5.0	.35	.0075	-.094	5.0-8.0	.4
18	0	0	0-5.0	-	0	0	0-5.0	-	.002	-.0095	5.0-8.0	.05
Fins	.065	0	0-1.75	.6	.1	-.12	1.75-8.0	.6	.1	-.12	1.75-8.0	.6

MACH NUMBER = 1.1

Lumped Force	C_N ($\alpha = 0$)	Offset	α Range, Degrees	X_{cp} Calibers	$C_{N\alpha_2}$	Offset	α Range, Degrees	X_{cp} Calibers	$C_{N\alpha_3}$	Offset	α Range, Degrees	X_{cp} Calibers
1	.0105	0	0-4.0	6.94	.007	.0135	4.0-8.0	7.1	.007	.0135	4.0-8.0	7.1
2	-.0025	0	0-2.0	6.8	0	-.005	2.0-5.0	6.8	.0015	-.013	5.0-8.0	6.85
3	.0045	0	0-5.9	6.4	.0085	-.0225	5.9-8.0	6.45	.0085	-.0025	5.9-8.0	6.45
4	-.008	0	0-1.6	5.85	-.003	-.0075	1.6-5.3	5.85	-.0065	.011	5.3-8.0	5.85
5	.0025	0	0-1.7	5.55	.0012	.002	1.7-8.0	5.5	.0012	.002	1.7-8.0	5.5
6	.015	0	0-2.5	5.25	.0105	.01	2.5-8.0	5.2	.0105	.01	2.5-8.0	5.2
7	-.00325	0	0-2.2	4.8	0	-.005	2.2-3.8	4.8	.0012	-.0095	3.8-8.0	4.85
8	.002	0	0-2.3	4.55	.00025	.00325	2.3-4.0	4.55	.00025	.00325	4.0-8.0	4.6
9	-.0125	0	0-1.0	4.15	-.00425	-.009	1.0-6.0	4.15	-.0075	.011	6.0-8.0	4.15
10	.0155	0	0-1.2	3.7	.01	.006	1.2-8.0	3.7	.01	.006	1.2-8.0	3.7
11	.006	0	0-2.4	3.5	.004	.005	2.4-8.0	3.5	.004	.005	2.4-8.0	3.5
12	-.006	0	0-1.5	3.25	-.0015	-.004	1.5-4.0	3.25	-.0015	-.004	4.0-8.0	3.3
13	.00925	0	0-1.5	2.7	.003	.0085	1.5-8.0	2.7	.003	.0085	1.5-8.0	2.75
14	-.00925	0	0-1.8	1.6	-.0025	-.0125	1.8-5.1	1.65	-.005	.0025	5.1-8.0	1.7
15	.011	0	0-1.6	.95	.0055	.0095	1.6-3.4	.95	.002	-.022	3.4-8.0	.95
16	.018	0	0-1.3	.6	.004	.02	1.3-5.0	.6	.006	.01	5.0-8.0	.6
17	-.015	0	0-2.4	.37	0	-.031	2.4-3.6	.4	.0085	.046	3.6-8.0	.45
18	.0005	0	0-3.0	.03	.0015	-.004	3.0-5.0	.06	.0025	-.0085	5.0-8.0	.1
Fins	.0725	0	0-2.75	.6	.1	-.12	2.75-8.0	.6	.1	-.12	2.75-8.0	.6

MACH NUMBER = 1.2

Lumped Force	C_N (α = 0)	Offset	α Range, Degrees	X_{c_p} Calibers	$C_{N\alpha_2}$	Offset	α Range, Degrees	X_{c_p} Calibers	$C_{N\alpha_3}$	Offset	α Range, Degrees	X_{c_p} Calibers
1	.01	0	0-4.5	6.9	.0075	.0105	4.5-8.0	7.05	.0075	.0105	4.5-8.0	7.05
2	-.0015	0	0-3.8	6.8	0	-.006	3.8-5.3	6.8	.002	-.016	5.3-8.0	6.85
3	.0055	0	0-1.4	6.4	.002	.0045	1.4-5.3	6.4	.006	-.0175	5.3-8.0	6.4
4	-.008	0	0-0.7	5.7	-.0035	-.004	0.7-5.0	5.7	-.005	.0025	5.0-8.0	5.65
5	.0005	0	0-4.0	5.525	-.00025	.002	4.0-6.0	5.525	-.00025	.002	6.0-8.0	5.5
6	.014	0	0-4.0	5.25	.011	.01	4.0-8.0	5.15	.011	.01	4.0-8.0	5.15
7	—	-	-	-	—	—	-	-	—	—	-	-
8	.002	0	0-2.9	4.45	.001	.0035	2.9-4.0	4.45	.001	.0035	4.0-8.0	4.65
9	-.009	0	0-1.0	4.05	-.0065	-.0025	1.0-2.6	4.05	-.0045	-.009	2.6-8.0	4.05
10	.00675	0	0-3.8	3.7	.003	.012	3.8-8.0	3.65	.003	.012	3.8-8.0	3.65
11	.00525	0	0-3.5	3.5	.001	.016	3.5-8.0	3.5	.001	.016	3.5-8.0	3.5
12	—	-	-	-	—	—	-	-	—	—	-	-
13	.0075	0	0-3.2	2.75	.005	.0085	3.2-8.0	2.75	.005	.0085	3.2-8.0	2.75
14	-.007	0	0-2.1	1.4	-.0035	-.0045	2.1-3.7	1.4	-.0015	-.0135	3.7-8.0	1.4
15	.007	0	0-3.4	.9	.002	.0135	3.4-4.8	.9	.0005	.0215	4.8-8.0	1.95
16	.0115	0	0-2.5	.6	.006	.017	2.5-4.3	.6	.0025	.0315	4.3-8.0	.6
17	-.0085	0	0-1.0	.4	0	-.0185	1.0-3.4	.4	.00325	-.03	3.4-8.0	.35
18	0	0	0-4.8	-	0	0	0-4.8	-	.0025	-.0135	4.8-8.0	.1
Fins	.071	0	0-8.0	.55	.071	0	0-8.0	.55	.071	0	0-8.0	.55

TABLE B-II (Continued)

MACH NUMBER = 1.28

Lumped Force	C_N ($\alpha = 0$)	Offset	α Range, Degrees	X_{cp} Calibers	$C_{N\alpha_2}$	Offset	α Range, Degrees	X_{cp} Calibers	$C_{N\alpha_3}$	Offset	α Range, Degrees	X_{cp} Calibers
1	.01125	0	0-4.4	6.85	.008	.016	4.4-8.0	6.95	.008	.016	4.4-8.0	6.95
2	-.0010	0	0-2.8	6.8	0	-.004	2.8-5.0	6.8	.0013	-.0105	5.0-8.0	6.85
3	.00325	0	0-8.0	6.35	.00325	0	0-8.0	6.35	.00325	0	0-8.0	6.35
4	-.009	0	0-1.4	5.65	-.0015	-.01	1.4-6.0	5.7	-.0035	.0035	6.0-8.0	5.7
5	0	0	0-1.0	-	.009	-.004	1.0-3.6	5.52	-.0035	.028	3.6-8.0	5.5
6	.013	0	0-4.1	5.25	.008	.0185	4.1-8.0	5.15	.008	.0185	4.1-8.0	5.15
7	—	-	-	-	—	—	-	-	—	—	-	-
8	.0035	0	0-2.4	4.45	.007	-.0085	2.4-4.0	4.5	.007	-.0085	4.0-8.0	4.55
9	-.0085	0	0-1.2	3.95	-.0045	-.004	1.2-4.2	4.0	-.003	-.011	4.2-8.0	4.0
10	.005	0	0-2.0	3.65	.0025	.0068	2.0-4.0	3.65	.0025	.0068	4.0-8.0	3.7
11	.0033	0	0-4.6	3.5	.0012	.0095	4.6-8.0	3.5	.0012	.0095	4.6-8.0	3.5
12	--	-	-	-	—	—	-	-	—	—	-	-
13	.0065	0	0-1.5	2.75	.005	.0025	1.5-4.3	2.75	.007	-.0105	4.3-8.0	2.75
14	-.006	0	0-1.8	1.25	-.003	-.0055	1.8-8.0	1.3	-.003	-.0055	1.8-8.0	1.3
15	.00475	0	0-1.8	.8	.002	.0055	1.8-3.4	.85	.0005	.01	3.4-8.0	.85
16	.0125	0	0-1.6	.6	.006	.021	1.6-4.0	.6	.002	.025	4.0-8.0	.6
17	-.005	0	0-3.0	.35	0	-.015	3.0-4.6	.35	.004	-.034	4.6-8.0	3.5
18	0	0	0-5.0	-	0	0	0-5.0	-	.0025	-.015	5.0-8.0	.1
Fins	.069	0	0-8.0	.45	.069	0	0-8.0	.45	.069	0	0-8.0	.45

DEFINITION OF LUMPED LOADS

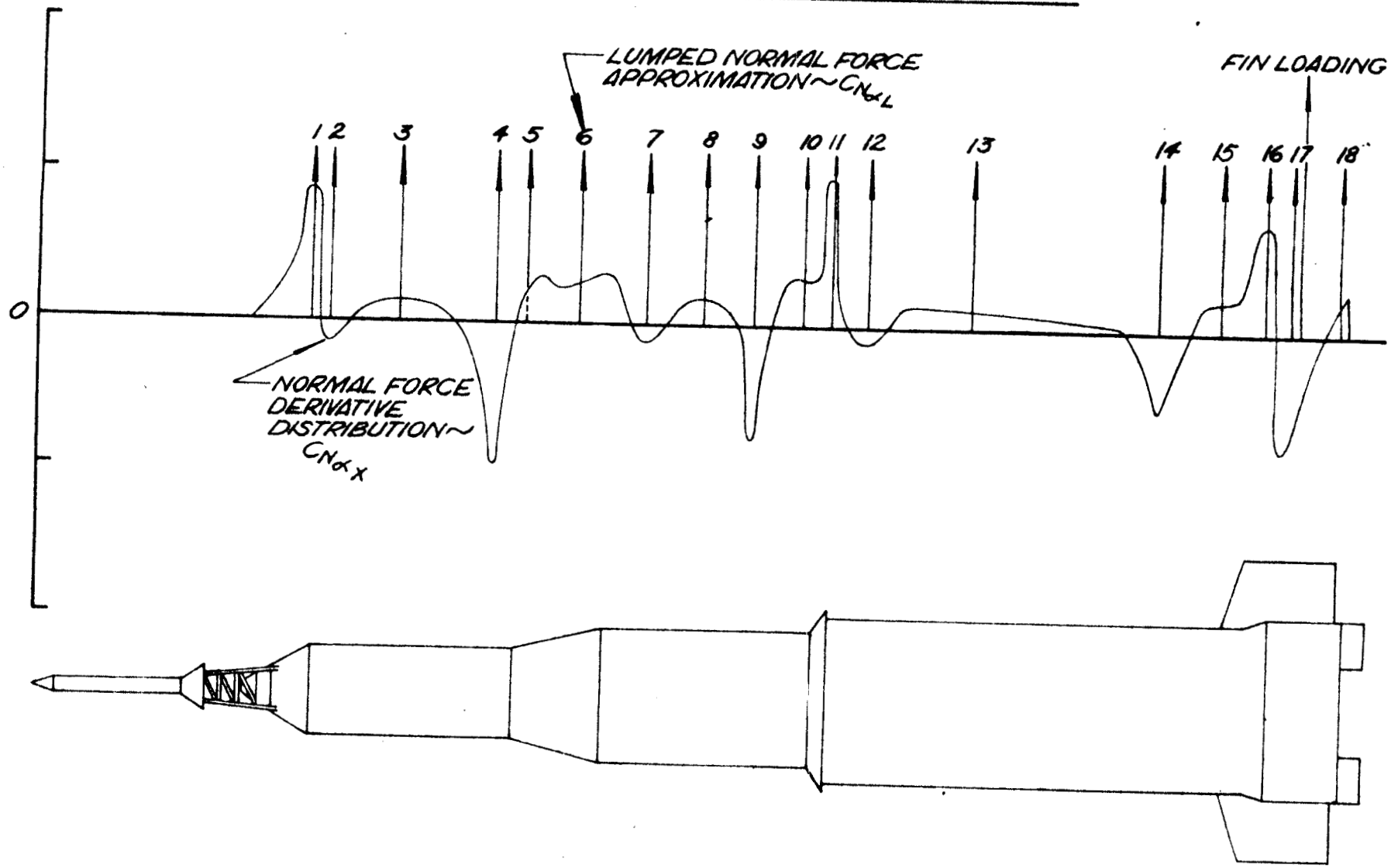

FIGURE B-1
PAGE B-12

PREPARED BY TM
DATE 8-1-63
CHECKED BY

LOCKHEED MISSILES & SPACE COMPANY
A GROUP DIVISION OF LOCKHEED AIRCRAFT CORPORATION

PAGE
MODEL
REPORT NO.

FIGURE B-2a
PAGE B-13

FLIGHT CONFIGURATION AND FLIGHT CONDITIONS
LUMPED NORMAL FORCE DERIVATIVE DISTRIBUTION
ALL MOTORS AT $\alpha = 0°$

DISK ON
DISK OFF

DISK ON AND OFF

DISK ON AND OFF

COMBINED FORCES

NORMAL FORCE DERIVATIVE DISTRIBUTION

FMS

MACH NUMBER

LUMPED NORMAL FORCE DERIVATIVE $\sim C_{N_\alpha}$, PER DEGREE

LUMPED NORMAL FORCE DERIVATIVE $\sim C_{N_\alpha}$, PER DEGREE

FORM LMSC 838D-1

FORM LMSC 830D-1

FLIGHT CONFIGURATION AND FLIGHT CONFIGURATION PLUS DISK LUMPED NORMAL FORCE DERIVATIVES AT $\alpha = 0°$

FINS AND CARRY-OVER

LUMPED FORCES

NORMAL FORCE DERIVATIVE DISTRIBUTION

LUMPED NORMAL FORCE DERIVATIVE ~ $C_{N_{\alpha x}}$, PER DEGREE

MACH NUMBER ~ M

PREPARED BY TM
DATE 8-15-63
CHECKED BY

LOCKHEED MISSILES & SPACE COMPANY
A GROUP DIVISION OF LOCKHEED AIRCRAFT CORPORATION

PAGE
MODEL
REPORT NO.

FIGURE B-26
PAGE B-44

FORM LMSC 635D-1

FLIGHT CONFIGURATION AND FLIGHT CONFIGURATION PLUS DISK FORCE COMPONENT CENTERS OF PRESSURE AT $\alpha = 0°$

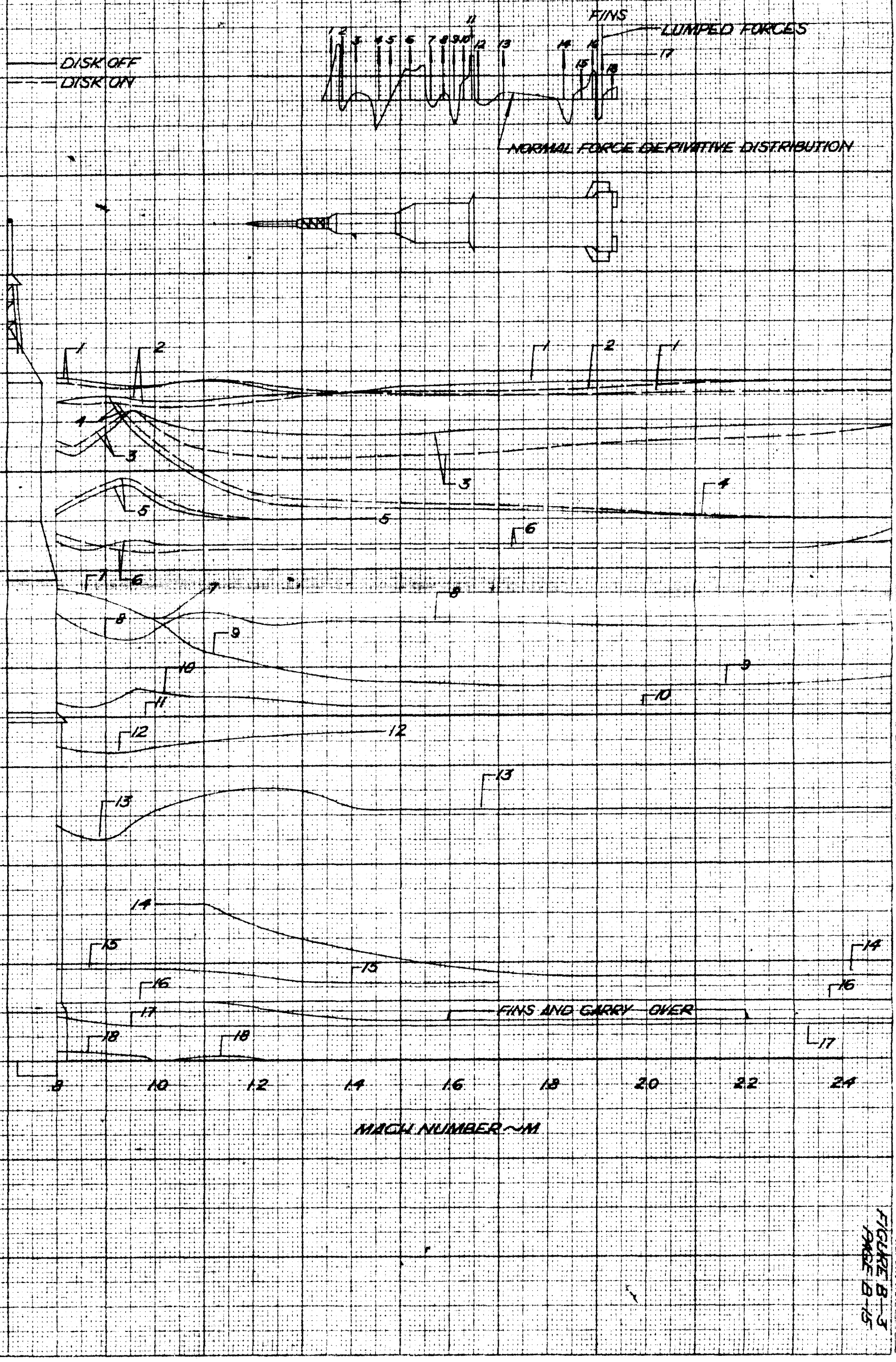

LOCKHEED MISSILES & SPACE COMPANY
A GROUP DIVISION OF LOCKHEED AIRCRAFT CORPORATION

PREPARED BY TM
DATE 7-31-63
CHECKED BY

PAGE
MODEL
REPORT NO.

FIGURE B-3
PAGE B-15

FORM LMSC 6380 1

BASIC CONFIGURATION AND BASIC CONFIGURATION DISK OFF
LUMPED NORMAL FORCE DERIVATIVES AT $\alpha = 0°$

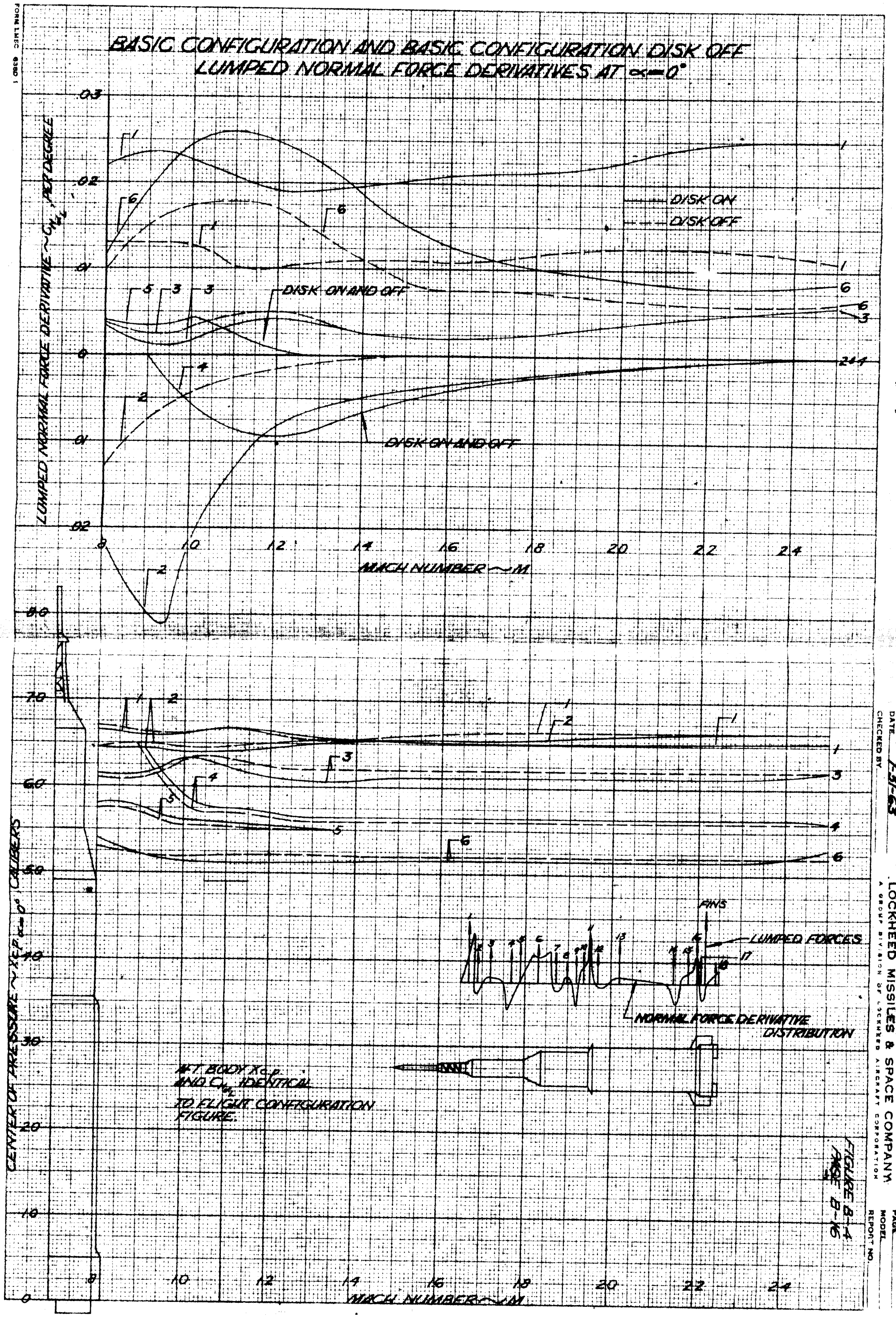

PREPARED BY TM
DATE 7-31-63
CHECKED BY

LOCKHEED MISSILES & SPACE COMPANY
A GROUP DIVISION OF LOCKHEED AIRCRAFT CORPORATION

PAGE
MODEL
REPORT NO.

FIGURE B-14
PAGE B-16